AFRL-RQ-WP-TR-2015-0138

THERMAL ENHANCEMENT OF SILICON CARBIDE (SiC) POWER ELECTRONICS AND LASER BARS:

Statistical Design Optimization of a Liquid-Cooled Power Electronic Heat Sink

James D. Scofield

Electrical Systems Branch
Power and Control Division

AUGUST 2015
Final Report

AIR FORCE RESEARCH LABORATORY
AEROSPACE SYSTEMS DIRECTORATE
WRIGHT-PATTERSON AIR FORCE BASE, OH 45433-7541
AIR FORCE MATERIEL COMMAND
UNITED STATES AIR FORCE

NOTICE AND SIGNATURE PAGE

Using Government drawings, specifications, or other data included in this document for any purpose other than Government procurement does not in any way obligate the U.S. Government. The fact that the Government formulated or supplied the drawings, specifications, or other data does not license the holder or any other person or corporation; or convey any rights or permission to manufacture, use, or sell any patented invention that may relate to them.

This report was cleared for public release by the USAF 88th Air Base Wing (88 ABW) Public Affairs Office (PAO) and is available to the general public, including foreign nationals.

Copies may be obtained from the Defense Technical Information Center (DTIC) (http://www.dtic.mil).

AFRL-RQ-WP-TR-2015-0138 HAS BEEN REVIEWED AND IS APPROVED FOR PUBLICATION IN ACCORDANCE WITH ASSIGNED DISTRIBUTION STATEMENT.

*//Signature//
JAMES D. SCOFIELD
Program Manager
Electrical Systems Branch
Power and Control Division

//Signature//
GREGORY L. FRONISTA, Chief
Electrical Systems Branch
Power and Control Division
Aerospace Systems Directorate

//Signature//
JOHN G. NAIRUS, Chief Engineer
Power and Control Division
Aerospace Systems Directorate

This report is published in the interest of scientific and technical information exchange, and its publication does not constitute the Government's approval or disapproval of its ideas or findings.

*Disseminated copies will show "//Signature//" stamped or typed above the signature blocks.

REPORT DOCUMENTATION PAGE

Form Approved
OMB No. 0704-0188

1. REPORT DATE *(DD-MM-YY)*	2. REPORT TYPE	3. DATES COVERED *(From - To)*
August 2015	Final	01 October 2007 – 23 September 2015

4. TITLE AND SUBTITLE
THERMAL ENHANCEMENT OF SILICON CARBIDE (SiC) POWER ELECTRONICS AND LASER BARS:
Statistical Design Optimization of a Liquid-Cooled Power Electronic Heat Sink

5a. CONTRACT NUMBER
In-house

5b. GRANT NUMBER

5c. PROGRAM ELEMENT NUMBER
62203F

6. AUTHOR(S)
James D. Scofield

5d. PROJECT NUMBER
3145

5e. TASK NUMBER
N/A

5f. WORK UNIT NUMBER
Q0M3

7. PERFORMING ORGANIZATION NAME(S) AND ADDRESS(ES)
Electrical Systems Branch (AFRL/RQQE)
Power and Control Division
Air Force Research Laboratory, Aerospace Systems Directorate
Wright-Patterson Air Force Base, OH 45433-7541
Air Force Materiel Command, United States Air Force

8. PERFORMING ORGANIZATION REPORT NUMBER
AFRL-RQ-WP-TR-2015-0138

9. SPONSORING/MONITORING AGENCY NAME(S) AND ADDRESS(ES)
Air Force Research Laboratory
Aerospace Systems Directorate
Wright-Patterson Air Force Base, OH 45433-7541
Air Force Materiel Command
United States Air Force

10. SPONSORING/MONITORING AGENCY ACRONYM(S)
AFRL/RQQE

11. SPONSORING/MONITORING AGENCY REPORT NUMBER(S)
AFRL-RQ-WP-TR-2015-0138

12. DISTRIBUTION/AVAILABILITY STATEMENT
Approved for public release; distribution unlimited.

13. SUPPLEMENTARY NOTES
PA Case Number: 88ABW-2015-4435; Clearance Date: 18 Sep 2015.

14. ABSTRACT

The objective of this project was to investigate the utilization of a design of experiments (DOE) methodology as an efficient means to realize an optimized configuration for a single phase, liquid-cooled, pin fin, heat sink for power electronic thermal management applications. The process being utilized in this effort is a computational fluid dynamics (CFD) software solution of a series of quarter fraction, two-level (2n-2) DOE runs over defined ranges of input factors, variables, or treatments. The software used on this project is the Navier-Stokes CFD solver Fluent™ package marketed by ANSYS, Inc., which is a finite volume discretization PDE solution technique. The output response variables of interest are computationally determined for each of the factorial run conditions and used in all subsequent statistical analysis. The ultimate goal is to ascertain whether a generic design algorithm for pin fin heat sinks can be realized using subject matter (SM) expertise coupled with a focused DOE methodology, thereby simplifying thermal management design for optimal heat transfer performance that can lead to acceptable power device junction temperatures and reliable operation.

15. SUBJECT TERMS
silicon carbide, power electronics thermal management, design of experiments

16. SECURITY CLASSIFICATION OF:			17. LIMITATION OF ABSTRACT:	18. NUMBER OF PAGES	19a. NAME OF RESPONSIBLE PERSON (Monitor)
a. REPORT	b. ABSTRACT	c. THIS PAGE			James D. Scofield
Unclassified	Unclassified	Unclassified	SAR	107	19b. TELEPHONE NUMBER *(Include Area Code)* N/A

Table of Contents

List of Figures

Figure **Page**

List of Tables

1 Objective

The objective of this project was to investigate the utilization of a Design of Experiments (DOE) methodology as an efficient means to realize an optimized configuration for a single phase, liquid cooled, pin fin, heat sink for power electronic thermal management applications. The process being utilized in this effort is a computational fluid dynamics (CFD) software solution of a series of quarter fraction, 2-level (2^{n-2}) DOE "runs" over defined ranges of input factors, variables, or treatments. The software used on this project is the Navier-Stokes CFD solver *Fluent*^{TM} package marketed by ANSYS, Inc., which is a finite volume discretization PDE solution technique. The output response variables of interest are computationally determined for each of the factorial run conditions and used in all subsequent statistical analysis. The ultimate goal is to ascertain whether a "generic" design algorithm for pin fin heat sinks can be realized using subject matter (SM) expertise coupled with a focused DOE methodology, thereby simplifying thermal management design for optimal heat transfer performance leading to acceptable power device junction temperatures and reliable operation. The complete solution leading to a final design for this problem is well beyond the scope of our class project; however, the statistical evaluation of the initial designed experiments evaluating the basic criteria leading to an idealized surrogate design model is well within the scope. Combinations of practical physical boundary conditions are chosen to avoid out of range nuisance or impractical variable effects, but to also enable indirect investigation of their relationship to the obtained optimal design, such as the case with cross sectional pin shape (circular, square). Critical design considerations that require practical bounds are: 1) pumping power due to the fact that excessive pressure and/or flow requirements result in impractically large pumps which exceed typical system cost, volume, and weight constraints; 2) inlet coolant temperature (this project uses single phase H_2O as the coolant fluid thus a 32 $^oF < T_{in} < 212\ ^oF$ maximal range limit); 3) fluid channel mass flow rates sufficient to ensure that turbulent flow (Re > ~ 2500) conditions exist; 4) input heat rate (Q_{in}) must be limited to the practical limit of SOTA power electronics packaging (< 200 W/cm^2) so that realistic solution sets are analyzed over ranges in which the fundamental electronic functionality is preserved (i.e. maintain junction temperatures below the rated device maximum), and 5) external system temperature boundary conditions are held constant (300 K) in simulations to eliminate associated nuisance effects. Constraint 1) will drive the bounds of practical pin fin array geometries since excessively dense coolant fluid channel obstruction will drive excessive pressure drops and pump sizing. In addition, pin geometries (length, diameter, array density, cross sectional shape) are, in principle, an infinitely variable set of parameters which while critically important, must necessarily be handled in a controlled design paradigm in order to initially allow us to determine the more fundamental physics derived factors of sink heat transfer importance. To this end, the CFD simulations and DOE analysis and experiment designs have been structured to initially evaluate two cross sectional geometries, circular and square pin fins which are evaluated as categoric factors to observe their direct influence on the response variables of interest (e.g., T_{max}, ΔP, h_{eff}). The primary reason for investigating this bifurcated fin analysis is twofold. First, valuable insight into the DOE methodology and the influence of different design analyses will be obtained, and secondly the fundamental flow, spatial layout, heat transfer physics can be understood and defined on each geometry, eliminating any potential confusion with shape-factor interactions. The analyzed results will be quantitatively compared analyzed directly in the full factorial ANOVA calculations in which each categoric factor (geometry) will yield an independent surrogate model equation for each response variable. These surrogate equation models can subsequently be compared to CFD run output response results for cases not included in the factorial design run list, as sort of an initial

validation of the DOE results. A well designed experiment should lead to very good agreement between CFD and surrogate models within the original design space, but the results outside these ranges will be dubious for the quarter fraction derived surrogates. In other words, the factorial results will give good analysis and indications of main and two-factor interactions of primary importance, but will require a higher fidelity RSM or similar follow-on experiment for refining our surrogate model to be of greater utility for prediction outside our original design space. This inclusion of a categoric geometry input factor was taken because it has been assumed by our SME's that pin shape will have a significant influence, but that it will ultimately be a higher level design choice between cross sectional shapes for fine tuning or tailoring in the final heat sink design process. Our analysis intends to determine the factuality of this statement or whether shape is a more fundamental factor easily elucidated by the simple fractional factorial process. To accomplish these goals we have designed a two-level fractional factorial experiment requiring 32 runs; i.e. a resolution IV 2^{7-2}. Two center points were included in the run matrix to estimate the anticipated curvature in response variables and provide the requisite DOF for pure error and lack of fit in the ANOVA analysis. We have used the State-Ease software "Design Expert" to perform the DOE analysis of the experiment and response statistics. Details of the experimental structure and the selected simulation response variables and the analysis of data are summarized in the sections that follow.

2 Introduction

Numerous comprehensive theoretical and experimental studies have been accomplished on the characterization and optimization of pin fin heat sinks [1,2,3,4,5]. Studies utilizing empirically derived correlation factors [6,7,8,9] to second law and exergy analysis [10,11,12] have been accomplished on the subject. However, using a statistically based DOE paradigm to accomplish a design objective has been given very little consideration. Given the large number of possible factors driving the optimal configuration, it is a perfect system for which to leverage the efficient power with which statistically designed experiments can distill the complex multi-factor interaction physics which dictate heat transfer performance in these "simple" thermal management components.

As an AFRL In House researcher responsible for conducting research in the area of power electronics, components, and electronics cooling, I have a keen interest in investigating the utility of this proposed approach to cold plate design. Several platforms currently under development have thermal performance limitations and could benefit significantly from more efficient heat transfer and rejection technologies. This situation, coupled with the fact that critical electronic component reliability and life expectancy depends fundamentally on operating temperature, necessitates that a more focused attention be paid to heat transfer effectiveness from device junctions to the cooling medium. In addition, because of the potentially large number of driving factors, a one factor at a time (OFAT) approach is not only infeasible, it is highly unlikely to lead to the best design. Furthermore, conventional thermal design approaches, based on lumped element thermal capacity models, are highly inefficient and usually require an engineering "safety" design margin factor to account for the large associated uncertainties and nuisance factors. Thus, a well-designed set of experiments, which are minimal yet sufficient for improved design purposes, are likely to only be realized using these statistically formalized techniques. It is my goal to begin the process of addressing this much broader thermal management problem by focusing on defining an efficient design optimization methodology. Due to the complexity of the problem, we will hopefully identify an initial set of design screening factors which are primary to achieving the stated objective. Figure 1 illustrates a typical electronics package configuration and shows the heat rejection pathway to the coolant medium. In most instances, the coolant fluid is passive or forced air or circulated liquid. More advanced two phase systems are required for some high heat flux applications, such as dual core microprocessors operating at several GHz frequencies and extremely high chip integration levels leading to significant waste heat fluxes. The power electronic components of interest for the purposes of this project have air, kerosene, PAO, water, or similar coolant single phase requirements. In these applications, Fourier conduction characterizes the heat transfer from the chip to the cold plate or heatsink. While critically important to power electronic device functionality and operational device junction temperatures, they are fundamental materials and thermal conductivity problems and are not within the scope of this project. The subject DOE analysis and design consideration in this project is targeting optimization of the heat sink portion of the electronics subsystem. As a result, our base physical model for *Fluent*^{Tm} CFD simulation purposes is shown in Figure 2 and is representative of a heat rate ($\Delta Q/\Delta t$) source (electronic device) located directly on top of the fluid channel containing the pin fin array heat sink. The heat sink array is modeled using aluminum ($k = 247$ W/mK) material properties which is a common material choice for this application due to its' extrudability, high conductivity (κ), and lightweight (ρ) characteristics. The following section details the DOE

experimental design approach, chosen input factors and ranges, response variables, and configuration details of the physical models utilized for the *Fluent*™ simulation runs.

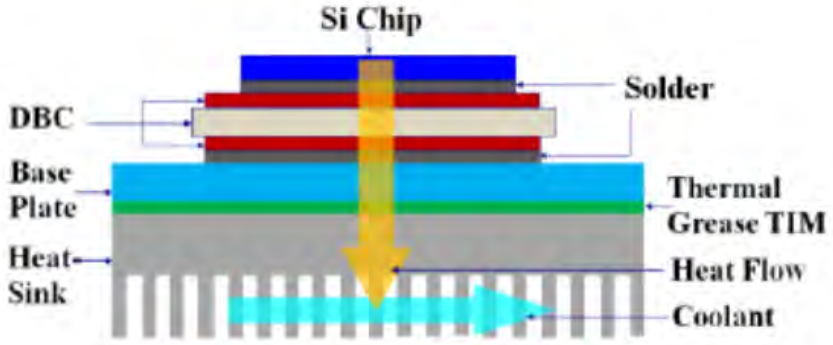

Figure 1. Typical Finned Heat Sink Electronics Cooling Configuration

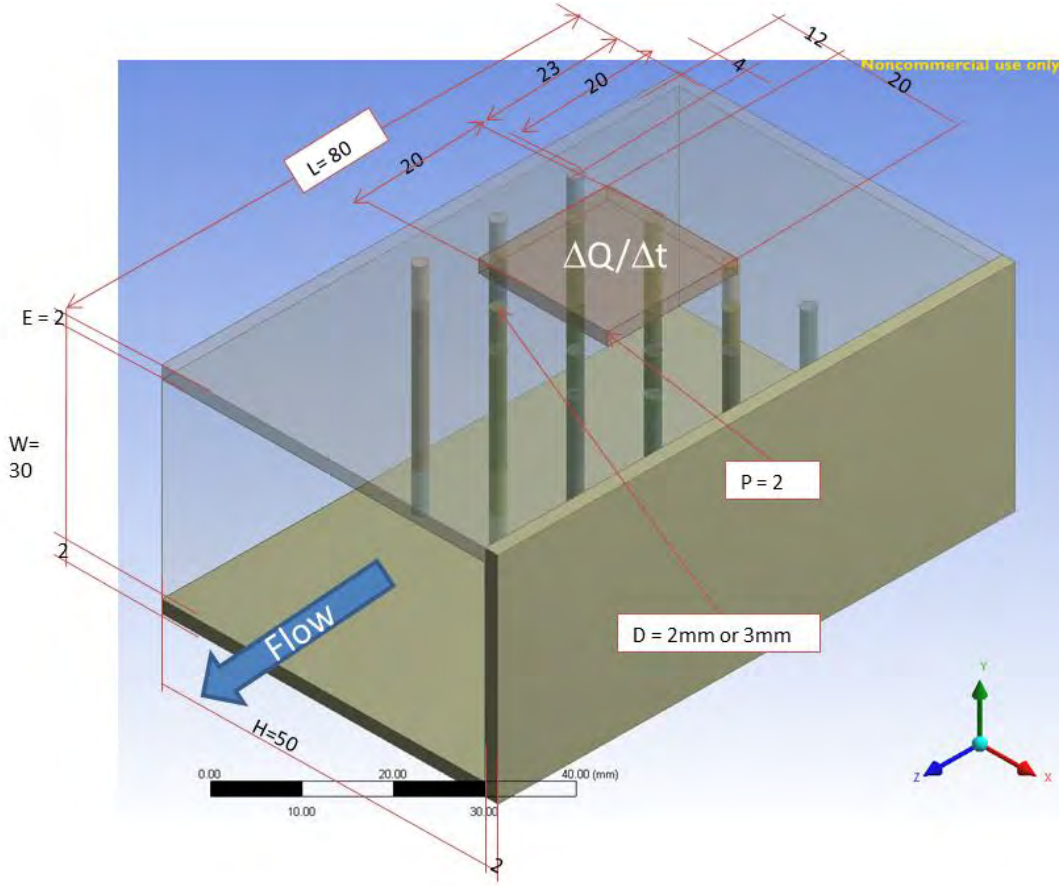

Figure 2. General Configuration Rendering of the *Fluent*™ Physical Finite Volume Model

3 Experiment Description

In this factorial screening design investigation there are seven physical input factors associated with three selected heat sink response variables. The physical parameter variables and units are: (A) pin diameter, d, mm; (B) pin spacing, S, mm; (C) heat rate in, Qin, W/cm^2; (D) temperature of the fluid, TFluidIn, K; (E) mass flow, mdot, kg/s; (F) offset angle, θ, degrees; and (G) pin geometry (circular vs. square). Table 1 organizes the six numerical input factors as well as their two level input computational values. The seventh factor, G, is qualitative. The pins are sized such that the circular cross-section of the cylindrical pins has a diameter equal to the edge dimension of the square cross-section pins. Figure 3 illustrates the angle (q), diameter (d), and spacing (s) relationships through a simple trigonometric identity. Output response variables chosen were: 1) peak temperature at the base of the pin fin array, T-max, 2) pressure drop across the test cell, ΔP, and 3) effective or overall heat transfer coefficient, h_{eff}. The factorial low and high levels, also shown in Table 1, have been tailored to both provide sufficient range variation as well as to reflect practical power electronics operational environmental conditions through consultation with our SME's. For example, the heat rate input range is varied over a reasonable range of energy rates commensurate with the heat rejection capability of SOTA discrete and module packaging thermal impedances, resulting in a physically realistic power device junction temperature peak. Similarly for the coolant fluid (H_2O in this case) temperature range listed in Table 1 as well as its mass flow rate. Pin-fin dimensions are driven by practical computational limitations (number of pins and computational time), flow channel obstruction (pump considerations), manageable fin heat flux, and manufacturing constraints. The experimental matrix computational test cells were designed with 8, 15, 18, 25, and 60 pin fins, and were dictated by the cell base area and the dimensional constraints of Figure 3.

Table 1. Quantitative Input Factors and Levels for the 2^{7-2} Resolution IV Fractional Factorial Design

A: Pin Diameter		B: Pin Spacing		C:Qin		D:TfluidIn		E:Mdot		F:Angle	
+	-	+	-	+	-	+	-	+	-	+	-
3	2	9	4	200	50	60	10	0.6	0.1	30	60
mm	mm	mm	mm	W/cm^2	W/cm^2	°C	°C	kg/s	kg/s	Deg	Deg

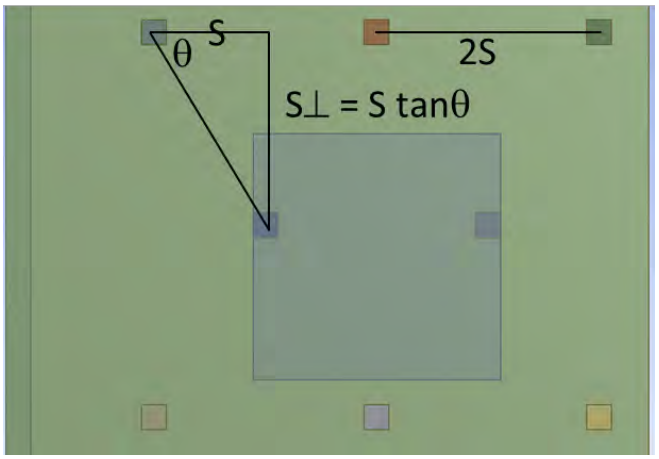

Figure 3. Top View of a Test Cell Pin Arrangement

(This view shows the relationship between pin diameter and spacing leading to pin locations and total pin number per fixed cell area.)

A two-level 2^{7-2} fractional factorial was designed using the ranges and parameters described above and computational CFD experiments run using the input factors of Table 1. A detailed summary of the results are described in the following section. As will be shown, the ANOVA and ancillary statistical analysis enabled a quantitative comparison between the two pin types, without the need to increase the number of experimental runs, while simultaneously screening the more physically fundamental heat transfer input variables driving the output responses of interest. A comparison of the resulting parsimonious surrogate models for each response variable is also summarized and compared to CFD computations of design space runs not included in the 32+2 factorial experimental runs. A higher resolution design will necessarily be required in a follow-on project after the present 2^{7-2} experimental screening of relevant factors and the elimination of non-statistically significant factors. The ultimate goal was to identify critical design parameter ranges that are ubiquitous to pin fin, single phase, fluid heat sink systems, as well as, to gain key insight into the use of DOE methods to efficiently arrive at the optimal design with a minimum probability of not being not wrong. As will be shown in the following sections, these goals were enabled by the DOE methodology.

4 DOE Experimental Design

As required by the statistical evaluation process we first identify and state the null hypothesis that we sought to evaluate: Since most of the input factors are quantitative, we anticipate that a regression model will be best suited for this analysis. Thus, our comparison between treatments and response variables will involve testing the hypothesis that the regression coefficients are all zero. Specifically;

Null Hypothesis

***Ho**: $\beta_1 = \beta_2 = \beta_3 = \beta_4 = \beta_5 = \beta_6 = \ldots = \beta_{ijkl\ldots} = 0$ i.e. variation of the input factors do not have an effect on the peak temperature of the heat sink base, the pressure drop across the fin array, or the effective heat transfer coefficient of the test cell.*

Alternative Hypothesis

***H1**: $\beta_{ijkl\ldots} \neq 0$ for at least one treatment pair for each of the response variables.*

Evaluation of this hypothesis been accomplished by conducting the ANOVA and associated statistical analysis of the response variable effects associated with varying the input factors as shown above. *Fluent*™ CFD software was used to numerically compute the response solutions deterministically as described above. The details of the factorial experiment design and the response variable analysis will be described in detail below.

The experimental design was based on a 2-level fractional factorial design to screen the relevant factors and interactions of primary interest, in addition to comparing alternative ANOVA analyses. Ultimately, since the factorial designed solution is not well suited for prediction; either a general factorial design or a response surface methodology will be required as a follow-on activity to achieve the desired final optimization results. However, our 2^{7-2} experiment will give good quantitative assessments of the main factors of primary importance as well as indications of strong two factor interactions. Some two-factor interactions and all three-factor and higher interaction relevance will not be determinable due to the aliasing structure resulting from the quarter fraction design.

As described in the previous section, the factors to be evaluated and their respective levels are re-summarized below:

1) Fin diameter (high level – 3 mm, low level 3 mm)
2) Pin Spacing (high level – 3x diameter, low level – 2x diameter)
3) offset angle (high level -45^o, low level 30^o)
4) Mass flow fluid velocity (high level – 0.6 m/s, low level – 0.1 m/s)
5) Heat flux input (high level – 200 W/cm2, low level 50 W/cm2)
6) Inlet Fluid T (high level – 60 ^{o}C, low level 10 ^{o}C)
7) Cross Sectional Geometry – (circular cylinder, square cylinder)

Since we are using a deterministic modeling experiment no nuisance variables are anticipated, especially since boundary conditions such as external environmental temperature, which would potentially be an uncontrollable nuisance variable, is held as constant in the simulations. In addition, the inlet coolant temperature is also assumed constant which in real physical systems would typically be variable and thus an additional complexity and likely an uncontrollable

nuisance variable. The physical model was developed based on the 2-D diagram of a circular pin array shown in Figure 4.

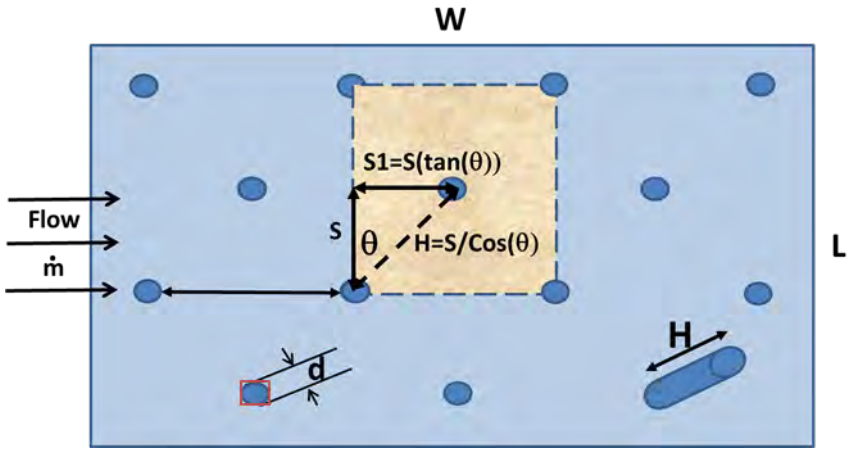

Figure 4. Pin Fin Layout Design and Input Parameters

The brown shaded region indicates a "unit" cell in the array design which is replicated laterally to populate the defined fin area in the fluid channel top surface as seen in the previous Figure 2. The input geometrical factors identified for intentional variation are shown in the Figure. S, is seen to be one half the transverse pin spacing, d is the pin diameter, θ reflects the alternate row pin location offset angle, while the remaining factors define the coolant fluid flow characteristics and input heat load. The Fluent™ physical model geometries were based on a fixed pin fin area (80 mm x 50 mm) and a fixed pin length of 28 mm. These values were chosen after consultation with our fluid dynamics SME's to be 1) sufficient to allow flow to fully develop prior to exiting the pin array 2) ensure turbulence around the pins, and 3) based on the estimated pin length required to maximize the standard heat transfer "*fin factor*", $[(Q_{dot})/[h_cPL(T_b-T_e)]=(1/\beta L)\tanh(\beta L)]$. In this "efficiency" ratio, the left side defines the ratio between the actual heat loss from a pin of length L and perimeter P, to the heat loss that would occur if the pin were at a fixed temperature T_b. The right hand side is a function of the non-dimensional factor βL, defined as the fin parameter and is given by $\beta L=(h_cP/\kappa A_c)^{0.5}L$, where the thermal conductivity, cross sectional area, and perimeter are defined by the pin construction. This non-dimensional factor is generated from the 1D solution to the second order differential heat transfer equation derived from an energy balance consideration of the heat flow down a pin *i.e.* $[d^2T/dx^2 - (hP/kA)(T-T_f) = 0]$, which is summarized in Figure 5.

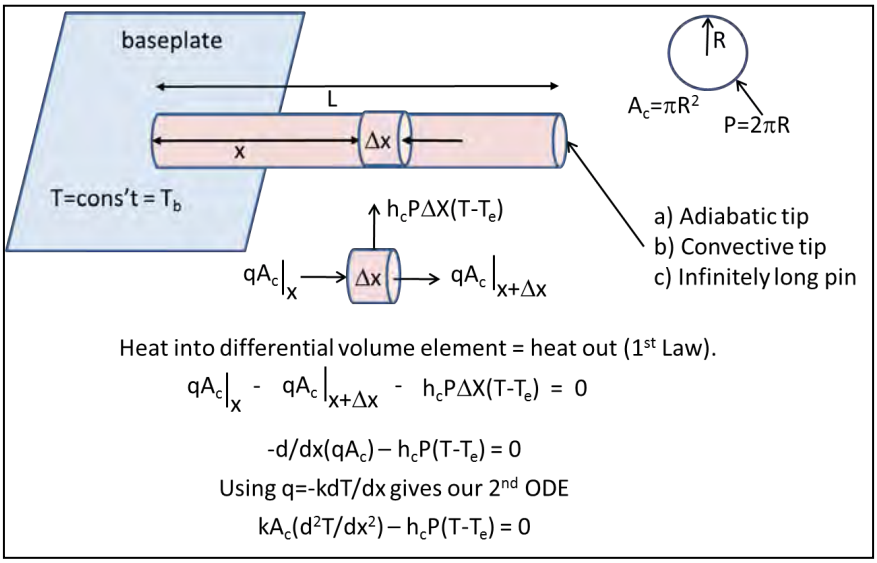

Figure 5. Geometry and Energy Balance Considerations

(The geometry and energy balance considerations lead to the fin efficiency factor and the 1D temperature distribution along the pin from which heat transfer into a fluid may be calculated.

When βL is small (thin long pins), fin efficiency is high. Practical manufacturing, heat capacity, and implementation considerations moderate the exploitation of this limiting case. While pin aspect ratio is potentially an important design consideration, our approach in this initial factorial screening design of experiments is to assume that only sufficient length is needed to result in a temperature drop along the length of the fin so that the pin tip approaches the fluid temperature. Additional length is therefore wasted and will not contribute to convective heat transfer to the fluid due to the negligible ΔT for $h[T_{pin} - T_{fluid}]$ to be significant. To ensure that this design assumption remains valid, T-distributions for each of the *Fluent*™ simulation runs have been assessed for the validity of this constraint. Turbulent flow was ensured by utilizing geometries and mass flow rate ranges such that the calculated Reynolds number would exceed 2000 and result in either turbulent to transition flow conditions. All 34 experimental run conditions were analyzed for this flow condition threshold prior to finalization of the input factor range values. Table 2 is a summary of the 44 run Reynolds number calculations shown in standard order. These values were calculated for the rectangular flow channel using the standard relationship between duct geometry and fluid properties given by

$$R_e = \rho VL/\mu = VL/\nu$$

,

where r, V, L, M, and n are the fluid density, mean velocity, characteristic dimension, dynamic viscosity, and kinematic viscosity, respectively. The relation for rectangular ducts in which the characteristic length is defined as 4 times the area divided by the wetted perimeter was used in the spreadsheet calculation shown in Table 2.

Table 2. Reynolds Number Calculations for the 44 Run Quarter Fraction Experiment

Cross area of channel	Perimeter of channel	Hight of fin	fin # in a row	Cross area over fins	Hydraulic diameter	Reynold number
A	P	H	n	A_f	D_h	Re
m^2	m	m		m^2	m	
0.0015	0.16	0.028	6	0.001164	0.0375	2,463
0.0015	0.16	0.028	6	0.001164	0.0375	2,463
0.0015	0.16	0.028	6	0.000996	0.0375	17,271
0.0015	0.16	0.028	6	0.000996	0.0375	17,271
0.0015	0.16	0.028	2	0.001388	0.0375	12,393
0.0015	0.16	0.028	2	0.001388	0.0375	12,393
0.0015	0.16	0.028	2	0.001332	0.0375	2,152
0.0015	0.16	0.028	2	0.001332	0.0375	2,152
0.0015	0.16	0.028	3	0.001332	0.0375	12,914
0.0015	0.16	0.028	3	0.001332	0.0375	12,914
0.0015	0.16	0.028	3	0.001248	0.0375	2,297
0.0015	0.16	0.028	3	0.001248	0.0375	2,297
0.0015	0.16	0.028	3	0.001332	0.0375	2,152
0.0015	0.16	0.028	3	0.001332	0.0375	2,152
0.0015	0.16	0.028	3	0.001248	0.0375	13,784
0.0015	0.16	0.028	3	0.001248	0.0375	13,784
0.0015	0.16	0.028	3	0.001332	0.0375	6,029
0.0015	0.16	0.028	3	0.001332	0.0375	6,029
0.0015	0.16	0.028	3	0.001248	0.0375	38,606
0.0015	0.16	0.028	3	0.001248	0.0375	38,606
0.0015	0.16	0.028	3	0.001332	0.0375	36,171
0.0015	0.16	0.028	3	0.001332	0.0375	36,171
0.0015	0.16	0.028	3	0.001248	0.0375	6,434
0.0015	0.16	0.028	3	0.001248	0.0375	6,434
0.0015	0.16	0.028	6	0.001164	0.0375	41,392
0.0015	0.16	0.028	6	0.001164	0.0375	41,392
0.0015	0.16	0.028	6	0.000996	0.0375	8,062
0.0015	0.16	0.028	6	0.000996	0.0375	8,062
0.0015	0.16	0.028	2	0.001388	0.0375	5,785
0.0015	0.16	0.028	2	0.001388	0.0375	5,785
0.0015	0.16	0.028	2	0.001332	0.0375	36,171
0.0015	0.16	0.028	2	0.001332	0.0375	36,171
0.0015	0.16	0.028	3	0.00129	0.0375	14,131
0.0015	0.16	0.028	3	0.00129	0.0375	14,131

As seen in the table, calculated Re number exceeded the value of 2000 set as our minimum baseline flow condition for all experiment runs.

Figure 6 shows two 2D top-view images of *Fluent*^{TM} physical models, one each for circular and square pins with the physical design factor dimensions shown to the right and which correspond to CFD runs 2 and 11. A total of 32 CFD physical models were similarly generated and run to cover the core range of input variables used in our designed factorial experiment. In addition, in order to satisfy the degrees of freedom required for Lack of Fit analysis and to account for potential curvature in the response variables, two center point models were run and replicated 10 times in Design Expert leading to a total of 44 experimental CFD runs. Table 3 shows an organized Design Expert summary of the initial 2^{7-2} fractional factorial designed experiment including response variables.

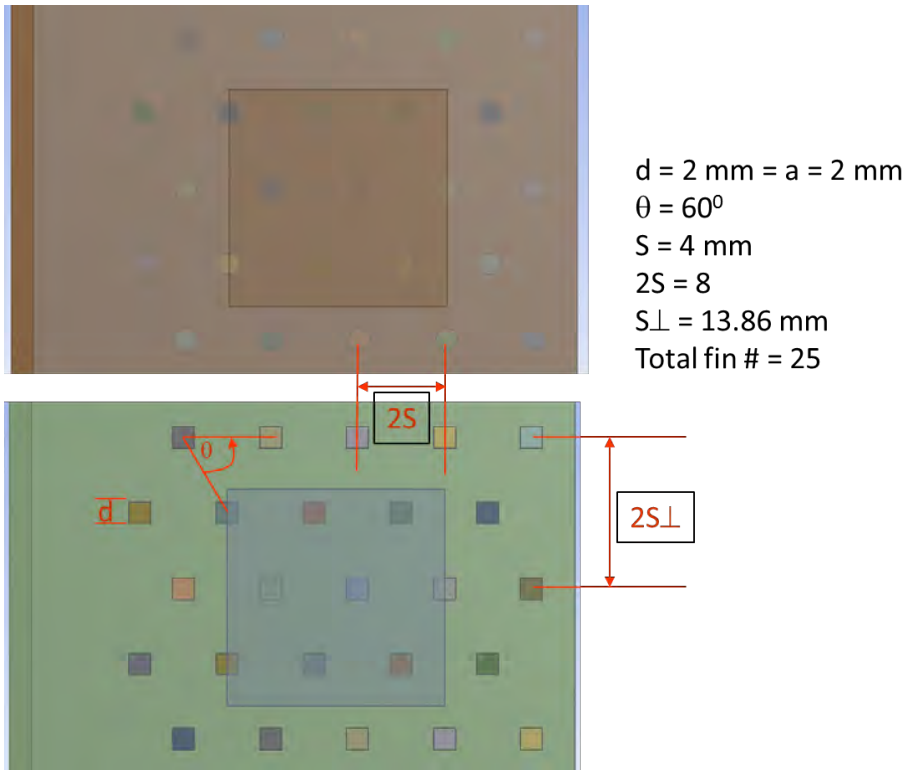

Figure 6. 2D Layout Configuration of the Pin Fin Arrays

(The pin fin arrays are for 2 mm diameter, 60^o offset, and 8 mm transverse spacing. As seen in the figure the d, S, and q factors result in a total of 25 pins in these 2 models.)

Table 3. Design Expert Summary for the 2^{7-2} Fractional Factorial CFD Experimental Design

File Version	8.0.7.1									
Study Type	Factorial		**Runs**	44						
Design Type	2 Level Factorial			**Blocks**	No Blocks					
Center Points	12									
Design Model	Reduced 3FI		**Build Time (ms)**		1.84					
Factor	**Name**	**Units**	**Type**	**Subtype**	**Minimum**	**Maximum**	**Coded**	**Values**	**Mean**	**Std. Dev.**
A	Diameter	mm	Numeric	Continuous	2.00	3.00	-1.000=2.00	1.000=3.00	2.50	0.43
B	Spacing	mm	Numeric	Continuous	4.00	9.00	-1.000=4.00	1.000=9.00	6.50	2.13
C	HeatRateIn	W/cm2	Numeric	Continuous	50.00	200.00	-1.000=50.00	1.000=200.00	125.00	63.96
D	TfluidIn	oC	Numeric	Continuous	10.00	60.00	-1.000=10.00	1.000=60.00	35.00	21.32
E	mdot	kg/s	Numeric	Continuous	0.10	0.60	-1.000=0.10	1.000=0.60	0.35	0.21
F	OffsetAngle	deg	Numeric	Continuous	30.00	60.00	-1.000=30.00	1.000=60.00	45.00	12.79
G	Geometry		Categoric	Nominal	Circular	Square			**Levels:**	2
Response	**Name**	**Units**	**Obs**	**Analysis**	**Minimum**	**Maximum**	**Mean**	**Std. Dev.**	**Ratio**	**Trans**
Y1	Tmax	oC	44	Factorial	25.1	208	101.586	41.6794	8.28685	None
Y2	h_avg	W/m2K	44	Factorial	2920.89	14333.4	8282.92	3051.98	4.90722	None
Y3	DeltaP	Pa	44	Factorial	6.22847	1246.31	182.937	240.151	200.1	None

Figure 7 shows the design alias structure of the Resolution IV 2^{7-2} fractional factorial design, calculated with Design Expert software. As a result of the extensive aliasing and concurrence with SME recommendation, a 3 factor interaction (3FI) model was considered a "full model" for all response factor analysis detailed in the following section.

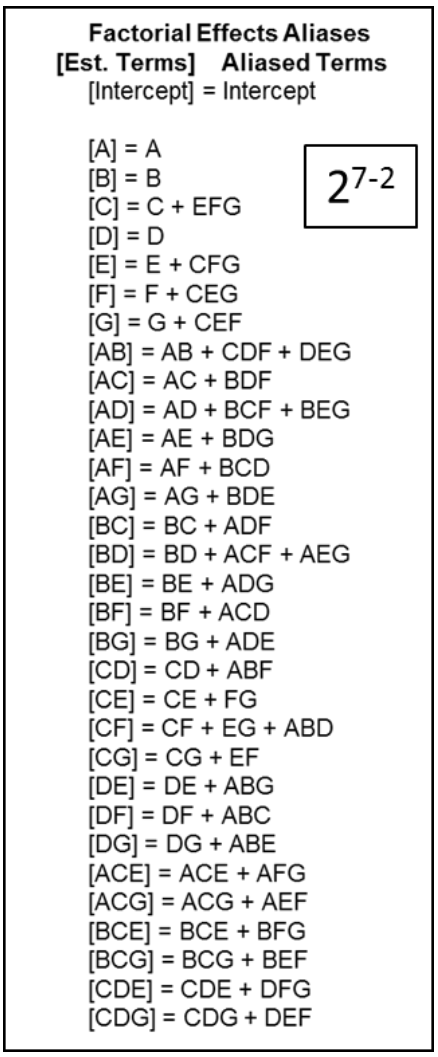

Figure 7. Design Expert Matrix Summary for the 2^{7-2} Resolution IV Design Showing Aliased Structure

Figure 8 illustrates the summary Design Expert experiment evaluation information for the fractional factorial design selected. The Design Expert defining relation for this design is shown along with the word length table illustrating the Resolution IV design definition based on the shortest defining relation word length, which is 4 in this case. The defining relation shown determines the aliasing structure of the quarter fraction design, which can be seen to be a minimum aberration design chosen to minimize aliasing between main effects and two factor interactions. For this case, it is easy to show that generators other than ABCD and ABDE will result in a more complex aliasing structure with both main effects two-factor interactions being aliased with each other and higher order interactions. Of primary note is the Degree of Freedom evaluation in Figure 8 showing the insufficiency of DOF for Lack of Fit analysis. Therefore we need to be careful since residual analysis may fail to detect a lack of fit. Pure Error analysis, however, does possess sufficient DOF and reduced model analysis will increase the Lack of Fit DOF to sufficient levels as will be shown below.

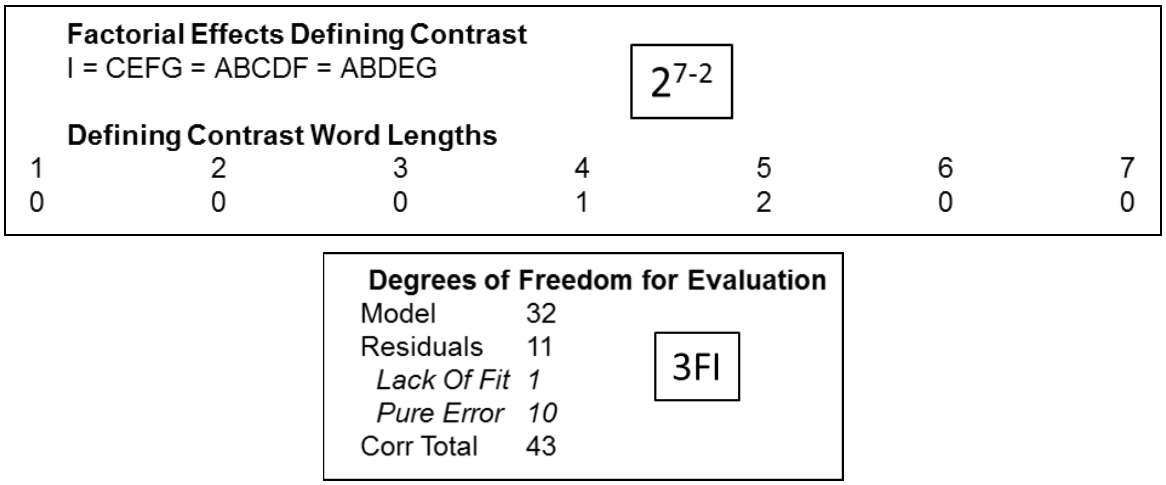

Figure 8. Design Expert Matrix Evaluation Summary for 3FI Model

(The model shows defining contrast terms and the analyzed DOF structure illustrating of the distribution of the n -1=43 DOF.)

Figure 9 shows the experiment evaluation list of aliased factors when a reduced order 2FI model is assumed. In this case the aliased structure does not change as shown in the figure; however, the "extra" DOF obtained from model reduction can now be redistributed across the LoF residual for evaluation. The model DOF is reduced commensurately, but should not be a concern for the analysis going forward as we will show in the following section that the ANOVA model F-value is shown to be statistically significant at 0.01%.

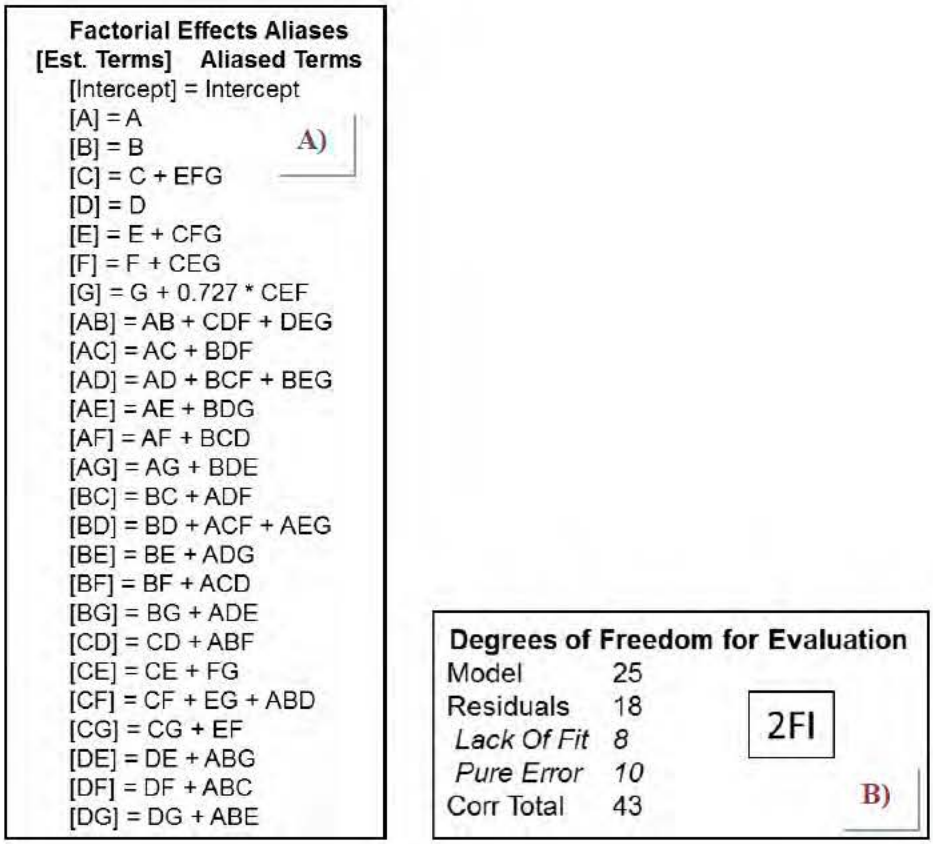

Figure 9. Reduced Model Order (2FI) Effects

(Effects are on A) aliasing (none) and B) DOF distribution. Sufficient DOF now exist for accurate detection of lack of fit.)

Design Expert software evaluation analysis also provides Fraction of Design Space (FDS) plots in which the curves indicate what fraction of the design space has a given variance for both the mean and prediction characteristics. In general, a lower and flatter FDS curve is better, although lower numerical value is more important than flatter. A lower curve translates to a higher Fraction of Design space such that more of the design has useful precision at a given Standard Error value.

Figure 10 shows both of these FDS plots for the mean A) and prediction B) characteristics. The relatively poor FDS for prediction error shown in Figure 10, (1.098σ for 50% of the design space), is characteristic of an aliased quarter fraction factorial design and further supports our previous comments regarding the usefulness of this design for identifying the primary factors of import and estimates for optimal input factor settings within the design space. The realization of higher fidelity surrogate models will require conducting follow-on fold-over, reduced parameter full factorial (ie. 2^4), RSM or similar DOE analysis on the ¼ fraction determined parameters of importance. Figure 9 A) does however show that within the design space the mean is known with a reasonable error estimate. At the same 50% of the design space value, the standard error of the mean is only 0.434 σ. When the 2FI model order reduction was invoked, the FDS changed only slightly as expected. As a final reflection of the designed experiment efficacy, Figure 10 shows the

3D FDS contour plots which is an assessment of the prediction capability of the selected experiment model for A) the “full” 3FI model and B) the reduced 2FI designed model.

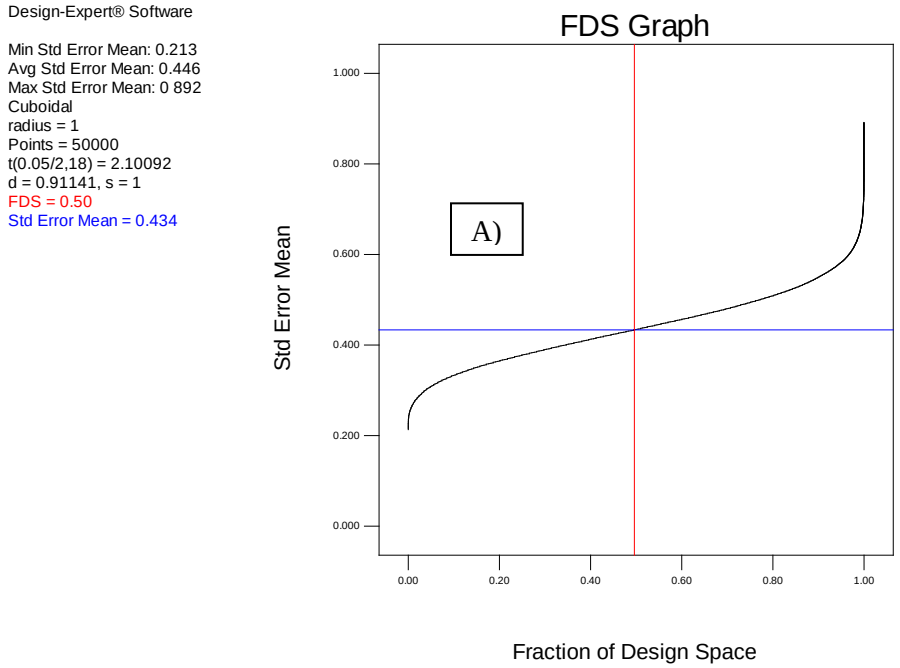

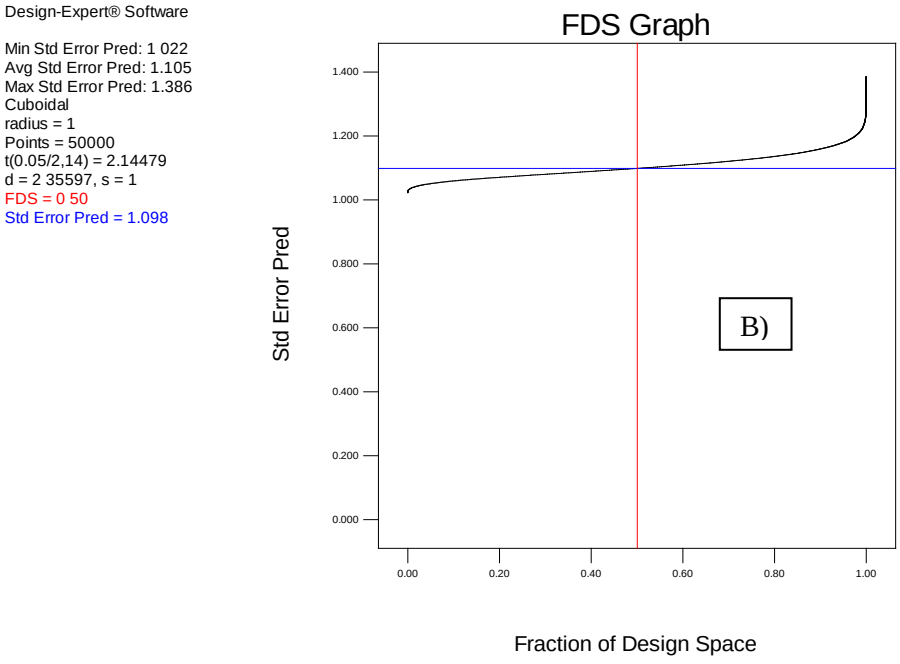

Figure 10. Fraction of Design Space Standard Error Evaluation Plot for the Quarter Fraction Designed Experiment

(A) μ and B) prediction error, respectively.)

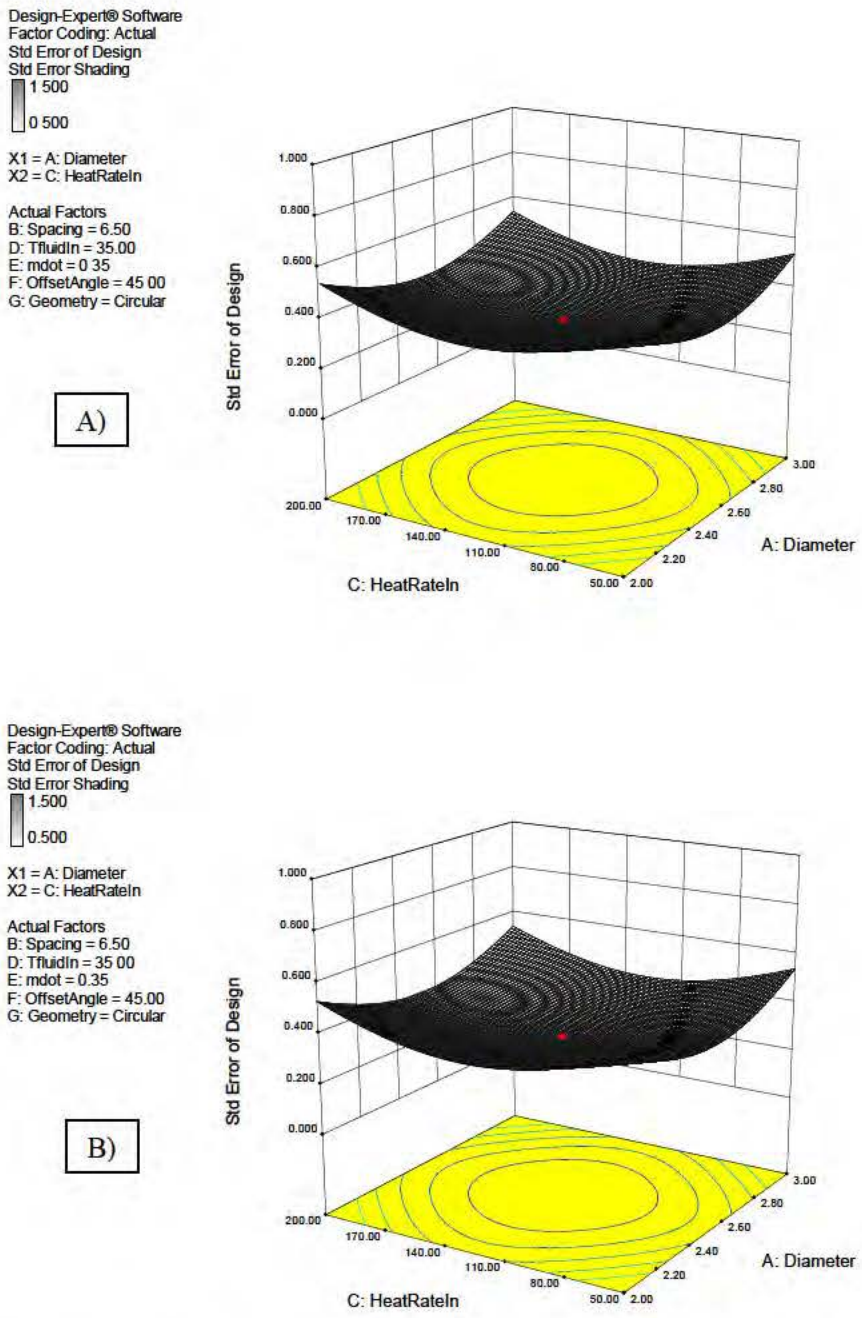

Figure 11. Contour plots of the standard prediction error of the chosen quarter fraction design.

In the figure the standard error of prediction, for areas only within the design space, again reflects an only slightly improved prediction capability for the reduced model due to the extensive aliasing of the quarter fraction design even for a reduced 2FI model. It should be noted that this analysis is representative of only the design, and not the response data.

Finally, Table 4 displays the full 2^{7-2} design matrix in standard order. Also included are the response variables (T_{max}, ΔP, and h_{avg}) values for *Fluent*™ simulation runs accomplished. Although the majority of these simulations were run on the MSCR supercomputer center, they still

necessitated several hours of run time and roughly 1-2 hours of time to download the results files for each case. The following section describes in detail the DOE analysis of the data shown in Table 4 and highlights the parameters identified of primary importance and compares the optimized analytical surrogate models with additional CFD runs as an initial validation exercise.

Table 4. Design Expert Matrix of the 2^{7-2} Runs and Response Factor Summary

Std	Run	Factor 1 A:Diameter mm	Factor 2 B:Spacing mm	Factor 3 C:HeatRateIn W/cm2	Factor 4 D:TfluidIn oC	Factor 5 E:mdot kg/s	Factor 6 F:OffsetAngle deg	Factor 7 G:Geometry	Response 1 Tmax oC	Response 2 h_avg W/m2K	Response 3 DeltaP Pa
16	1	3.00	9.00	200.00	60.00	0.10	60.00	Circular	103	9833.72	345.18
26	2	3.00	4.00	50.00	60.00	0.60	60.00	Circular	130	8875.96	626.14
21	3	2.00	4.00	200.00	10.00	0.60	30.00	Circular	84.4	14333.4	170.517
11	4	2.00	9.00	50.00	60.00	0.10	60.00	Square	127	4856.74	18.0949
29	5	2.00	4.00	200.00	60.00	0.60	60.00	Square	208	7881.01	6.22847
42	6	2.50	6.50	125.00	35.00	0.35	45.00	Square	99	8349.1	157.102
9	7	2.00	4.00	50.00	60.00	0.10	30.00	Circular	112	12202.5	207.525
3	8	2.00	9.00	50.00	10.00	0.10	30.00	Circular	27.5	9070.51	736.822
39	9	2.50	6.50	125.00	35.00	0.35	45.00	Circular	105	9573.44	102.618
2	10	3.00	4.00	50.00	10.00	0.10	30.00	Circular	35.4	2920.89	28.4708
25	11	2.00	4.00	50.00	60.00	0.60	30.00	Square	134	10908.3	398.955
5	12	2.00	4.00	200.00	10.00	0.10	30.00	Square	39.7	12656.1	115.202
4	13	3.00	9.00	50.00	10.00	0.10	60.00	Square	25.1	6605.88	1246.31
36	14	2.50	6.50	125.00	35.00	0.35	45.00	Square	99	8349.1	157.102
22	15	3.00	4.00	200.00	10.00	0.60	60.00	Square	83.3	13442.3	226.533
31	16	2.00	9.00	200.00	60.00	0.60	30.00	Circular	157	13575.3	157.118
18	17	3.00	4.00	50.00	10.00	0.60	30.00	Square	90.4	4997.8	17.3551
12	18	3.00	9.00	50.00	60.00	0.10	30.00	Circular	119	3668.92	28.1231
8	19	3.00	9.00	200.00	10.00	0.10	30.00	Square	49.1	3743.08	14.0985
43	20	2.50	6.50	125.00	35.00	0.35	45.00	Circular	105	9573.44	102.618
33	21	2.50	6.50	125.00	35.00	0.35	45.00	Circular	105	9573.44	102.618
37	22	2.50	6.50	125.00	35.00	0.35	45.00	Circular	105	9573.44	102.618
13	23	2.00	4.00	200.00	60.00	0.10	60.00	Circular	159	6009.78	9.84772
30	24	3.00	4.00	200.00	60.00	0.60	30.00	Circular	207	5536.18	8.44347
41	25	2.50	6.50	125.00	35.00	0.35	45.00	Circular	105	9573.44	102.618
10	26	3.00	4.00	50.00	60.00	0.10	60.00	Square	103	10440.3	385.323
27	27	2.00	9.00	50.00	60.00	0.60	60.00	Circular	140	4305.43	31.4539
34	28	2.50	6.50	125.00	35.00	0.35	45.00	Square	99	8349.1	157.102
19	29	2.00	9.00	50.00	10.00	0.60	30.00	Square	80.8	12307.1	355.032
14	30	3.00	4.00	200.00	60.00	0.10	30.00	Square	149	5006.06	12.6081
38	31	2.50	6.50	125.00	35.00	0.35	45.00	Square	99	8349.1	157.102
6	32	3.00	4.00	200.00	10.00	0.10	60.00	Circular	39.2	10128.7	155.623
32	33	3.00	9.00	200.00	60.00	0.60	60.00	Square	156	12154	215.468
24	34	3.00	9.00	200.00	10.00	0.60	30.00	Circular	89.7	5012.06	18.1101
40	35	2.50	6.50	125.00	35.00	0.35	45.00	Square	99	8349.1	157.102
44	36	2.50	6.50	125.00	35.00	0.35	45.00	Square	99	8349.1	157.102
23	37	2.00	9.00	200.00	10.00	0.60	60.00	Square	92	5943.23	12.7593
7	38	2.00	9.00	200.00	10.00	0.10	60.00	Circular	50.9	5700.14	9.26896
35	39	2.50	6.50	125.00	35.00	0.35	45.00	Circular	105	9573.44	102.618
17	40	2.00	4.00	50.00	10.00	0.60	60.00	Circular	92.2	6496.01	12.3799
1	41	2.00	4.00	50.00	10.00	0.10	60.00	Square	36.7	4193.91	18.5118
20	42	3.00	9.00	50.00	10.00	0.60	60.00	Circular	79.4	10903.5	647.625
15	43	2.00	9.00	200.00	60.00	0.10	30.00	Square	111	10107.5	202.07
28	44	3.00	9.00	50.00	60.00	0.60	30.00	Square	135	3096.83	53.7058

5 Experiment Results and Analysis

In order to do a complete assessment of the designed experiment, comparative reduced model analysis for each of the response variables was accomplished in addition to the 3FI baseline. These comparative analyses were done both with and without transformation of the response data, when doing so is indicated by Box-Cox and other residual analysis, to identify improvements to the resulting models for each response variable. In addition, as a comparison to the parsimonious model obtained for each response variable, a main effects only analysis was also accomplished to determine the efficacy of a simple model (no interactions) for screening purposes. To accomplish these objectives, the response factor evaluations were initiated by assessing the results of the T_{max} variable first, which as defined in prior sections is the maximum temperature at the pin-fin/channel surface interface and relates to an assessment of maximum power semiconductor device junction temperatures and reliability.

5.1 Tmax Response Variable Evaluation

Full model 3FI evaluation of T_{max} starts with a selection of model terms and residual plot generation. Figure 11 shows the Design Expert Half-Normal residual plot with the full model terms all selected for inclusion in the ANOVA analysis. This model term selection tool is preferred over the Normal residual plot but can be satisfactorily supplanted by the Pareto Chart tool which explicitly shows the t-statistic level and the relative magnitude of the effects. Figure 12 shows the companion Pareto Chart for the Figure 11 evaluation for reference purposes.

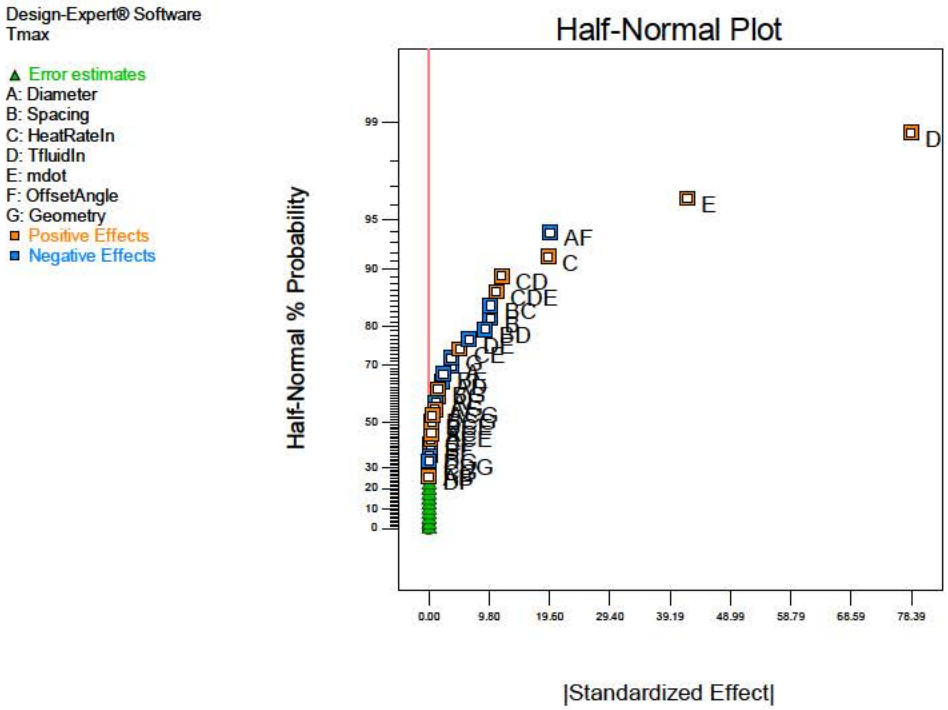

Figure 12. Half Normal Plot of the Full 3FI Model Term Selection Tool for the T_{max} Response

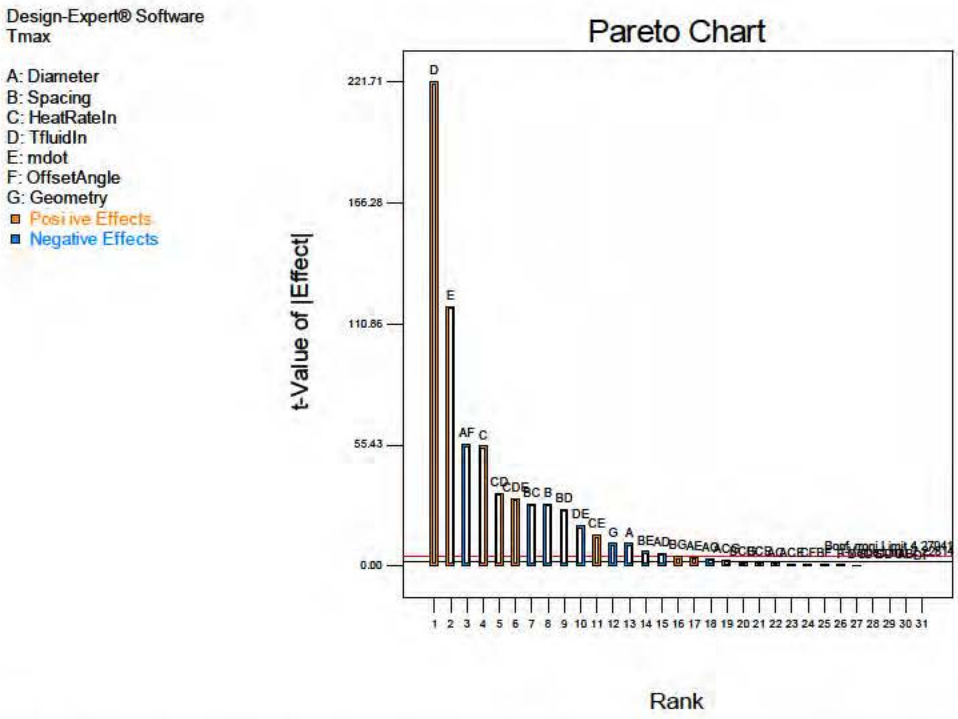

Figure 13. Pareto Chart Model Term Selection Tool Results for the 3FI Model Used for Figure 11.

Of note for the Pareto chart, are the indications of magnitude for input factors T_{fluid} (D), m_{dot} (E), $Heat_{ratein}$ (C), and fin diameter/offset angle interaction (AF) as dominant factors driving the T_{max} response, which are expected. Thus, even for an extensive aliased unbalanced quarter fraction model, the primary input factors of importance are indicated. Subsequent to the model term selection, the ANOVA analysis is accomplished in the Design Expert software tool. Figure 13 shows the results of that analysis for the full 3FI, untransformed evaluation of T_{max}. It should be noted that due to the extensive aliasing structure, some model graphs and diagnostics could not be generated without eliminating some two and three factor terms. This was completed for the reduced factor model analysis to follow the full 3FI model, as well as the determination of a need for response variable transformation.

Table 5. ANOVA Summary for Full 3FI Model T_{max} Evaluation

ANOVA Summary				
	Adjusted F-value	**Model p-value**	**Unadjusted F-value**	**Model p-value**
Model	6.366E+007	< 0.0001	9095.27	< 0.0001
Curvature	6.366E+007	< 0.0001		
Lack of Fit				

Immediately notable from the observation of the ANOVA summary full 3FI data in Table 5 is the large difference between the Adjusted F-Value and the Unadjusted F-Value. This is our first indication that curvature is statistically significant and the model will have dubious prediction value outside the factorial points. Tables 6 and 7 show the full ANOVA analysis data for both models summarized in Table 5.

Table 6. Full 3FI ANOVA Analysis for T_{max} in which Curvature is Included in Model Coefficients

ANOVA for selected factorial model (Aliased)
Analysis of variance table [Partial sum of squares - Type III]

Source	Sum of Squares	df	Mean Square	F Value	p-value Prob > F
Model	74695.45	32	2334.23	6.366E+007	< 0.0001
A-Diameter	*107.31*	*1*	*107.31*	*6.366E+007*	*< 0.0001*
B-Spacing	*808.02*	*1*	*808.02*	*6.366E+007*	*< 0.0001*
C-HeatRateIn	*3018.64*	*1*	*3018.64*	*6.366E+007*	*< 0.0001*
D-TfluidIn	*49156.80*	*1*	*49156.80*	*6.366E+007*	*< 0.0001*
E-mdot	*14137.21*	*1*	*14137.21*	*6.366E+007*	*< 0.0001*
F-OffsetAngle	*0.45*	*1*	*0.45*	*6.366E+007*	*< 0.0001*
G-Geometry	*29.87*	*1*	*29.87*	*6.366E+007*	*< 0.0001*
AB	*0.045*	*1*	*0.045*	*6.366E+007*	*< 0.0001*
AC	*1.62*	*1*	*1.62*	*6.366E+007*	*< 0.0001*
AD	*34.86*	*1*	*34.86*	*6.366E+007*	*< 0.0001*
AE	*17.11*	*1*	*17.11*	*6.366E+007*	*< 0.0001*
AF	*3100.78*	*1*	*3100.78*	*6.366E+007*	*< 0.0001*
AG	*10.13*	*1*	*10.13*	*6.366E+007*	*< 0.0001*
BC	*810.03*	*1*	*810.03*	*6.366E+007*	*< 0.0001*
BD	*677.12*	*1*	*677.12*	*6.366E+007*	*< 0.0001*
BE	*45.13*	*1*	*45.13*	*6.366E+007*	*< 0.0001*
BF	*0.72*	*1*	*0.72*	*6.366E+007*	*< 0.0001*
BG	*18.91*	*1*	*18.91*	*6.366E+007*	*< 0.0001*
CD	*1118.65*	*1*	*1118.65*	*6.366E+007*	*< 0.0001*
CE	*202.01*	*1*	*202.01*	*6.366E+007*	*< 0.0001*
CF	*0.85*	*1*	*0.85*	*6.366E+007*	*< 0.0001*
CG	*0.061*	*1*	*0.061*	*6.366E+007*	*< 0.0001*
DE	*341.91*	*1*	*341.91*	*6.366E+007*	*< 0.0001*
DF	*1.250E-003*	*1*	*1.250E-003*	*6.366E+007*	*< 0.0001*
DG	*0.18*	*1*	*0.18*	*6.366E+007*	*< 0.0001*
EF	*0.000*	*0*			
EG	*0.000*	*0*			
FG	*0.000*	*0*			
ABC	*0.000*	*0*			
ABD	*0.000*	*0*			
ABE	*0.000*	*0*			
ABF	*0.000*	*0*			
ABG	*0.000*	*0*			
ACD	*0.000*	*0*			
ACE	*1.28*	*1*	*1.28*	*6.366E+007*	*< 0.0001*
ACF	*0.000*	*0*			
ACG	*8.20*	*1*	*8.20*	*6.366E+007*	*< 0.0001*
ADE	*0.000*	*0*			
ADF	*0.000*	*0*			
ADG	*0.000*	*0*			
AEF	*0.000*	*0*			
AEG	*0.000*	*0*			
AFG	*0.000*	*0*			
BCD	*0.000*	*0*			
BCE	*1.90*	*1*	*1.90*	*6.366E+007*	*< 0.0001*
BCF	*0.000*	*0*			
BCG	*2.88*	*1*	*2.88*	*6.366E+007*	*< 0.0001*
BDE	*0.000*	*0*			
BDF	*0.000*	*0*			
BDG	*0.000*	*0*			
BEF	*0.000*	*0*			
BEG	*0.000*	*0*			
BFG	*0.000*	*0*			
CDE	*963.60*	*1*	*963.60*	*6.366E+007*	*< 0.0001*
CDF	*0.000*	*0*			
CDG	*0.061*	*1*	*0.061*	*6.366E+007*	*< 0.0001*
CEF	*22.21*	*1*	*22.21*	*6.366E+007*	*< 0.0001*
CEG	*0.000*	*0*			
CFG	*0.000*	*0*			
DEF	*0.000*	*0*			
DEG	*0.000*	*0*			
DFG	*0.000*	*0*			
EFG	*0.000*	*0*			
Curvature	2.82	1	2.82	6.366E+007	< 0.0001
Pure Error	0.000	10	0.000		
Cor Total	74698.27	43			

Table 7. Full 3FI ANOVA Analysis for T_{max} in which Curvature is Not Included in Model Coefficients

ANOVA for selected factorial model (Aliased)
Analysis of variance table [Partial sum of squares - Type III]

Source	Sum of Squares	df	Mean Square	F Value	p-value Prob > F
Model	74695.45	32	2334.23	9095.27	< 0.0001
A-Diameter	*107.31*	*1*	*107.31*	*418.14*	*< 0.0001*
B-Spacing	*808.02*	*1*	*808.02*	*3148.43*	*< 0.0001*
C-HeatRateIn	*3018.64*	*1*	*3018.64*	*11762.06*	*< 0.0001*
D-TfluidIn	*49156.80*	*1*	*49156.80*	*1.915E+005*	*< 0.0001*
E-mdot	*14137.21*	*1*	*14137.21*	*55085.22*	*< 0.0001*
F-OffsetAngle	*0.45*	*1*	*0.45*	*1.76*	*0.2117*
G-Geometry	*108.00*	*1*	*108.00*	*420.82*	*< 0.0001*
AB	*0.045*	*1*	*0.045*	*0.18*	*0.6835*
AC	*1.62*	*1*	*1.62*	*6.31*	*0.0289*
AD	*34.86*	*1*	*34.86*	*135.84*	*< 0.0001*
AE	*17.11*	*1*	*17.11*	*66.67*	*< 0.0001*
AF	*3100.78*	*1*	*3100.78*	*12082.10*	*< 0.0001*
AG	*10.13*	*1*	*10.13*	*39.45*	*< 0.0001*
BC	*810.03*	*1*	*810.03*	*3156.26*	*< 0.0001*
BD	*677.12*	*1*	*677.12*	*2638.38*	*< 0.0001*
BE	*45.13*	*1*	*45.13*	*175.83*	*< 0.0001*
BF	*0.72*	*1*	*0.72*	*2.81*	*0.1221*
BG	*18.91*	*1*	*18.91*	*73.69*	*< 0.0001*
CD	*1118.64*	*1*	*1118.64*	*4358.77*	*< 0.0001*
CE	*202.00*	*1*	*202.00*	*787.11*	*< 0.0001*
CF	*0.85*	*1*	*0.85*	*3.29*	*0.0969*
CG	*0.061*	*1*	*0.061*	*0.24*	*0.6348*
DE	*341.91*	*1*	*341.91*	*1332.25*	*< 0.0001*
DF	*1.250E-003*	*1*	*1.250E-003*	*4.871E-003*	*0.9456*
DG	*0.18*	*1*	*0.18*	*0.70*	*0.4201*
EF	*0.000*	*0*			
EG	*0.000*	*0*			
FG	*0.000*	*0*			
ABC	*0.000*	*0*			
ABD	*0.000*	*0*			
ABE	*0.000*	*0*			
ABF	*0.000*	*0*			
ABG	*0.000*	*0*			
ACD	*0.000*	*0*			
ACE	*1.28*	*1*	*1.28*	*4.99*	*0.0473*
ACF	*0.000*	*0*			
ACG	*8.20*	*1*	*8.20*	*31.96*	*0.0001*
ADE	*0.000*	*0*			
ADF	*0.000*	*0*			
ADG	*0.000*	*0*			
AEF	*0.000*	*0*			
AEG	*0.000*	*0*			
AFG	*0.000*	*0*			
BCD	*0.000*	*0*			
BCE	*1.90*	*1*	*1.90*	*7.41*	*0.0199*
BCF	*0.000*	*0*			
BCG	*2.88*	*1*	*2.88*	*11.22*	*0.0065*
BDE	*0.000*	*0*			
BDF	*0.000*	*0*			
BDG	*0.000*	*0*			
BEF	*0.000*	*0*			
BEG	*0.000*	*0*			
BFG	*0.000*	*0*			
CDE	*963.60*	*1*	*963.60*	*3754.66*	*< 0.0001*
CDF	*0.000*	*0*			
CDG	*0.061*	*1*	*0.061*	*0.24*	*0.6348*
CEF	*69.65*	*1*	*69.65*	*271.39*	*< 0.0001*
CEG	*0.000*	*0*			
CFG	*0.000*	*0*			
DEF	*0.000*	*0*			
DEG	*0.000*	*0*			
DFG	*0.000*	*0*			
EFG	*0.000*	*0*			
Residual	2.82	11	0.26		
Lack of Fit	*2.82*	*1*	*2.82*		
Pure Error	*0.000*	*10*	*0.000*		
Cor Total	74698.27	43			

Recall that the adjusted ANOVA is essentially the results that would have been obtained if the center points had not be included in the design. In this ANOVA analysis curvature sum of squares (SS) is removed from the Lack of Fit SS and factorial coefficients generated as if center point data were not included. If curvature is significant only factorial points may be predicted using the adjusted model. The unadjusted ANOVA analysis uses all the data, including center points, to estimate model coefficients using the standard regression analysis. Since the quadratic terms are aliased, curvature cannot be modeled, and if significant, this model cannot be used for prediction. When viewing the full ANOVA analysis tables it becomes more apparent that the untransformed "full" 3FI model is not suitable for surrogate model usage and likely has dubious prediction capability. The tabular data shows that curvature is indeed likely significant and even though the unadjusted model ANOVA results have p-value indicators for factors of statistical significance at the 5% level, the likely significance of curvature makes the results for this model suspect. In addition, due to the extensive aliasing of the higher order interaction terms, the SS values cannot be calculated and are thus show as zero in the table. This further prevents the use of diagnostic tools which require the residuals. Thus the typical Normal and Box-Cox screening tools are unavailable for this full 3FI model. Additionally, the R-squared statistics, which is a measure of the total variability explained by the model, shown in Table 8 below is another indicator of the poor prediction capability of this model. Although the R^2 and Adjusted-R^2 values are large and approach unity as desired, these statistics are misleading. The R^2 value of 1.0 is artificially high due to the inclusion of large numbers of terms in the model which also inflates the Adjusted-R^2 value. Greater insight is always obtained by considering the Prediction R^2 and the prediction error sum of squares (PRESS) values. Both of these statistics also indicate that the present model is severely lacking in prediction capability, even within the factorial design space. First, the Prediction R^2 value, which is a measure of the ability of the model to explain variability in new data, indicates that only ~85% of the variability can be accounted for by the model. Secondly, the PRESS value, which indicates the ability of the model to predict new data, is very large. Small values of PRESS are reflective of good model prediction capabilities and thus our very large value (10602) is further indication of problems with curvature and aliasing. Model reduction, response data transformation, and/or elimination of outliers are the only way to improve the model characteristics. Of course, bad data can also be the cause, but due to the deterministic modeling "experiment" conducted for this project, this is an unlikely cause. As we shall see in the following paragraphs, model reduction improves this situation dramatically.

Table 8. R^2 Statistics for the Full 3FI Model for T_{max} Response Evaluation

Std. Dev.	0.51	R-Squared	1.0000
Mean	101.59	Adj R-Squared	0.9999
C.V. %	0.50	Pred R-Squared	0.8581
PRESS	10602.25	Adeq Precision	416.887

As the initial T_{max} ANOVA analysis has shown, the full untransformed 3FI model must be modified to improve the prediction characteristics and thus additional analysis is of dubious value without first exercising these options. In addition, due to the extensive aliasing structure of the full model there are no error terms (SS terms are zero) from which to generate the typical model residual diagnostics. Thus, the typical model assessment tools cannot be used to determine model efficacy for this response variable. Even the Box-Cox plot cannot be used to determine the need for a response variable transformation. Therefore, further analysis of the full 3FI model is not

warranted before model reduction regression is exercised to eliminate statistically insignificant and aliased terms. Before that however, for comparison purposes the coded factor model equation resulting from the current full untransformed analysis is shown below as Equation I.

Equation I. Final Coded Factor Model Equation for the Full 3FI Untransformed ANOVA Analysis

$$
\begin{aligned}
Tmax = {} & +101.59 - 1.83 * A - 5.03 * B + 9.71 * C + 39.19 * D + 21.02 * E + 0.12 * F \\
& -3.00 * G - 0.037 * A * B + 0.23 * A * C - 1.04 * A * D + 0.73 * A * E \\
& - 9.84 * A * F - 0.56 * A * G - 5.03 * B * C - 4.60 * B * D - 1.19 * B * E \\
& + 0.15 * B * F + 0.77 * B * G + 5.91 * C * D + 2.51 * C * E + 0.16 * C * F \\
& +0.044 * C * G - 3.27 * D * E + 6.250E\text{-}003 * D * F - 0.075 * D * G \\
& + 0.20 * A * C * E + 0.51 * A * C * G + 0.24 * B * C * E + 0.30 * B * C * G \\
& +5.49 * C * D * E - 0.044 * C * D * G + 2.82 * C * E * F
\end{aligned}
$$

Additionally, the actual value equation cannot be generated due to the excessive aliasing of the current model. Lastly, response surface 3D plots for the Tmax factor are shown below in Figures 13-26 which are our initial indicators of the main factors of importance for this response variable. Due to the extensive aliasing and lack of adequate residuals from this full 3FI evaluation, these trends should be taken as qualitative indicators to compare to more rigorous reduced and/or transformed data evaluation subsequently. However, review of the plots reveals some trends which have relevance to the subsequent evaluation to be described. First, a comparison between the surface plots which indicate a strong influence on the maximum temperature response factor and the half-Normal and Pareto Charts of the analysis shown in Figures 11 and 12, illustrate that even the highly aliased, full 3FI model provides a good indication of the factors of primary importance for this response variable. The Pareto Chart magnitude bars suggest that input factors D, E, AF, and C have the greatest effect on Tmax in descending order of prominence. This is in agreement with Figures 15, 20, 23, 26, 28 which indicate that Tfluidin has the greatest effect on Tmax. In addition, Figures 16, 21, 24, and 27 also seem to indicate a strong, but slightly less dominant influence on cooling fluid mass flow, Mdot. The response curve of Figure 19 reflects a predicted strong two factor interaction term AF (pin diameter-offset angle) as well as a nonlinearity which may require transformation. Finally, factor C (Heatratein) is also suggested as a non-negligible main effect from Figures 14, 19, 22, 26, and 27. These indicators are intuitively dominant as might be expected from SME consideration. The fluid temperature will strongly influence convective heat transfer through larger ΔT as the water temperature is lowered. Similarly, the "amount" of fluid flowing through the channel (Mdot) will also enhance convective heat transfer via increased Reynolds number. Finally, the pin fin diameter and offset angle determine flow resistance and are highly interactive in influencing Reynolds number and convection. Finally, there should be no surprise to see that Tmax is influenced by the amount of energy delivered by the heat source. Agreement with the model selection statistics (half normal and Pareto charts) should not be surprising. What is impressive is that the DOE methodology is capable of qualitative physically valid factor screening even with a highly aliased fractional data set. One other thing of note to mention regarding the Figures 13-28 is the limited prediction capability even within the factorial design space. The red balls present above the surface plots are the factorial data points and can be seen to lie above the prediction surfaces. This simply confirms the prior comments regarding the dubious prediction capability of the full 3FI untransformed model with significant aliasing. The full permutation of input factor plot combinations will not be included in the report from this point forward for brevity considerations, and only the relevant statistical analysis required for experiment evaluation will be provided.

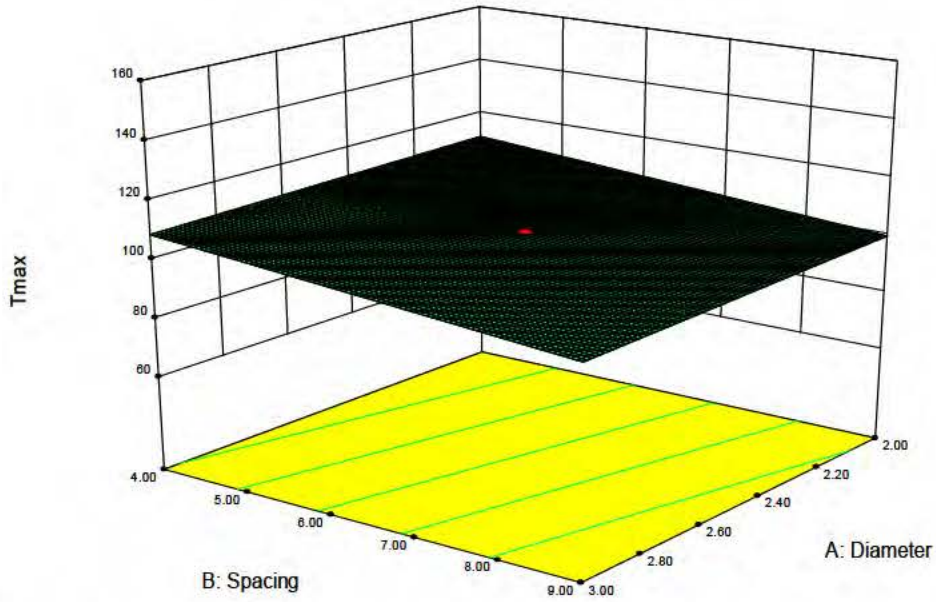

Figure 14. Response Surface Plot for Pin Fin Spacing and Diameter Input Variables

(Full 3FI untransformed evaluation.)

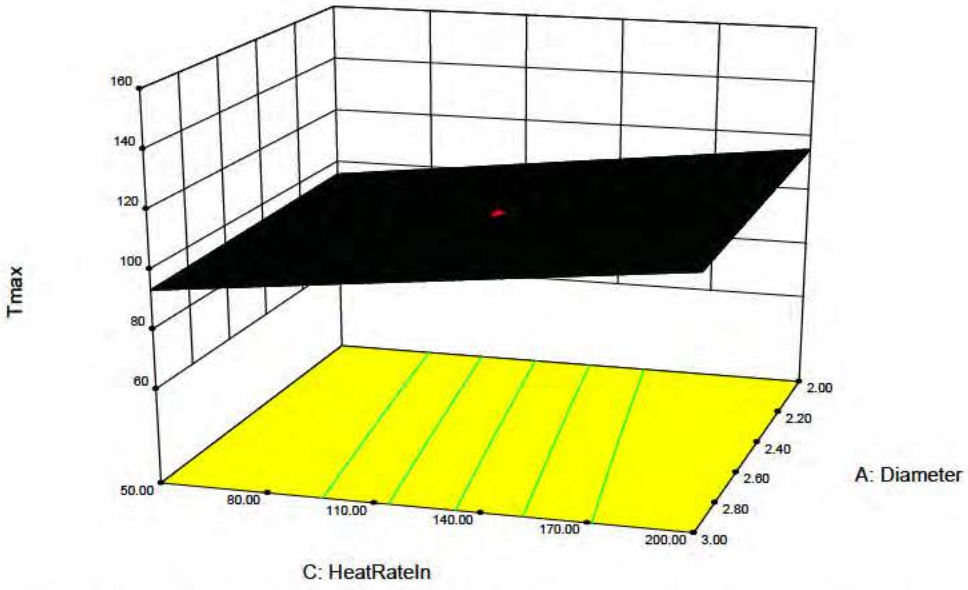

Figure 15. Response Surface Plot for Pin Fin Diameter and $Heat_{ratein}$ Variables

(Full 3FI untransformed evaluation.)

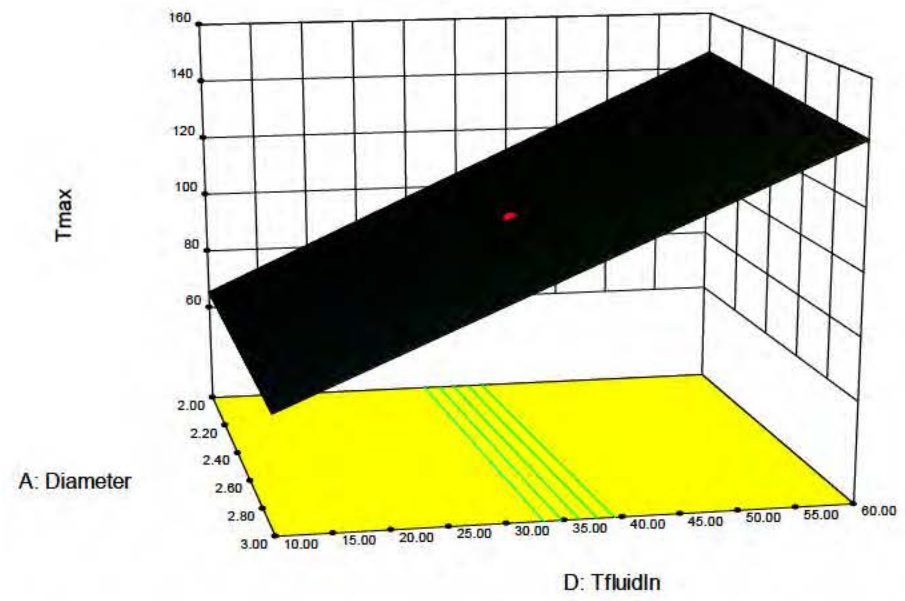

Figure 16. Response Surface Plot for Pin Fin Diameter and $T_{fluidin}$ Variables

(Full 3FI untransformed evaluation.)

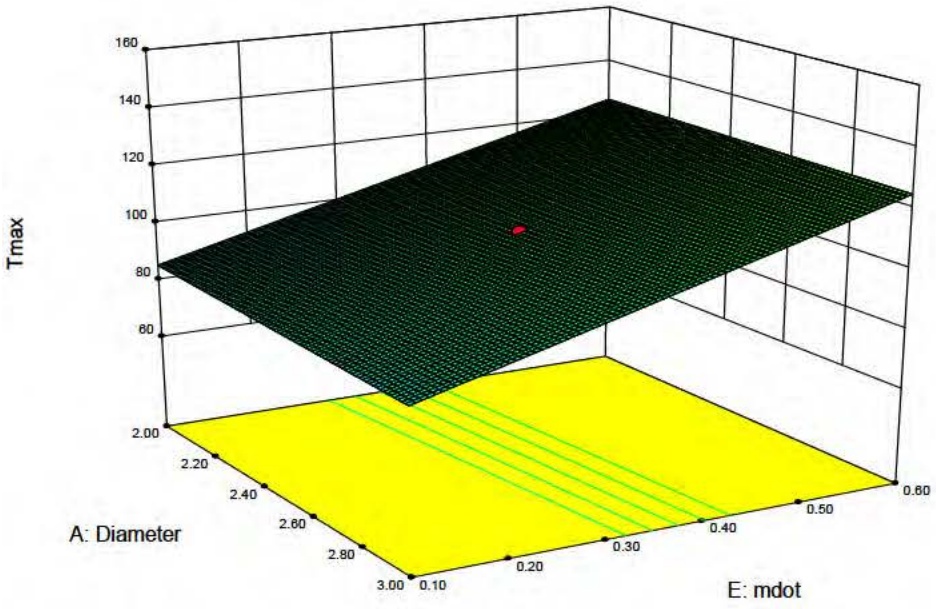

Figure 17. Response Surface Plot for Pin Fin Diameter and M_{dot} Variables

(Full 3FI untransformed evaluation.)

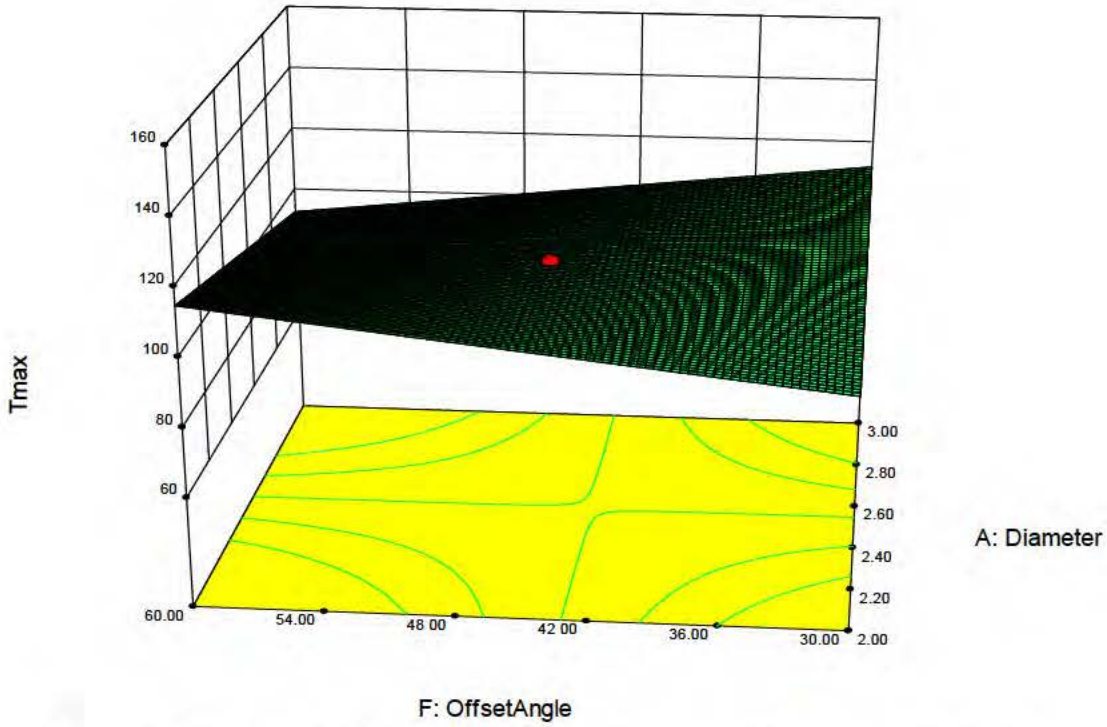

Figure 18. Response Surface Plot for Pin Fin Diameter and Offset Angle (θ) Variables

(Full 3FI untransformed evaluation.)

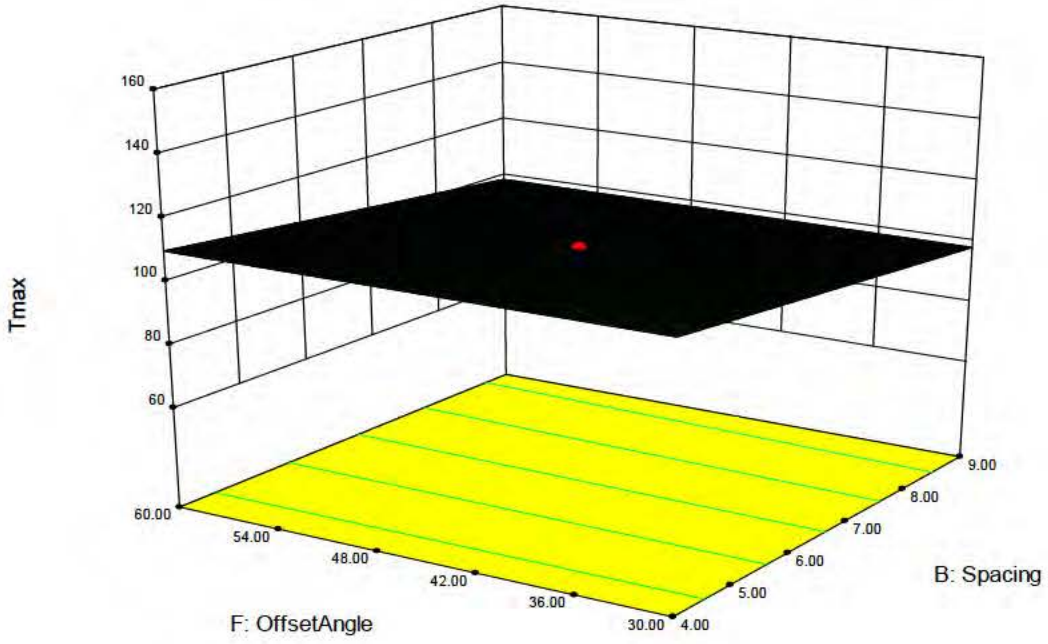

Figure 19. Response Surface Plot for Pin Fin Offset Angle and Pin Spacing Variables

(Full 3FI untransformed evaluation.)

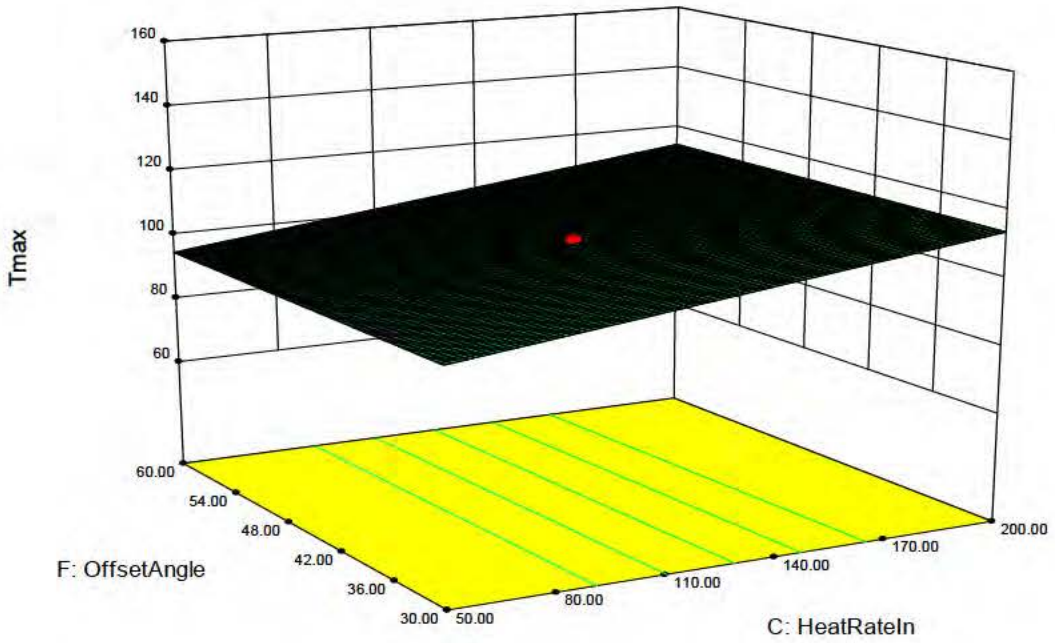

Figure 20. Response Surface Plot for Pin Fin Offset Angle and $Heat_{ratein}$ Variables
(Full 3FI untransformed evaluation.)

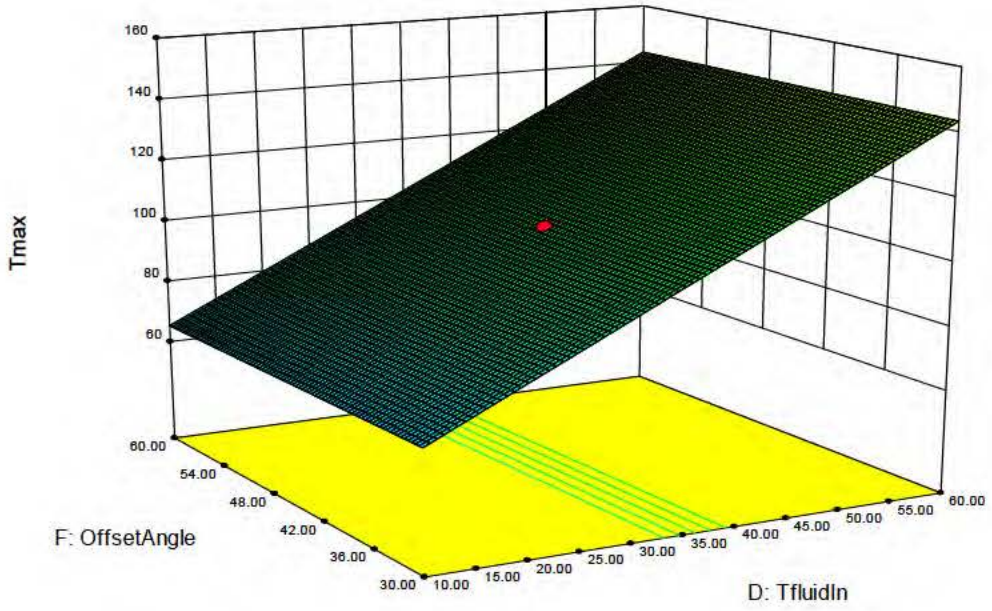

Figure 21. Response Surface Plot for Pin Fin Offset Angle and $T_{fluidin}$ Variables
(Full 3FI untransformed evaluation.)

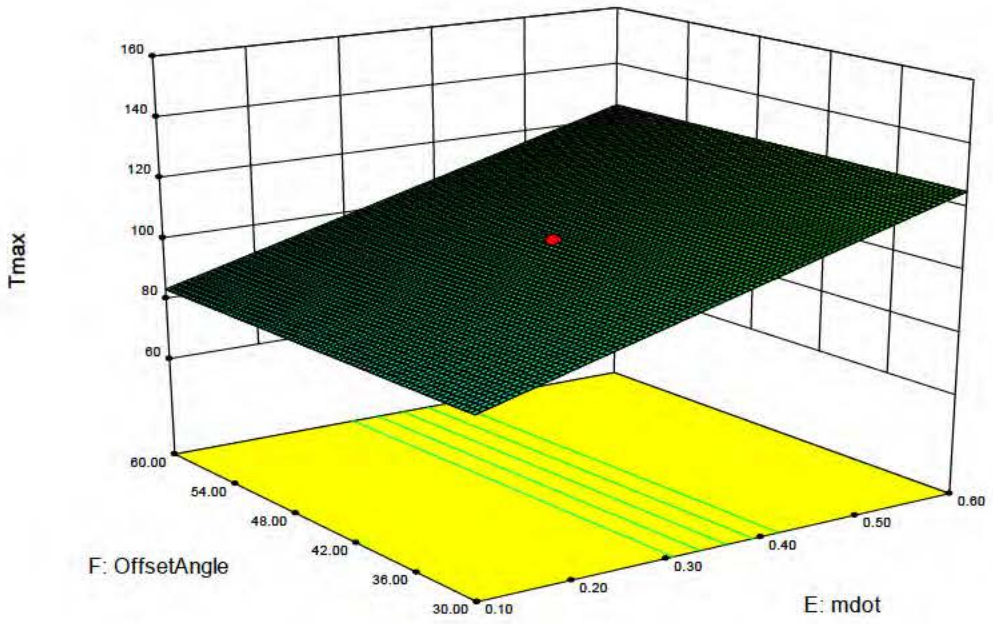

Figure 22. Response Surface Plot for Pin Fin Offset Angle and M_{dot} Variables

(Full 3FI untransformed evaluation.)

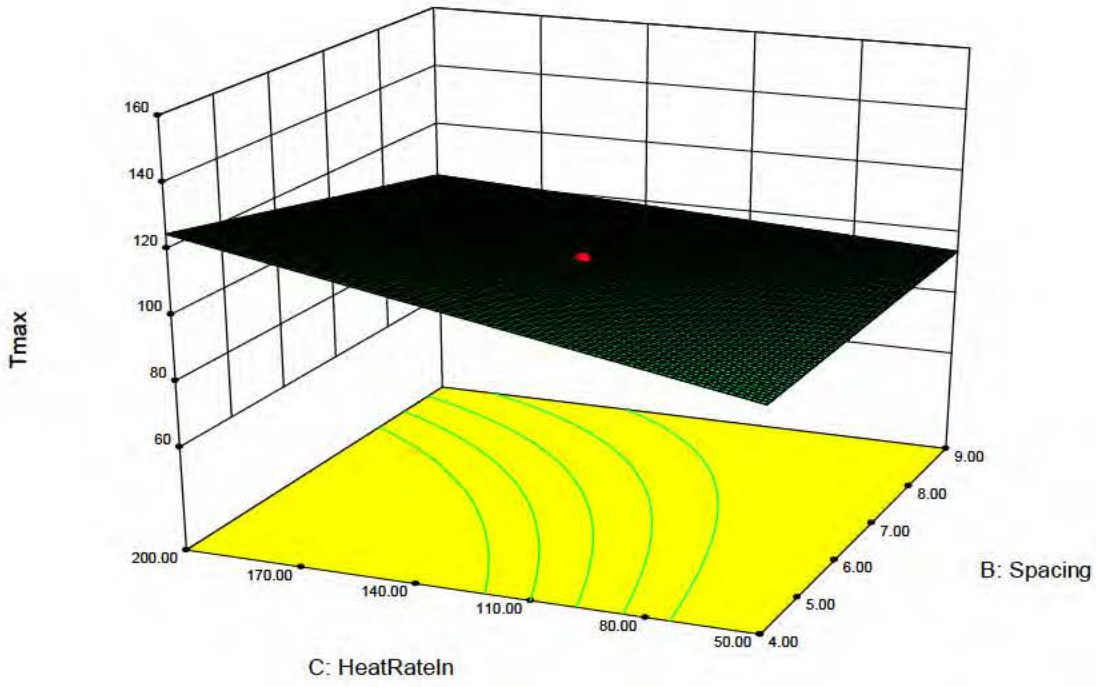

Figure 23. Response Surface Plot for $Heat_{ratein}$ and Pin Fin Spacing Variables

(Full 3FI untransformed evaluation.)

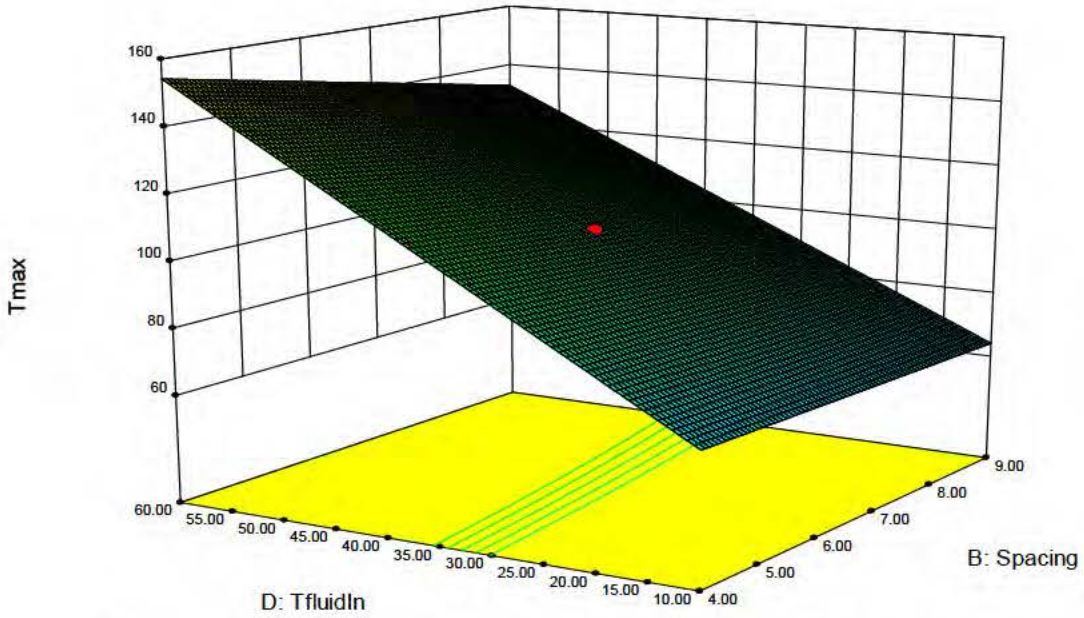

Figure 24. Response Surface Plot for Pin Fin Spacing and $T_{fluidin}$ Variables

(Full 3FI untransformed evaluation.)

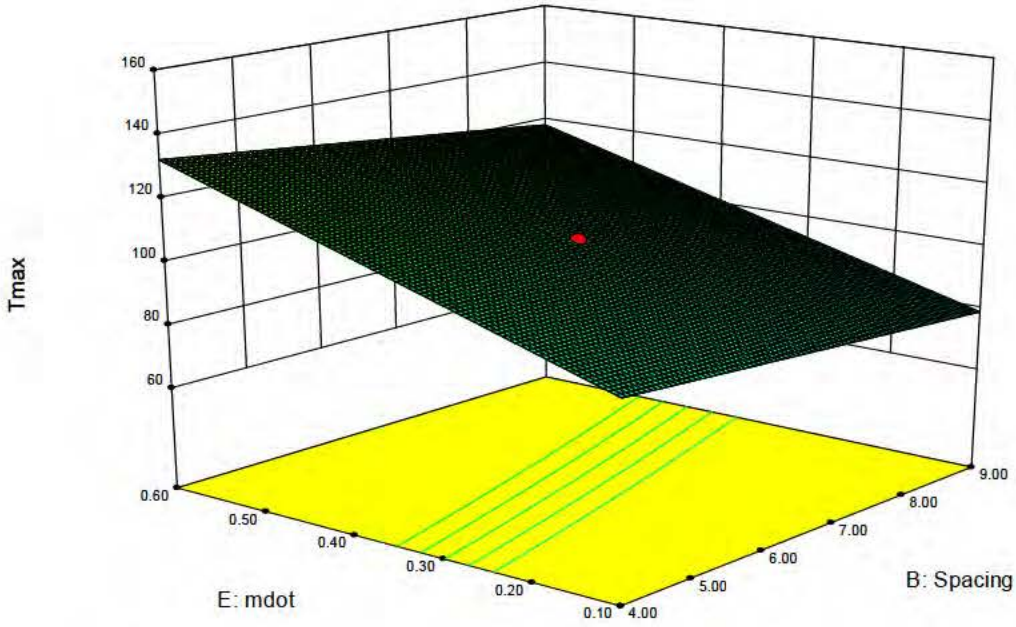

Figure 25. Response Surface Plot for Pin Fin Spacing and M_{dot} Variables

(Full 3FI untransformed evaluation.)

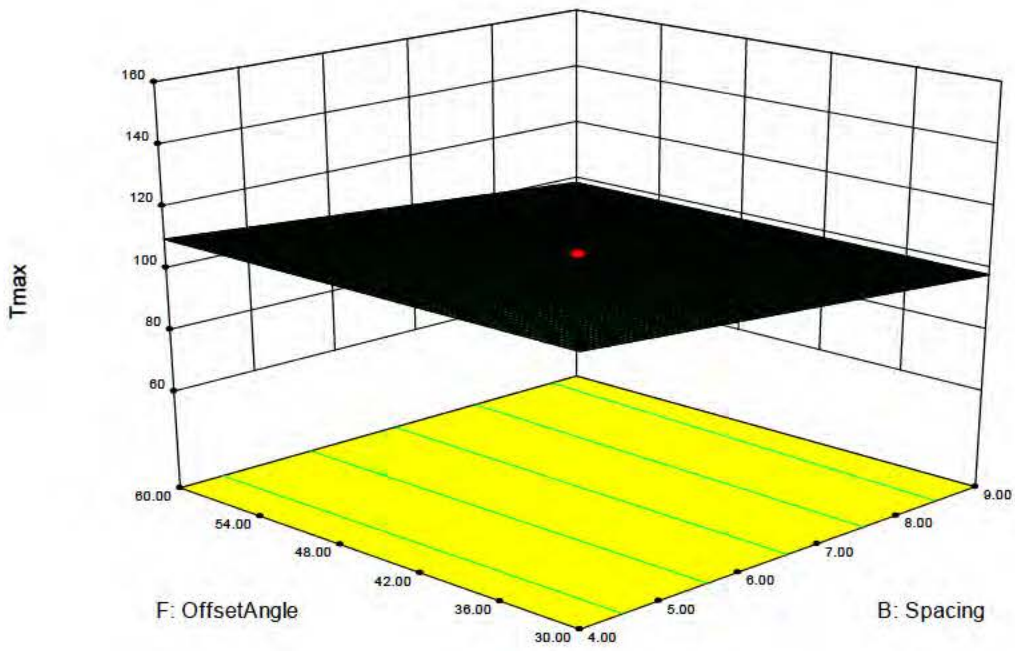

Figure 26. Response Surface Plot for Pin Fin Spacing and Pin Fin Offset Angle Variables

(Full 3FI untransformed evaluation.)

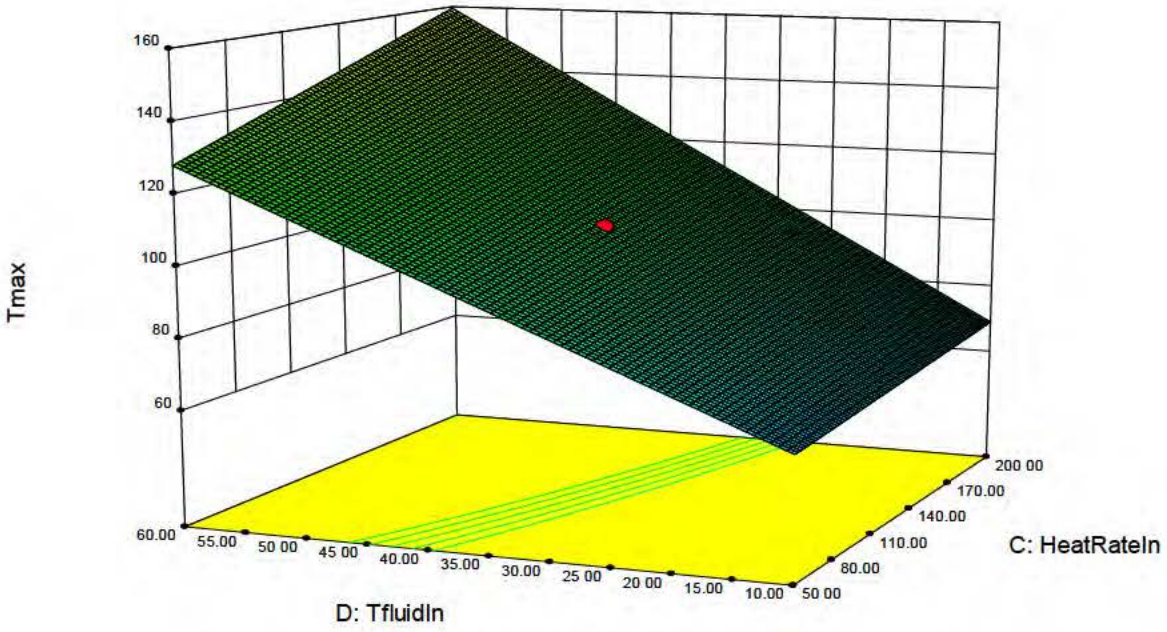

Figure 27. Response Surface Plot for $Heat_{rateim}$ and $T_{fluidin}$ Variables

(Full 3FI untransformed evaluation.)

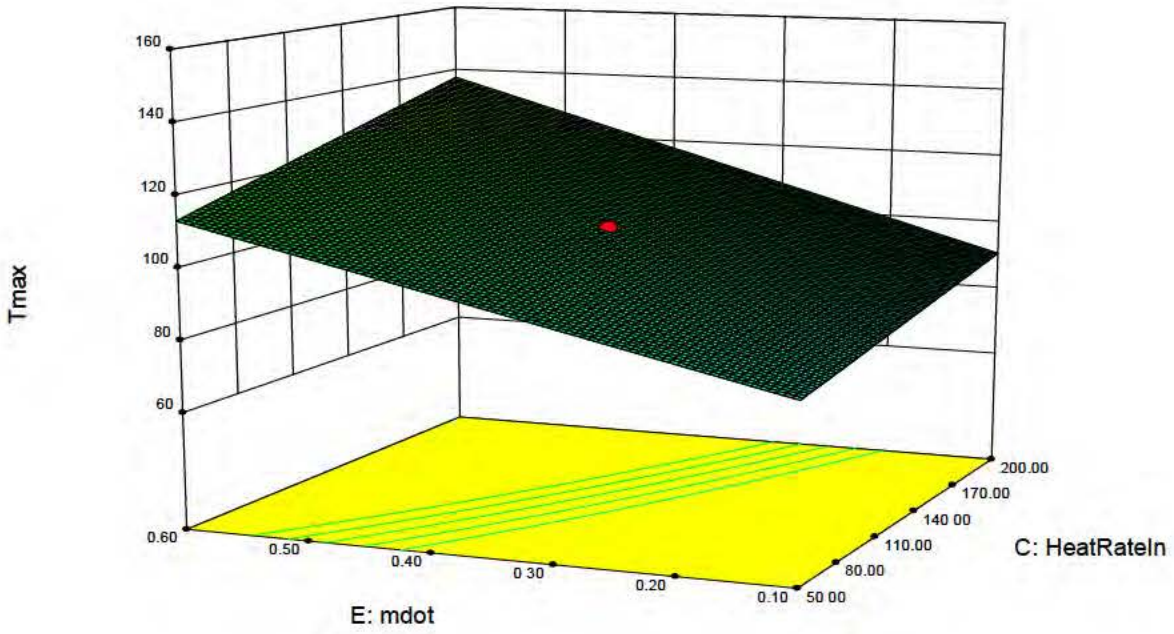

Figure 28. Response Surface Plot for $Heat_{rateim}$ and M_{dot} Variables

(Full 3FI untransformed evaluation.)

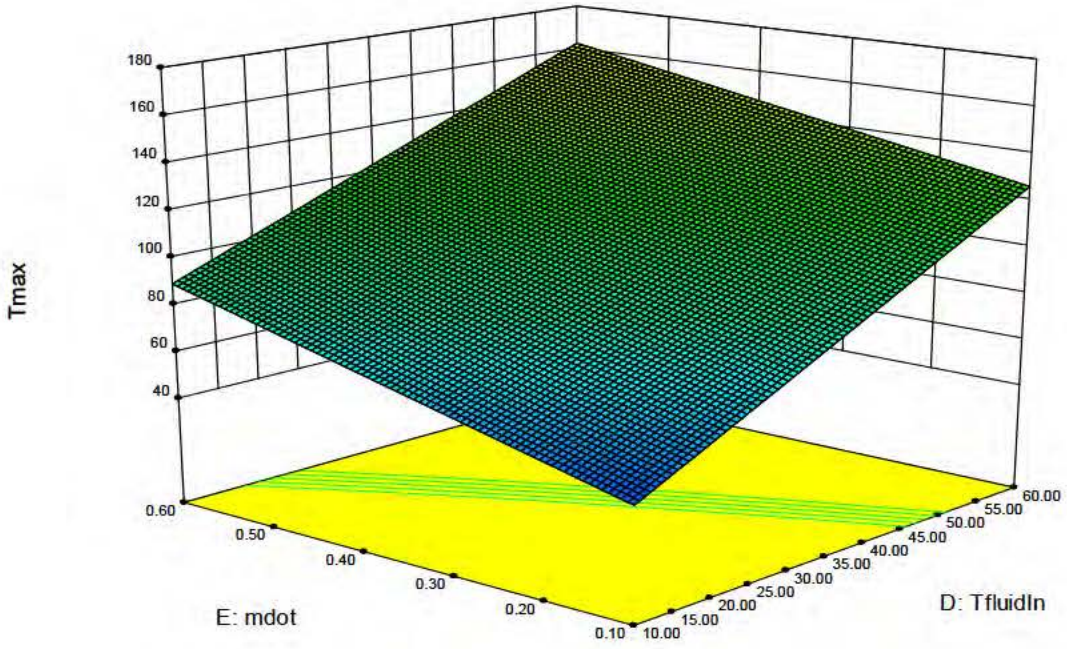

Figure 29. Response Surface Plot for M_{dot} and $T_{fluidin}$ Variables

(Full 3FI untransformed evaluation)

Subsequent to the full 3FI untransformed analysis, a transformation was applied to the data to determine if better results might be obtained. Both quadratic and power transforms were run, but

results were inferior to the full untransformed analysis. This is not surprising as this does nothing to alleviate the aliasing and associated lack of residuals. Table 9 shows the ANOVA summary and Table 10 shows the R^2 analysis for both cases.

Table 9. ANOVA Summary for A) Square Root and B) y^2 Transformations of T_{max} Data

A)

ANOVA Summary

	Adjusted F-value	Model p-value	Unadjusted F-value	Model p-value
Model	6.366E+007	< 0.0001	66.33	< 0.0001
Curvature	6.366E+007	< 0.0001		

B)

ANOVA Summary

	Adjusted F-value	Model p-value	Unadjusted F-value	Model p-value
Model	6.366E+007	< 0.0001	30.32	< 0.0001
Curvature	6.366E+007	< 0.0001		

As can be seen from the small model F-value, and large discrepancy between adjusted and unadjusted calculations, this model is likely worse for prediction, even within the factorial space, than the full untransformed model. This is further supported by the R^2 analysis of Table 10 in which we see negative prediction R^2 and large PRESS values.

Table 10. R^2 Analysis for A) Square Root and B) y^2 Transformations of T_{max} Data

A)

Std. Dev.	0.31	R-Squared	0.9948
Mean	9.85	Adj R-Squared	0.9798
C.V. %	3.15	Pred R-Squared	-18.3638
PRESS	3964.26	Adeq Precision	35.084

B)

Std. Dev.	1965.08	R-Squared	0.9888
Mean	12017.48	Adj R-Squared	0.9562
C.V. %	16.35	Pred R-Squared	-41.1074
PRESS	1.595E+011	Adeq Precision	25.052

Thus, as expected, improved model characteristics can only be realized using a regression reduced model to eliminate aliasing, generate the required residuals, and provide the necessary DOF for Lack of Fit and Pure Error analysis. To this end a backward regression analysis was performed in Design Expert for two cases of the T_{max} response data analysis. First a full 3FI model, with higher order terms ignored, was subjected to a backward regression of the model by iteratively removing insignificant model terms with p-values greater than the chosen alpha value (5%) until no terms remain with insignificant p-values. This modified model is then subjected to the normal ANOVA, regression diagnostics, and response surfaces assessments to determine if the reduced model did slightly improve model prediction capabilities compared to previous analysis of the full model. Table 11 shows the resulting ANOVA summary for the reduced 3FI model.

Table 11. T_{max} Response ANOVA Summary for Reduced 3FI Model Using Backward Regression

ANOVA Summary				
	Adjusted F-value	**Model p-value**	**Unadjusted F-value**	**Model p-value**
Model	6.366E+007	< 0.0001	398.60	< 0.0001
Curvature	6.366E+007	< 0.0001		
Lack of Fit				

While the unadjusted model F-Value increase is seen as an improvement over the full model analysis, the ANOVA for the model adjusted for curvature has not improved and DOF is still insufficient for Lack of Fit residual analysis. Furthermore, the Adjusted ANOVA analysis still indicates that curvature is statistically significant and thus an additional indication of predictability issues even within the factorial space. An assessment of the associated R^2 statistics also shows that the model still has problems. Table 12 shows that prediction R^2 and PRESS both indicate a continued lack of predictability, even for this reduced 3FI model, indicating the need for further reduction to achieve acceptable prediction capability.

Table 12. R^2 Analysis for the Backward Regression Reduced 3FI Model

Std. Dev.	2.46	R-Squared	0.9990
Mean	101.59	Adj R-Squared	0.9965
C.V. %	2.42	Pred R-Squared	0.0885
PRESS	68085.05	Adeq Precision	87.529

Finally, a lack of residuals continues to prevent the generation of diagnostic plots for further model assessment. Of note, the model still indicates the same four prominent factors controlling T_{max} response, D, E, AF, and C, again showing the robust nature of the higher level factorial screening properties of the DOE process. In addition, the reduction of insignificant terms reduces aliasing to a level allowing actual factor model equations in addition to the coded factor expression. The poor predictability of this model, however, does not warrant further evaluation without additional order reduction first. To this end, a further reduction in the model to only include up to 2FI terms was similarly analyzed and described below.

The ANOVA summary for the full 2FI model is shown in Table 13.

Table 13. T_{max} Response ANOVA Summary for the Full 2FI Model

ANOVA Summary				
	Adjusted F-value	**Model p-value**	**Unadjusted F-value**	**Model p-value**
Model	48.20	< 0.0001	50.48	< 0.0001
Curvature	0.59	0.5644		

For the first time we now have reasonable values for the Adjusted Model F-value and furthermore, curvature is seen to be not statistically significant indicating that the model may be suitable for prediction. However, the small F-Values for both ANOVA model terms are cause for caution and further review of the R^2 analysis confirms that the full 2FI model is only a modest

improvement. As with the previous evaluations, prediction R^2 values do not approach the Adjusted R^2 statistic as desired and PRESS is seen to be extremely large, once again indicating poor model characteristics and the need for further reduction and/or transformation. A quick glance at the full ANOVA data in Table 15 reveals the reason for the marginal suitability of the reduced full-2FI model. While reduction of model order from 3FI increased the DOF metric to satisfactory values for Lack of Fit and Pure Error assessment, the model retains many terms that are not statistically significant. This is seen by looking at the p-value column of values. Since the alpha level has been chosen at 5% significance we can see that only input factors B, C, D, E, AF, BC, BD, CD, DE are significant model terms (p-value <0.05). Thus degrees of freedom are being used on insignificant terms and residual analysis is inclusive of these same terms which degrade the prediction capability of the model. Backward regression to eliminate insignificant terms is warranted for this 2FI model to further refine and improve model characteristics. Before summarizing the backward regression 2FI model, a cursory glance at model diagnostics is information since sufficient residuals now are available for plot generation.

Table 14. R^2 Analysis for the Full 2FI Model.

Std. Dev.	7.64	R-Squared	0.9859
Mean	101.59	Adj R-Squared	0.9664
C.V. %	7.52	Pred R-Squared	0.6800
PRESS	23903.96	Adeq Precision	29.429

Table 15. Full 2FI ANOVA Results for T_{max} Analysis

ANOVA for selected factorial model (Aliased)
Analysis of variance table [Partial sum of squares - Type III]

Source	Sum of Squares	df	Mean Square	F Value	p-value Prob > F
Model	73647.87	25	2945.91	50.48	< 0.0001
A-Diameter	*107.31*	*1*	*107.31*	*1.84*	*0.1918*
B-Spacing	*808.02*	*1*	*808.02*	*13.85*	*0.0016*
C-HeatRateIn	*3018.65*	*1*	*3018.65*	*51.73*	*< 0.0001*
D-TfluidIn	*49156.80*	*1*	*49156.80*	*842.37*	*< 0.0001*
E-mdot	*14137.21*	*1*	*14137.21*	*242.26*	*< 0.0001*
F-OffsetAngle	*0.45*	*1*	*0.45*	*7.733E-003*	*0.9309*
G-Geometry	*39.33*	*1*	*39.33*	*0.67*	*0.4224*
AB	*0.045*	*1*	*0.045*	*7.711E-004*	*0.9782*
AC	*1.62*	*1*	*1.62*	*0.028*	*0.8695*
AD	*34.86*	*1*	*34.86*	*0.60*	*0.4496*
AE	*17.11*	*1*	*17.11*	*0.29*	*0.5948*
AF	*3100.78*	*1*	*3100.78*	*53.14*	*< 0.0001*
AG	*10.13*	*1*	*10.13*	*0.17*	*0.6819*
BC	*810.03*	*1*	*810.03*	*13.88*	*0.0015*
BD	*677.12*	*1*	*677.12*	*11.60*	*0.0031*
BE	*45.13*	*1*	*45.13*	*0.77*	*0.3908*
BF	*0.72*	*1*	*0.72*	*0.012*	*0.9128*
BG	*18.91*	*1*	*18.91*	*0.32*	*0.5762*
CD	*1118.65*	*1*	*1118.65*	*19.17*	*0.0004*
CE	*202.01*	*1*	*202.01*	*3.46*	*0.0792*
CF	*0.85*	*1*	*0.85*	*0.014*	*0.9056*
CG	*0.061*	*1*	*0.061*	*1.050E-003*	*0.9745*
DE	*341.91*	*1*	*341.91*	*5.86*	*0.0263*
DF	*1.250E-003*	*1*	*1.250E-003*	*2.142E-005*	*0.9964*
DG	*0.18*	*1*	*0.18*	*3.085E-003*	*0.9563*
EF	*0.000*	*0*			
EG	*0.000*	*0*			
FG	*0.000*	*0*			
Residual	1050.40	18	58.36		
Lack of Fit	*1050.40*	*8*	*131.30*		
Pure Error	*0.000*	*10*	*0.000*		
Cor Total	74698.27	43			

Figure 29 is the Normal plot of residuals used to determine the validity of the assumption that the residuals follow a normal distribution. If it is a valid assumption, the residuals should follow a linear trend. The residual data points in Figure 29 are indicative of a deviation from the normality assumption and the slight "S" shape distribution may suggest that a transformation may be prudent. However, the residual versus predicted and residual versus run plots shown in Figure 30 do not show non-random character and thus are not indicative of a transform requirement. Additionally, the Design Expert generated Box-Cox plot of Figure 31, the primary diagnostic tool to determine transform requirement and type, does not indicate that a transform is warranted. Furthermore, the large Ln(ResidualSS) minimum value (~6.75) is indicative of continued poor prediction characteristics of the model. Thus, further model reduction was the approach taken and will be summarized below.

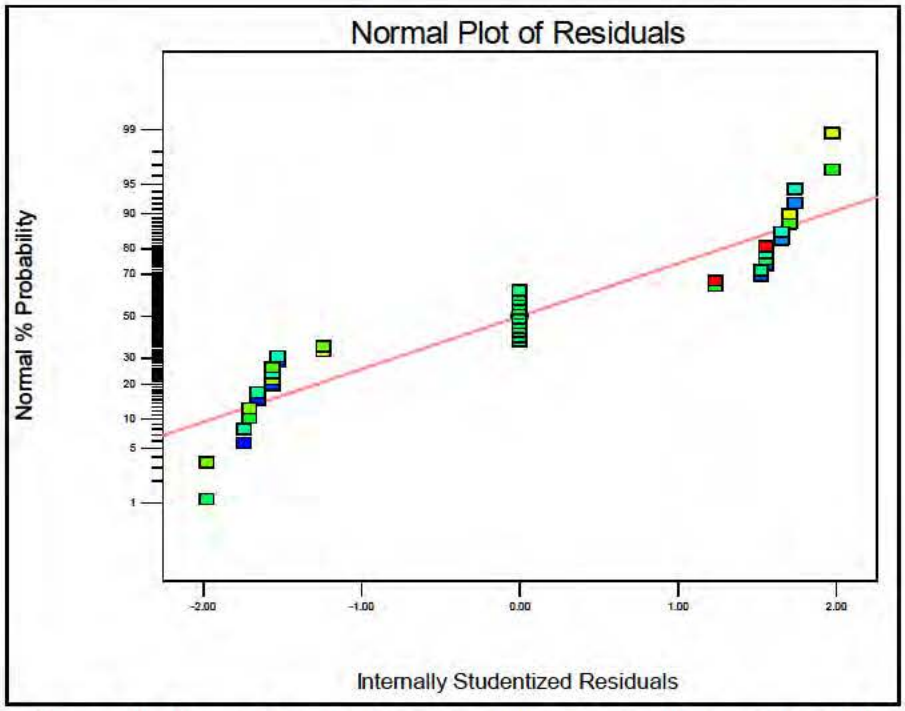

Figure 30. Normal Residual Diagnostic Plot for the Full T_{max} 2FI Model

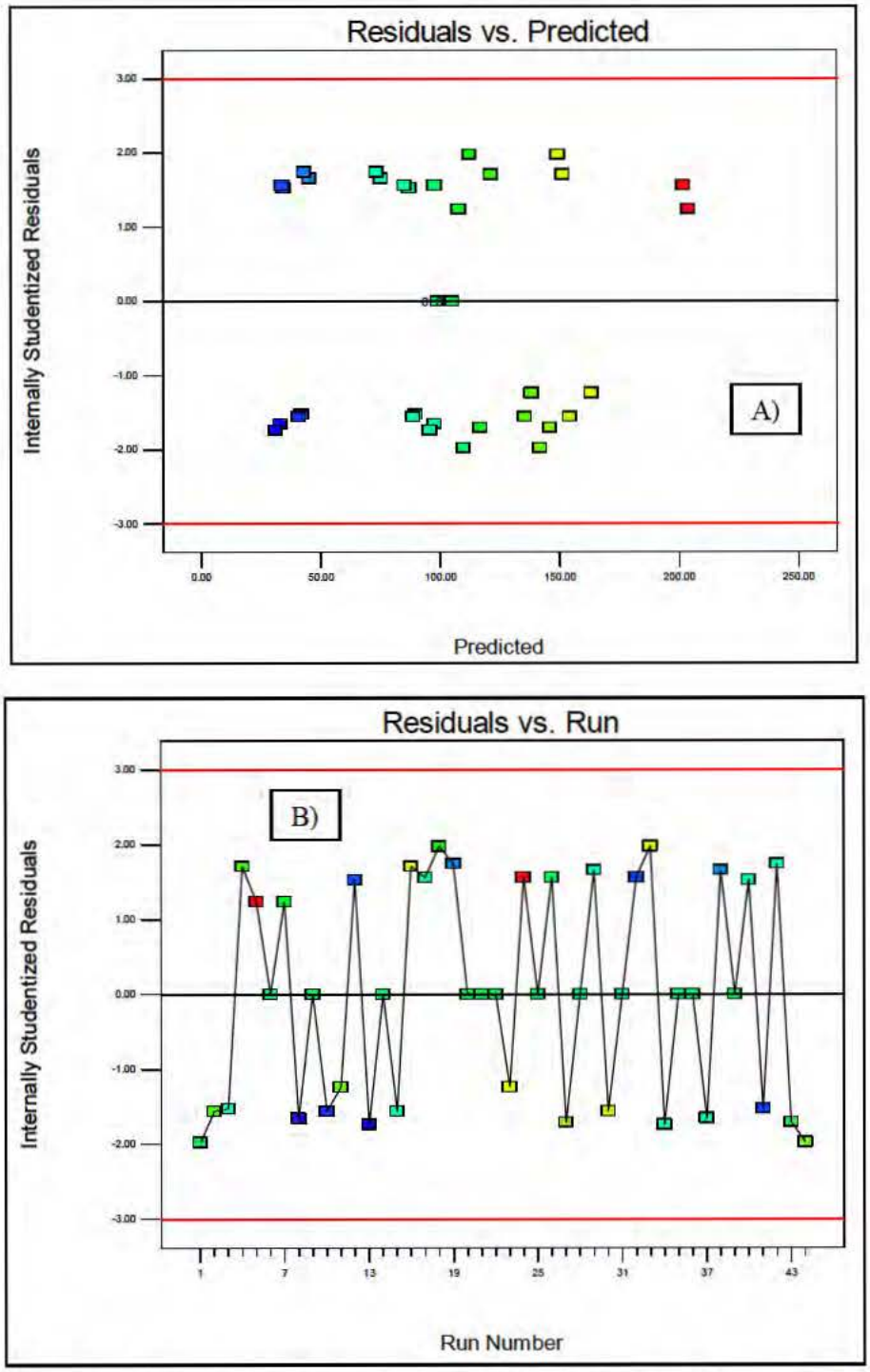

Figure 31. A) Residual vs. Prediction and B) Residual vs. Run Diagnostic Plots

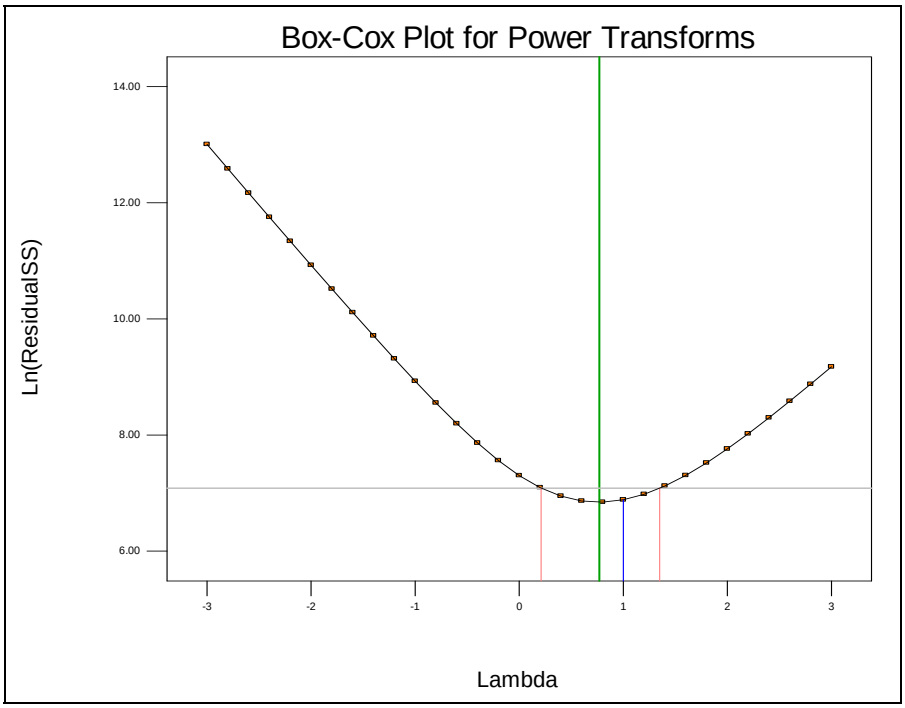

Figure 32. Box-Cox Diagnostic Plot for the Full T_{max} 2FI Model

Subsequent to the full 2FI Design Expert Tmax response analysis, a backward regression model reduction approach was taken to eliminate the statistically insignificant terms from the full 2FI model. Table 16 shows the Design Expert Effects List of Model, Error, and Aliased terms, effect magnitudes, SS, and %contribution after backward reduction.

Table 16. Effects List Showing Model, Aliased, and Error Terms after 2FI Model Backward Reduction

	Term	Effect	SumSqr	% Contribution
Require	Intercept			
Model	A-Diameter	-3.6625	107.311	0.14366
Model	B-Spacing	-10.05	808.02	1.08171
Model	C-HeatRateIn	19.425	3018.64	4.04112
Model	D-TfluidIn	78.3875	49156.8	65.8071
Model	E-mdot	42.0375	14137.2	18.9258
Model	F-OffsetAngle	0.2375	0.45125	0.000604097
Error	G-Geometry	-0.35	0.98	0.00131194
Error	AB	-0.075	0.045	6.02424E-005
Error	AC	0.45	1.62	0.00216872
Error	AD	-2.0875	34.8612	0.0466694
Error	AE	1.4625	17.1113	0.0229072
Model	AF	-19.6875	3100.78	4.15107
Error	AG	-1.125	10.125	0.0135545
Model	BC	-10.0625	810.031	1.0844
Model	BD	-9.2	677.12	0.906473
Error	BE	-2.375	45.125	0.0604097
Error	BF	0.3	0.72	0.000963878
Error	BG	1.5375	18.9112	0.0253169
Model	CD	11.825	1118.64	1.49755
Model	CE	5.025	202.005	0.270428
Error	CF	0.325	0.845	0.00113122
Error	CG	0.0875	0.06125	8.19965E-005
Model	DE	-6.5375	341.911	0.457723
Error	DF	0.0125	0.00125	1.6734E-006
Error	DG	-0.15	0.18	0.000240969
Aliased	EF	Aliased		
Aliased	EG	Aliased		
Aliased	FG	Aliased		
	Lenth's ME	1.0027		
	Lenth's SME	1.74421		

The analysis still shows the dominance of the same four main effects (B, C, D, and E) that has carried forward from the initial 3FI full model analysis. It is also notable that the Effects List shows that the backward regression resulted in the elimination of the geometry (circular/square cross section) main effect due to its' insignificance in influencing the maximum temperature response variable. In addition, the reduced model analysis indicates that interaction term CE is now statistically significant along with the 5 interaction terms (AF, BC, BD, CD, DE) projected to be statistically significant from the full 2FI ANOVA p-value assessment shown in Table 15. These dominant factors are also seen by viewing the half-normal Pareto graphs in Figures 32 and 33, respectively in which retained model terms are shown as deviations from linearity (half-normal) and the t-value associated with each effect. Even more explicit is the associated ANOVA analysis for the reduced 2FI model shown in Table 17.

Table 17. ANOVA Analysis for Backward Reduced 2FI Model

ANOVA Summary

	Adjusted F-value	Model p-value	Unadjusted F-value	Model p-value
Model	151.00	< 0.0001	155.68	< 0.0001
Curvature	0.070	0.7937		

ANOVA for selected factorial model
Analysis of variance table [Partial sum of squares - Type III]

Source	Sum of Squares	df	Mean Square	F Value	p-value Prob > F
Model	73478.93	12	6123.24	155.68	< 0.0001 significant
A-Diameter	*107.31*	*1*	*107.31*	*2.73*	*0.1087*
B-Spacing	*808.02*	*1*	*808.02*	*20.54*	*< 0.0001*
C-HeatRateIn	*3018.64*	*1*	*3018.64*	*76.74*	*< 0.0001*
D-TfluidIn	*49156.80*	*1*	*49156.80*	*1249.74*	*< 0.0001*
E-mdot	*14137.21*	*1*	*14137.21*	*359.42*	*< 0.0001*
F-OffsetAngle	*0.45*	*1*	*0.45*	*0.011*	*0.9154*
AF	*3100.78*	*1*	*3100.78*	*78.83*	*< 0.0001*
BC	*810.03*	*1*	*810.03*	*20.59*	*< 0.0001*
BD	*677.12*	*1*	*677.12*	*17.21*	*0.0002*
CD	*1118.64*	*1*	*1118.64*	*28.44*	*< 0.0001*
CE	*202.00*	*1*	*202.00*	*5.14*	*0.0306*
DE	*341.91*	*1*	*341.91*	*8.69*	*0.0060*
Residual	1219.34	31	39.33		
Lack of Fit	*1219.34*	*21*	*58.06*		
Pure Error	*0.000*	*10*	*0.000*		
Cor Total	74698.27	43			

Of immediate note is the fact that the ANOVA for the curvature adjusted model now has a reasonable F-value. The associated p-value shows that curvature is not statistically significant based on the probability of an F-value this large occurring due to random variation is 79.4%. Furthermore, close agreement between the adjusted and unadjusted model F-values is further evidence of the insignificance of curvature for the Tmax reduced 2FI case. One other item of significance from the ANOVA table is the statistical insignificance of the pin-fin diameter (A) and offset angle geometry (F) factor main effects. They have however, been retained in the reduced model for hierarchy reasons because of the significance of the diameter-angle interaction term (AF). The R2 analysis summary associated with the ANOVA for this case is shown in Table 18.

Table 18. R^2 Analysis for the Reduced 2FI Tmax Model

Std. Dev.	6.27	R-Squared	0.9837
Mean	101.59	Adj R-Squared	0.9774
C.V. %	6.17	Pred R-Squared	0.9575
PRESS	3173.37	Adeq Precision	50.821

We now see good agreement between the prediction R2 and the adjusted R2 values with both > 0.95 indicating that the model is suitable for navigating the design space. The large value of PRESS simply indicates that the model will be marginally effective at predicting the results of a new experiment, which is understood from the beginning that this is a factor screening exercise. Follow-on designs will be required for model optimization.

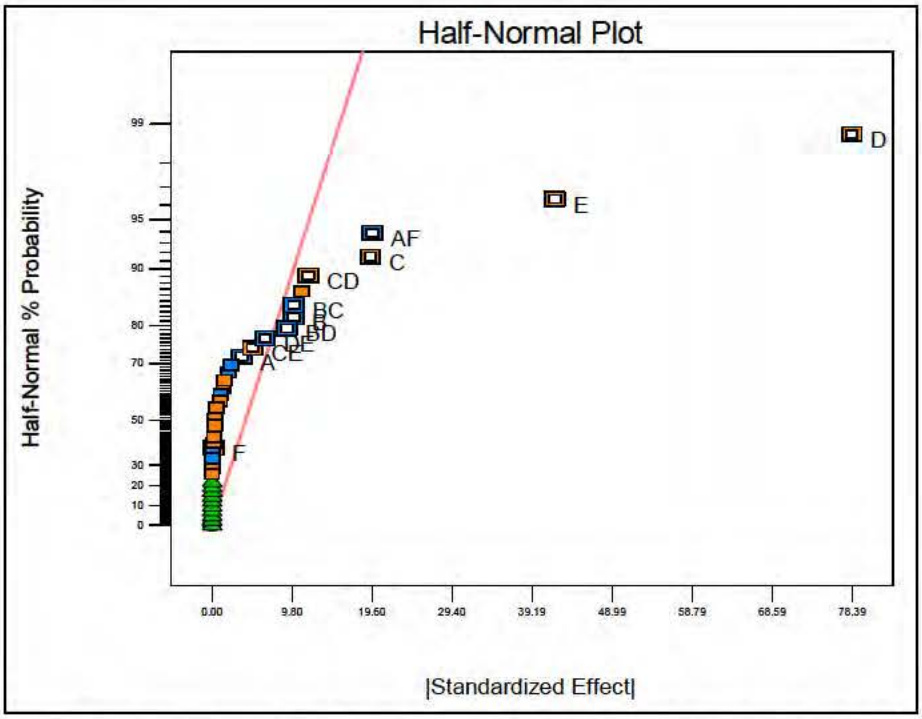

Figure 33. Half Normal Plot for Backward Regression Reduced 2FI T_{max} Model

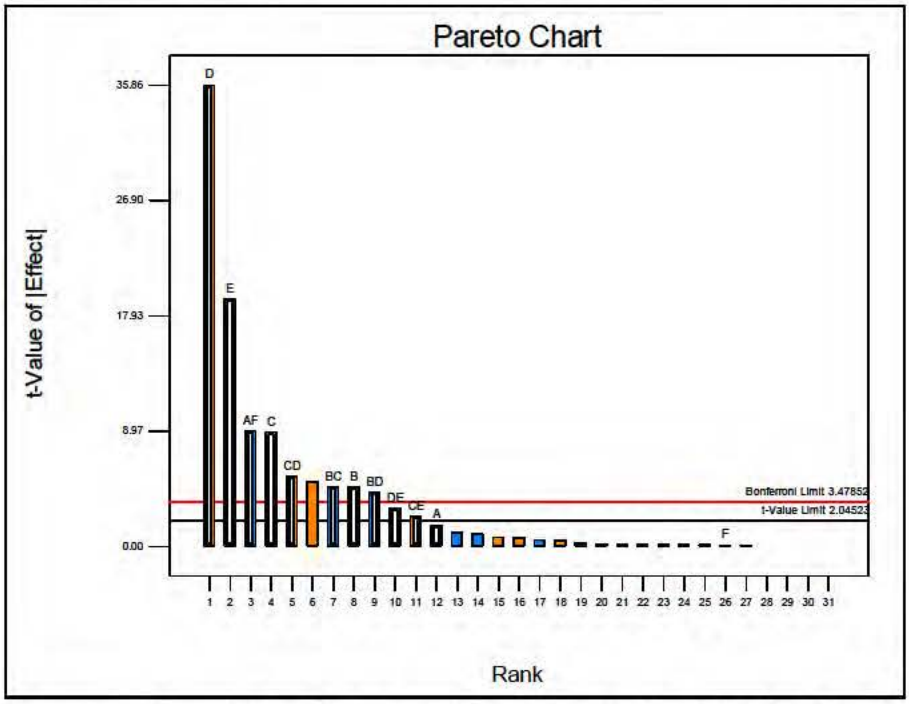

Figure 34. Pareto Chart for Backward Regression Reduced 2FI T_{max} Model

The only analysis remaining is to assess the diagnostic plots for variance normality and to determine whether a data transformation is warranted. First, as can be seen in Figure 34 the normal plot of residuals now much more closely follows a linear characteristic indicating that our normal distribution of variance assumption in likely valid. In addition, the residuals versus predicted and run number plots of Figure 35 reflect a random scatter of points which supports the

normality assumption and contraindicates the need for a transformation, and the absence of lurking time dependent variables, respectively. The Box-Cox plot for this analysis is shown in Figure 36, which still does not indicate the need for a transformation on this response data set. This is concluded since, as seen in the plot, the 95% confidence interval contains unity (λ=1). It is once again noteworthy that the minimum Box-Cox plot value is still reflective of a larger than desired variance (i.e. lower Ln(ResidualSS) means smaller variance). This is not unexpected due to the use of a quarter fraction factorial experiment design and again highlights the primary utility for this experiment as an initial dominant input factor screening tool.

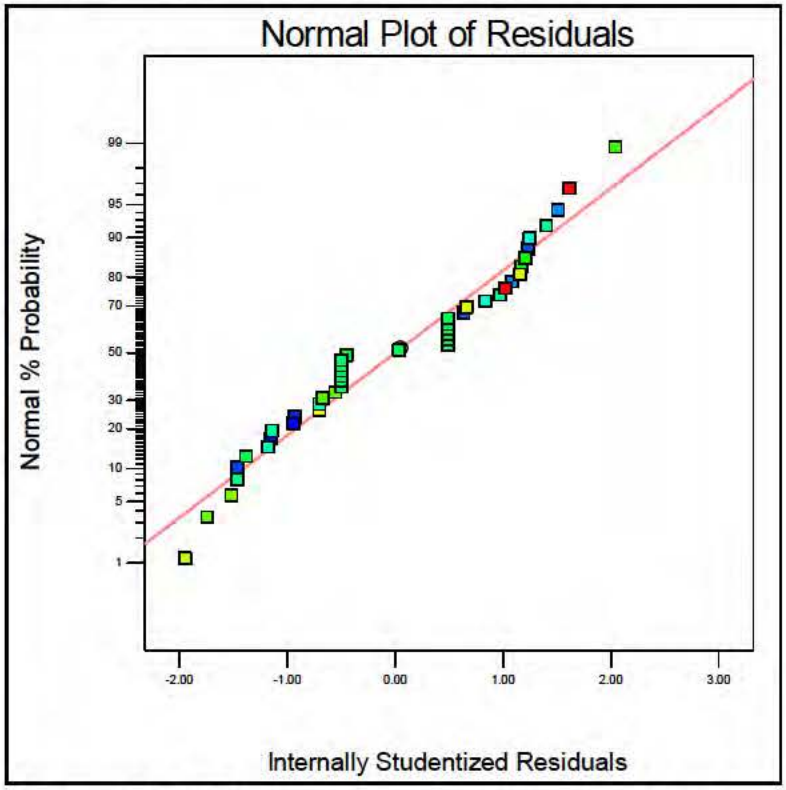

Figure 35. Normal Plot of Residuals for the Reduced 2FI Model for T_{max} Response

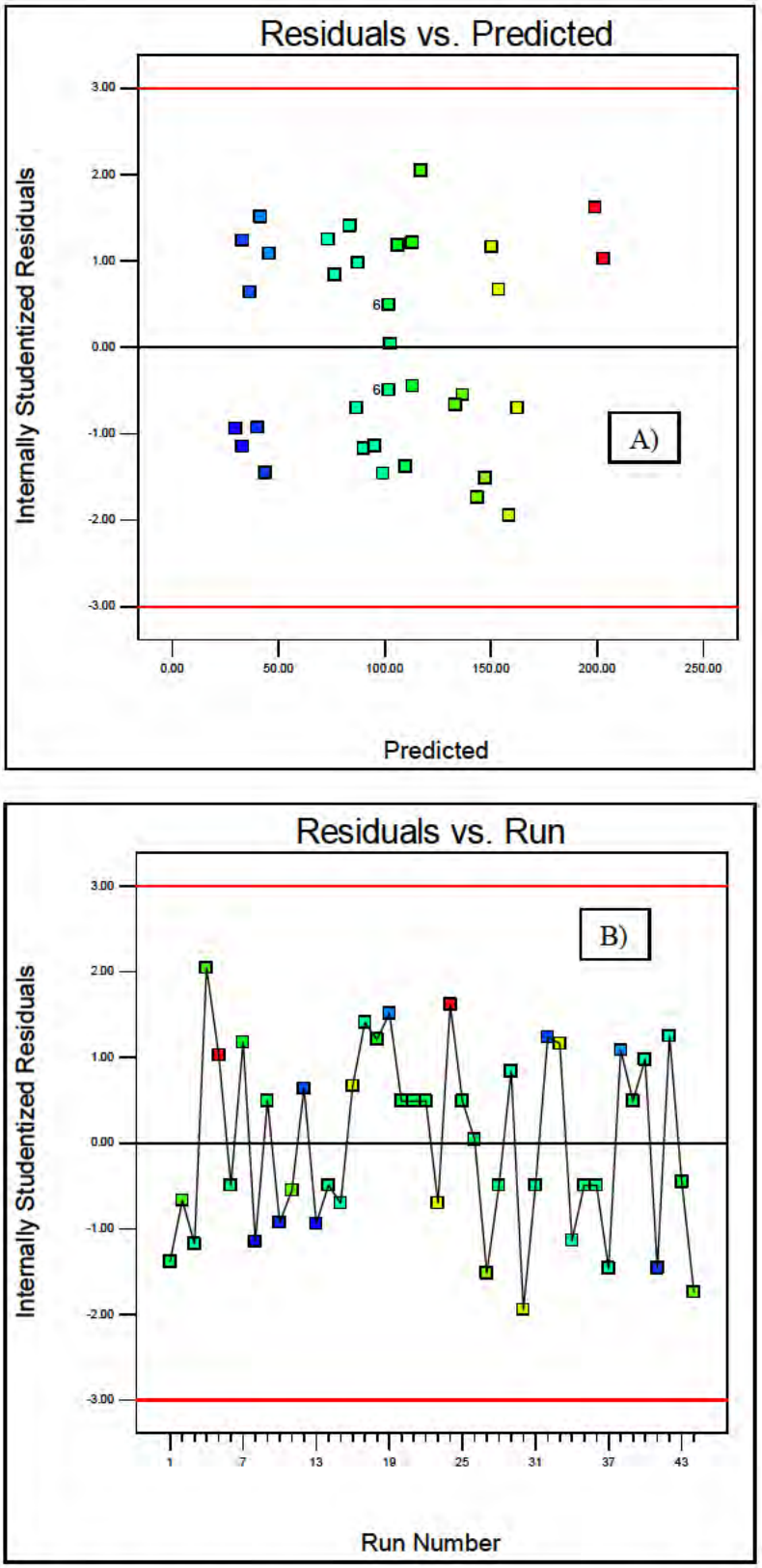

Figure 36. A) Residuals vs. Predicted and B) Residuals vs. Run Diagnostic Plots for 2FI Reduced Model

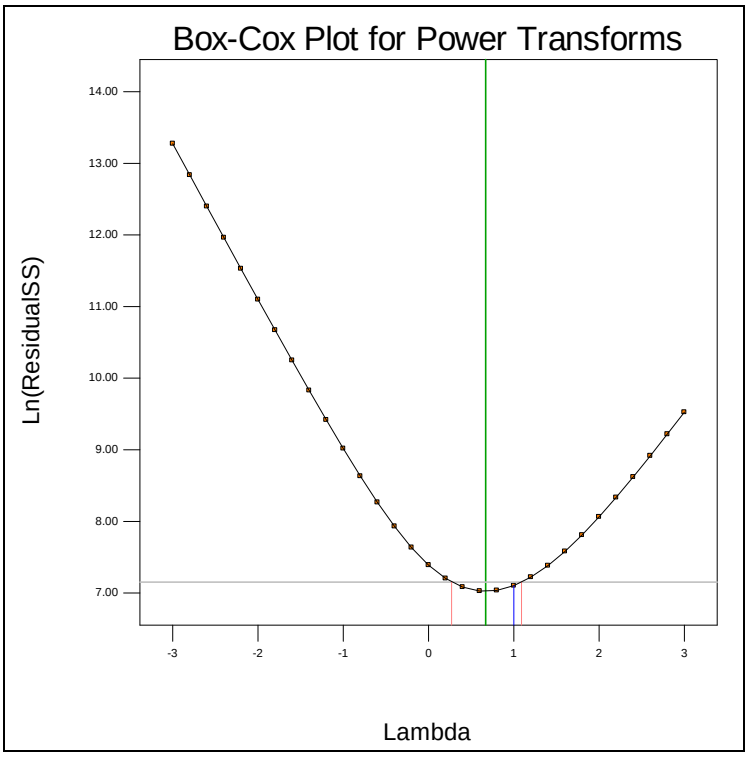

Figure 37. Box-Cox Diagnostic Plot for the Reduced T_{max} 2FI ANOVA Model.

The superiority of the ANOVA model for the reduced 2FI model is highlighted by the improved R^2, diagnostic plot behavior, as well as the 3D response surface graphs of the design space predictions. By each of these measures, the model suitability for prediction within the design space has been significantly improved by the backward regression reduction procedure. This is most readily apparent by noting that all of the prior response surface plots (Figures 15 through 27) indicated that the un-optimized models were not able to accurately model even the factorial design points. This was indicated by the red design point shown on these plots illustrating that the ANOVA model response surfaces did not contain the design points. The full set of response surface plots for this reduced 2FI model is shown in Appendix A. It is notable that the most statistically significant interaction term, AF, which exhibited nonlinear behavior, is the remaining response surface plot that misses the factorial design point. This is not surprising due to the inability of the fractional factorial model to account for nonlinear behavior since the terms required to model quadratic behavior are aliased. However, as stated previously, the quarter fraction design is highly suitable for providing clear estimates of the main effects of importance as long as 3FI terms can be neglected. We initially made that assumption based on SME input.

Equations 2 and 3 below show the resulting reduced 2FI ANOVA model final equations for both coded variables and actual factors. These are the equations that will be carried forward as the "parsimonious" T_{max} model for validation and optimization usage.

Equation 2. *Coded Variables Reduced 2FI*

$$T_{max} = + 101.59 - 1.83 * A - 5.03 * B + 9.71 * C + 39.19 * D + 21.02 * E + 0.12 * F$$
$$- 9.84 * A * F - 5.03 * B * C - 4.60 * B * D + 5.91 * C * D + 2.51 * C * E - 3.27 * D * E$$

Equation 3. *Actual Factors Reduced 2FI*

$$T_{max} = -149.98439 + 55.4 * Diameter + 3.92017 * Spacing + 0.14665 * HeatRateIn + 1.83503 * TfluidIn + 85.63000 * mdot + 3.28917 * OffsetAngle - 1.31250 * Diameter * OffsetAngle - 0.026833 * Spacing * HeatRateIn - 0.0736 * Spacing * TfluidIn + 3.15333E-003 * HeatRateIn * TfluidIn + 0.13400 * HeatRateIn * mdot - 0.523 * TfluidIn * mdot$$

As a final assessment of the T_{max} ANOVA model space, the analysis was run one additional time to generate a main effects only model and equation set which can be compared to the reduced 2FI model above for its effectiveness in screening important factors. Table 19 shows the effects list and the % contribution of each effect when all higher order terms are suppressed. This analysis continues to reflect the dominance of the B, C, D, and E factors seen throughout the entire range of model order analyses. Thus, it appears initially that the main effects only model could possibly be sufficient for screening purposes. Similarly, the ANOVA summary shows consistency between both the adjusted and unadjusted results. In addition, the ANOVA analysis indicate significance of the models while curvature was found to be not significant. R^2 analysis indicates that the model may be suitable to explore the design space. A cursory review of the effects list illustrates that geometry factors F and G are no longer statistically significant now that the dominance of the AF interaction has been removed. The final equations for the main effects model are shown as Equation 4, 5, and 6 below. The insignificance of G is reflected by the similarity of Equations 5 and 6. In fact, only the y-intercept value differs slightly between the two.

Table 19. Effects List for Main Effects Only Model Analysis for Tmax ANOVA Model

	Term	Effect	SumSqr	% Contribution
Model	A-Diameter	-3.6625	107.311	0.14366
Model	B-Spacing	-10.05	808.02	1.08171
Model	C-HeatRateIn	19.425	3018.64	4.04112
Model	D-TfluidIn	78.3875	49156.8	65.8071
Model	E-mdot	42.0375	14137.2	18.9258
Model	F-OffsetAngle	0.2375	0.45125	0.000604097
Model	G-Geometry	-0.35	0.98	0.00131194

Table 20. ANOVA Summary for the Main Effects Only Analysis for Tmax

ANOVA Summary

	Adjusted F-value	Model p-value	Unadjusted F-value	Model p-value
Model	44.40	< 0.0001	46.56	< 0.0001
Curvature	0.17	0.8465		

Table 21. R^2 Analysis for the Main Effects Only Model

Std. Dev.	14.37	R-Squared	0.9005
Mean	101.59	Adj R-Squared	0.8812
C.V. %	14.14	Pred R-Squared	0.8314
PRESS	12597.46	Adeq Precision	25.067

Review of the normal residual diagnostic plot in Figure 37, for the main effects model, shows reasonable linearity and only a slight "S" shape near the central points. However, in the residual

vs. predicted diagnostic plot of Figure 38 the observed "horn" shape of the data scatter indicates the possible need for a data transformation. This is further supported by the Box-Cox analysis in Figure 39 which recommends a λ=1/2 transformation. The data was once again run through the analysis for a main effects only model but with the square root transform applied to the response data. Review of the ANOVA summary and R^2 analysis indicated little change for the untransformed results. However, the residual vs. predicted plot was improved as seen in Figure 39, with a more random scatter of the data points. The Box-Cox plot of Figure 40 now reflects a prediction interval centered on the l=0.5 and close to the optimal calculated value of 0.66. Thus, the transformed model is selected as the final for main effects screening comparison. The three modified main effects only equations are listed below as Equation 7 a-c.

Equation 4. *Coded Factor Main Effects Model*

Tmax = +101.59 - 1.83 * A -5.03 * B +9.71 * C +39.19 * D +21.02 * E +0.12 * F -0.95 * G

Equation 5. *Actual Factor Model for Circular Fin Geometry for Main Effects Only*

GeometryCircular
Tmax = +23.91182 -3.66250 * Diameter -2.01000 * Spacing +0.12950 * HeatRateIn
+1.56775 * TfluidIn +84.07500 * mdot +7.91667E-003 * OffsetAngle

Equation 6. *Actual Factor Model for Square Fin Geometry for Main Effects Only*

GeometrySquare
Tmax = +22.02091 -3.66250 * Diameter -2.01000 * Spacing +0.12950 * HeatRateIn
+1.56775 * TfluidIn +84.07500 * mdot +7.91667E-003 * OffsetAngle

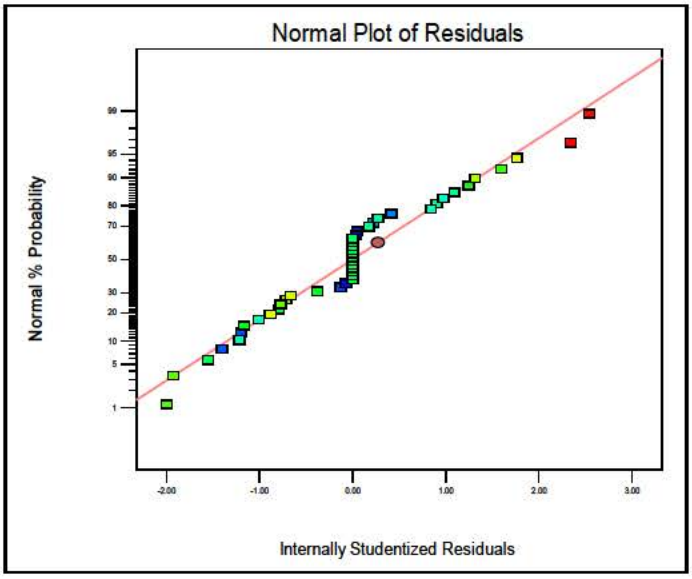

Figure 38. Normal Residual Plot for Main Effects Only Model

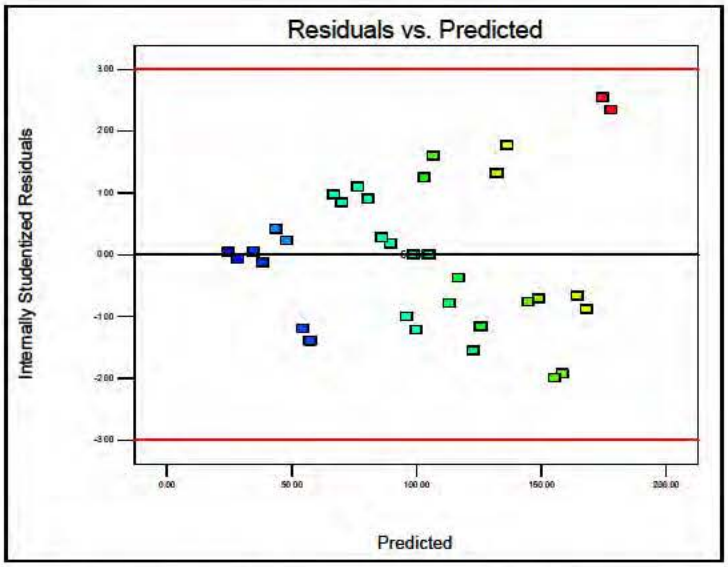

Figure 39. Residual vs. Predicted Diagnostic for Main Effects Model

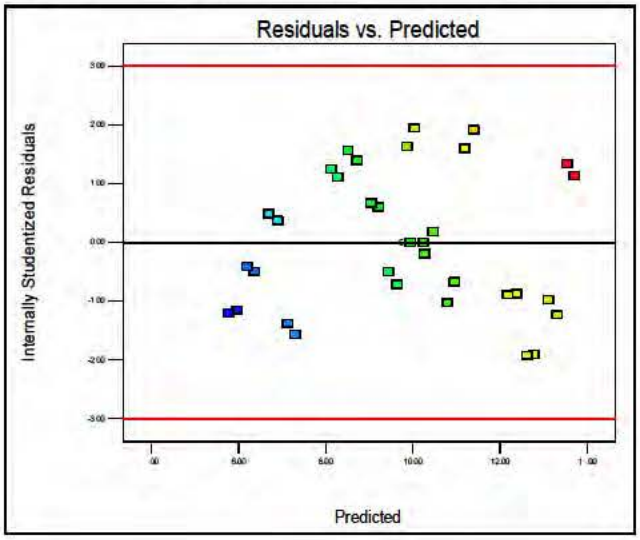

Figure 40. Residual vs. Predicted Diagnostic Plot for the Transformed (λ=0.5) Main Effects Model

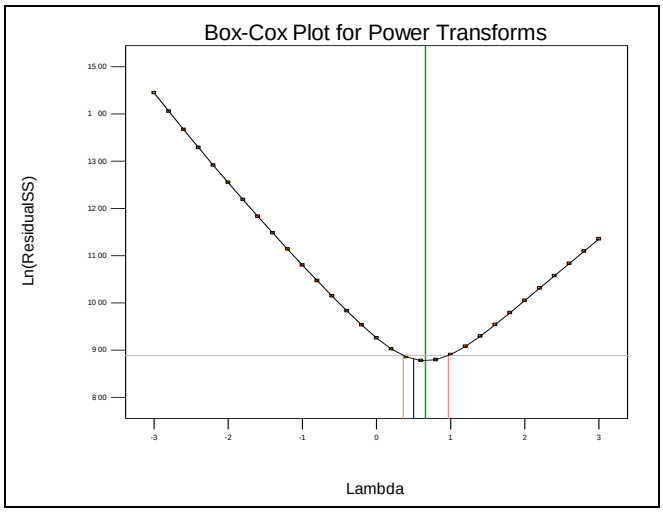

Figure 41. Box-Cox Diagnostic Plot for the Transformed (λ=0.5) Main Effects Model

Equation 7. *a) Actual Factor, b) Actual Factor Circular, and c) Actual Factor Square Transformed Main Effects*

a)
Sqrt(Tmax) = +9.85 -0.091 * A -0.21 * B +0.46 * C +2.04 * D +1.16 * E +4.666E-004 * F -0.047 * G

b)
Sqrt(Tmax) = +5.62629 -0.18182 * Diameter -0.082964 * Spacing +6.16666E-003 * HeatRateIn
+0.081647 * TfluidIn +4.65856 * mdot +3.11067E-005 * OffsetAngle

c)
Sqrt(Tmax) = +5.53152 -0.18182 * Diameter -0.082964 * Spacing +6.16666E-003 * HeatRateIn
+0.081647 * TfluidIn +4.65856 * mdot +3.11067E-005 * OffsetAngle

A quick survey of the model response surface graphs shows that this main effects model has sacrificed some prediction fidelity on the design space, which is indicated by the response surface being below the factorial design points. That is acceptable if the model is shown to be adequate for screening the dominant main effects and used only for that purpose. As a result, for our purposes we will utilize the reduced 2FI model going forward.

With the T_{max} response factor data analyzed we only need now to optimize the input factors to yield the minimum T_{max} response. However, before we complete that analysis we need to complete the response analysis on the remaining two output factors, average heat transfer coefficient (h_{avg}) and pressure drop (DeltaP). The results of those analyses will be summarized in the following sections.

5.2 h_{avg} Response Variable Evaluation

The Design Expert analysis of the average heat transfer coefficient response variable mirrors the approach taken above for T_{max}. Initially, a full 3FI model was assessed followed by a comparison to a backward regression reduction and analysis of that full model. Subsequently, a reduced full 2FI model was similarly assessed for predictability and statistical significance and that was also followed-up by a backward regression reduction to eliminate statistically insignificant

factors and improve predictability and utility. During each ordered model analysis, the need for a transformation was assessed, which was also accomplished for the remaining response factors. Similarly, main-effects only model equations were also generated to use for screening efficacy comparison. As the evaluations above were excessively detailed and explicit, the remaining two response factor analyses will be significantly abbreviated and only summary ANOVA, R^2, and other relevant diagnostic plots will be included and discussed in the paragraphs to follow. Response surface plots of the parsimonious h_{avg} model are also included in the Appendix for reference following those for T_{max}.

To this end, Table 22 a)-d) show the ANOVA summary information for each of the evaluated order model cases described above. In addition, the summary R^2 analysis for each of these cases is shown in Table 23 as well. As with the prior evaluation of T_{max}, the extensive aliasing of the quarter fraction designed experiment leads to very poor model characteristics for the higher order models, even when reduced via backward regression to eliminate insignificant terms. The lack of residuals for the full and reduced 3FI models manifests itself in the unrealistically high Adjusted F-value in the ANOVA calculations for these cases. In addition, the R^2 evaluation yields similarly unrealistically high values of R^2 due to the inclusion of statistically insignificant model terms, as seen in Table 23 for both 3FI models. In addition, the negative values of prediction R^2 (1-$PRESS/SS_{Total}$) due to the extremely large PRESS values indicates an inability to even use this model on the factorial design space. As before, the lacks of residuals prevents the generation of diagnostic plots for normality assumption verification and transform requirement determination. Thus, as expected, the 3FI models are not of utility for this highly aliased quarter fraction design. Once the 3FI terms are suppressed and the aliasing structure with the main factors is eliminated, the ANOVA model predictability improves dramatically. This is reflected by the agreement now between the adjusted and unadjusted ANOVA F-values and much improved R^2 statistics.

Table 22. ANOVA Summary Table for h_{avg} Factor Evaluating Several Model Order Cases
a) Full 3FI Model, b) Reduced 3FI Model, c) Full 2FI Model, d) Reduced 2FI Model

a)

ANOVA Summary

	Adjusted F-value	Model p-value	Unadjusted F-value	Model p-value
Model	6.366E+007	< 0.0001	17.79	< 0.0001
Curvature	6.366E+007	< 0.0001		

b)

ANOVA Summary

	Adjusted F-value	Model p-value	Unadjusted F-value	Model p-value
Model	6.366E+007	< 0.0001	13.99	< 0.0001
Curvature	6.366E+007	< 0.0001		

c)

ANOVA Summary

	Adjusted F-value	Model p-value	Unadjusted F-value	Model p-value
Model	18.24	< 0.0001	11.30	< 0.0001
Curvature	6.53	0.0084		

d)

ANOVA Summary

	Adjusted F-value	Model p-value	Unadjusted F-value	Model p-value
Model	65.17	< 0.0001	50.99	< 0.0001
Curvature	10.73	0.0024		

Table 23. R^2 Summary Analysis Table for h_{avg} Factor Evaluating Several Model Order Cases
a) Full 3FI Model, b) Reduced 3FI Model, c) Full 2FI Model, d) Reduced 2FI Model

a)

Std. Dev.	830.81	R-Squared	0.9810
Mean	8282.92	Adj R-Squared	0.9259
C.V. %	10.03	Pred R-Squared	-70.1928
PRESS	2.851E+010	Adeq Precision	15.862

b)

Std. Dev.	948.07	R-Squared	0.9731
Mean	8282.92	Adj R-Squared	0.9035
C.V. %	11.45	Pred R-Squared	-24.2991
PRESS	1.013E+010	Adeq Precision	14.306

c)

Std. Dev.	1154.61	R-Squared	0.9401
Mean	8282.92	Adj R-Squared	0.8569
C.V. %	13.94	Pred R-Squared	0.0147
PRESS	3.947E+008	Adeq Precision	13.679

d)

Std. Dev.	950.94	R-Squared	0.9210
Mean	8282.92	Adj R-Squared	0.9029
C.V. %	11.48	Pred R-Squared	0.8717
PRESS	5.139E+007	Adeq Precision	26.93

Although the suppressing the 3FI terms improves the model characteristics, both the ANOVA summary and R^2 tables for the two 2FI cases shows that a backward regression reduced model is

superior. Increases in F-values for the model and good agreement between the prediction R^2 and the R^2 adjusted for the number of model factors indicate that the reduced model is superior for navigating the design space. However, the statistical significance of curvature for even the reduced 2FI model is a first indication that our data may require transformation. Review of the diagnostic plots of Figures 41 and 42 support both the normality assumption and the potential need for a transformation. The expanding residual vs. predicted data distribution suggestion of the need for a transform is verified by the Box-Cox plot of Figure 43.

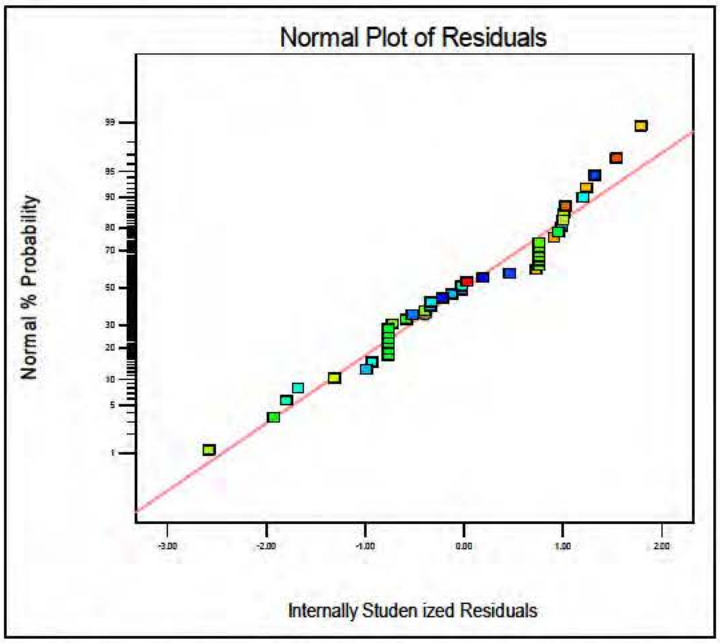

Figure 42. Normal Residual Plot for h_{avg} Reduced 2FI ANOVA Model

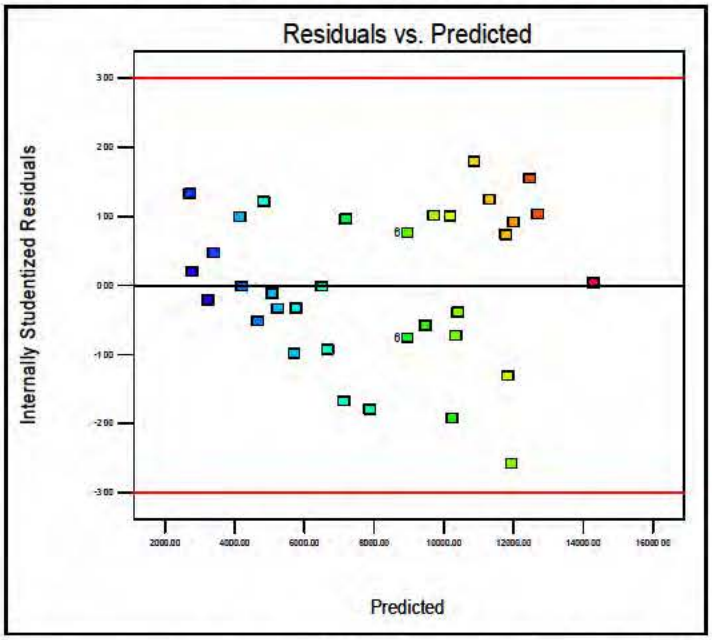

Figure 43. Residuals vs. Predicted Data for h_{avg} Reduced 2FI ANOVA Model

Thus, an additional h_{avg} response data analysis was conducted to include the recommended λ=1/2 transformation applied to the reduced 2FI model. Table 14 shows the ANOVA summary

and R^2 analysis for the transformed model data. As seen from the data the transform improved the agreement between prediction R^2 and adjusted R^2 while also yielding a PRESS value indicative of improved prediction capability. Figure 44 shows the residuals vs. predicted data plot for the transformed h_{avg} data showing a more random distribution of points reflecting an appropriate application of data transformation. Interestingly, all of the models evaluated predict that interaction factor AF (pin diameter-offset angle) is the most dominant term driving the h_{avg} response, followed in order by main effects C (Heatreatin), A (diameter), B (spacing), and then interaction DE (Tfluid-Mass flow rate). This is physically reasonable when considering that heat transfer coefficient is often calculated from the Nusselt number which is proportional to the Reynolds number, that is a strong function of the flow geometry, and mass flow rate. Furthermore, the conventional definition of h is the proportionality coefficient between heat rate in and the temperature difference and thus the inclusion of $Heat_{ratein}$ factor is appropriate. Thus, this apportionment of primary input factor importance for this response is considered fundamentally sound and consistent with the underlying physics of the system under consideration.

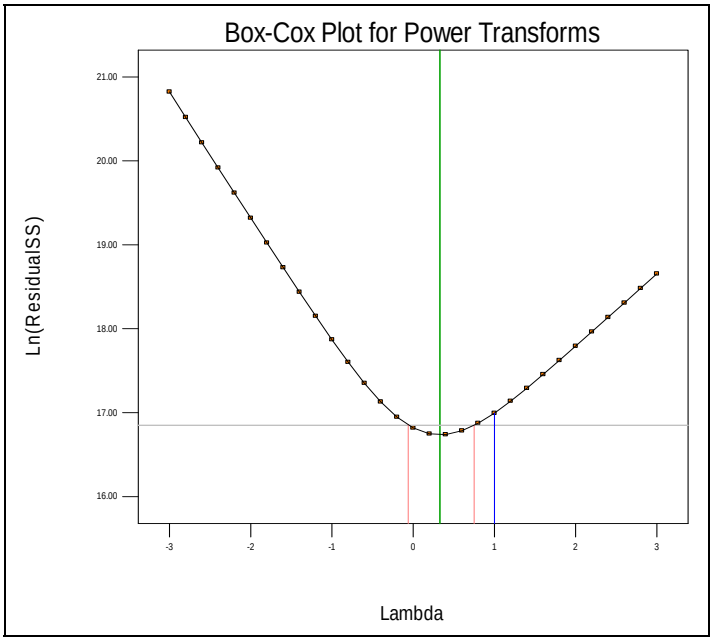

Figure 44. Box-Cox Plot for h_{avg} Reduced 2FI ANOVA Model

Table 24. ANOVA and R^2 Summary for Transformed, Reduced 2FI Model for h_{avg}

ANOVA Summary				
	Adjusted F-value	**Model p-value**	**Unadjusted F-value**	**Model p-value**
Model	83.36	< 0.0001	49.34	< 0.0001
Curvature	25.14	< 0.0001		

Std. Dev.	5.54	R-Squared	0.9185
Mean	89.35	Adj R-Squared	0.8999
C.V. %	6.20	Pred R-Squared	0.8753
PRESS	1643.77	Adeq Precision	26.477

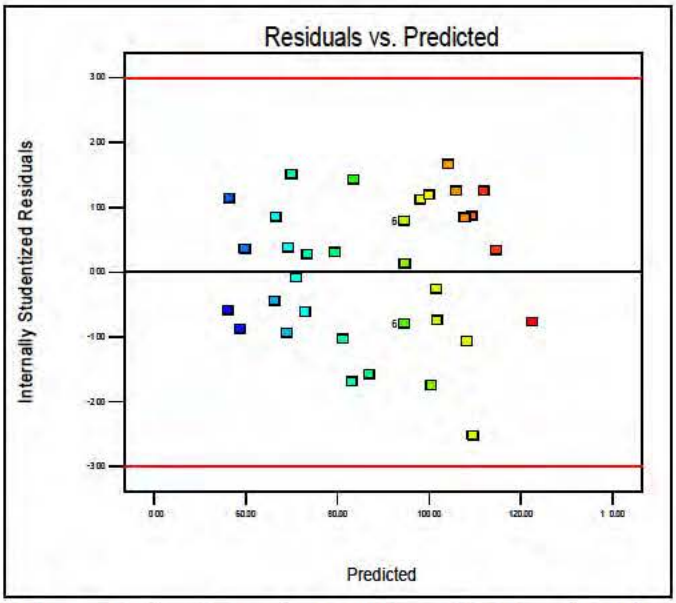

Figure 45. Residuals vs. Predicted Data for Transformed, Reduced 2FI h_{avg} ANOVA Model.

As a result of the improved predictability of the reduced and transformed 2FI data model, this was selected as the most appropriate model to proceed forward with to optimization and validation. Equations 8 and 9 list the coded and actual factor equations, respectively for this model As was done for the T_{max} model, Equation 10 and 11 show the main effects only equations, which also required a transformation with $\lambda=1/2$, for best predictability based on ANOVA analysis. Associated Response surface plots are included in Appendix B and clearly reflect the dominance of the interaction geometry term AF. The analysis now turns to the final response factor analysis, the pressure drop across the test cell, ΔP.

Equation 8. *Coded Factor Equation for Transformed and Reduced 2FI Model for h_{avg}*

$$\text{Sqrt}(h_{avg}) = +89.35 - 4.49 * A - 2.73 * B + 4.58 * C + 0.17 * D + 3.88 * E + 0.60 * F + 17.52 * A * F - 2.69 * D * E$$

Equation 9. *Actual Factor Equation for Transformed and Reduced 2FI Model for h_{avg}*

$$\text{Sqrt}(h_{avg}) = +361.39963 - 114.13032 * \text{Diameter} - 1.09036 * \text{Spacing} + 0.061038 * \text{HeatRateIn} + 0.15739 * \text{TfluidIn} + 30.56912 * \text{mdot} - 5.80154 * \text{OffsetAngle} + 2.33660 * \text{Diameter} * \text{OffsetAngle} - 0.43041 * \text{TfluidIn} * \text{mdot}$$

Equation 10. *Coded Factor Equation for Transformed Main Effects Only Model for h_{avg}*

$$\text{Sqrt(h\_avg)} = +89.35 - 4.49 * A - 2.73 * B + 4.58 * C + 0.17 * D + 3.88 * E + 0.60 * F - 0.95 * G$$

Equation 11. *Actual Factor Equations for Transformed Main Effects Only Model for h_{avg}*

GeometryCircular

$$\text{Sqrt(h\_avg)} = +104.75031 - 8.98336 * \text{Diameter} - 1.09036 * \text{Spacing} + 0.061038 * \text{HeatRateIn} + 6.74746E\text{-}003 * \text{TfluidIn} + 15.50462 * \text{mdot} + 0.039958 * \text{OffsetAngle}$$

GeometrySquare
Sqrt(h_avg) =+102.85930 -8.98336 * Diameter -1.09036 * Spacing +0.061038 * HeatRateIn
+6.74746E-003 * TfluidIn +15.50462 * mdot +0.039958 * OffsetAngle

5.3 ΔP Response Variable Evaluation

The ΔP response analysis will be presented with simply the optimized reduced model obtained following the same stepwise analysis as the preceding two response factors. It should be obvious by now that the aliasing of the quarter fraction factorial experiment leads to no useful information for model orders greater than 2FI. Even for factor screening we have shown that a main effects only model is superior thus we present only the 2FI and reduced 2FI model analysis summary below. As will be shown below, the ΔP data required a log (λ=0) transformation to provide acceptable predictability over the design space. Table 25 shows the same ANOVA summary data for full 2FI, reduced 2FI, and transformed and reduced 2FI models.

Table 25. ANOVA Summaries for Models
The following models are summarized: a) Full 2FI Model, b) Reduced 2FI Model, and c) Transformed and Reduced 2FI Model for ΔP

a)

ANOVA Summary	Adjusted F-value	Model p-value	Unadjusted F-value	Model p-value
Model	9.52	< 0.0001	8.01	< 0.0001
Curvature	2.69	0.0982		

b)

ANOVA Summary	Adjusted F-value	Model p-value	Unadjusted F-value	Model p-value
Model	20.99	< 0.0001	18.39	< 0.0001
Curvature	5.38	0.0273		

c)

ANOVA Summary	Adjusted F-value	Model p-value	Unadjusted F-value	Model p-value
Model	214.77	< 0.0001	104.40	< 0.0001
Curvature	41.17	< 0.0001		

As was the case for the previous response factor analysis, model order reduction and elimination of non-significant input factors improves the project predictability of our model. This is reflected by the increasing F-value with model reduction and ultimately transformation and the identification of the significance of curvature for reduced models. Table 26 shows the same improvement with order reduction and transformation for the R^2 analysis. In each case of order reduction the agreement between the important prediction R^2 and adjusted R^2 improves, also reflected by the decreasing PRESS statistic. Figure 45 and 46 are the relevant residual diagnostic plots for determining the need for a data transformation and they clearly indicate said scaling of the data is required. The Box Cox analysis results in a recommendation of a $\log_{10}$ transformation

(λ=0), which is what was used to generate the ANOVA summary and R^2 transformed data in the tables.

Table 26. R^2 Analysis for Models

a) Full 2FI Model, b) Reduced 2FI Model, and c) Transformed and Reduced 2FI Model for ΔP

Std. Dev.	106.57	a)	R-Squared	0.9176
Mean	182.94		Adj R-Squared	0.8031
C.V. %	58.26		Pred R-Squared	-0.6260
PRESS	4.032E+006		Adeq Precision	15.152

Std. Dev.	99.27	b)	R-Squared	0.8768
Mean	182.94		Adj R-Squared	0.8291
C.V. %	54.27		Pred R-Squared	0.6898
PRESS	7.692E+005		Adeq Precision	19.300

Std. Dev.	0.17	c)	R-Squared	0.9321
Mean	1.92		Adj R-Squared	0.9232
C.V. %	8.82		Pred R-Squared	0.9135
PRESS	1.39		Adeq Precision	32.691

Figure 47 shows the post transformed model residual vs. predicted plot with the desired random data scatter characteristic suggesting that the appropriate transform was invoked. Interestingly, the criticality of the applied transform in this instance is highlighted by the fact that the untransformed analysis showed that the primary input effects dictating ΔP response was AF (pin diameter-offset angle), C ($Heat_{ratein}$), and BD (pin spacing-$Fluid_{temp}$), in that order of their percent contribution. However, after the Log transformation was applied, the backward regression reduced 2FI model analysis indicated otherwise. In this case primary factors of importance were identified to be AF, C. B, and A. Thus, the untransformed model, although providing reasonable prediction statistic results (R^2, ANOVA results) would have led to an inappropriate attempt to optimize the response factors using incorrect primary input factor s of importance. The dominance of the geometry interaction term in this case is physically expected since the pin diameter (d) and offset angle (θ) primarily dictate channel conductance or restriction to flow. The other factors are truly minor in comparison for ΔP optimization as can be seen by reviewing the Effects List shown below in Table 27. At 82.4% the AF interaction factor clearly dominates.

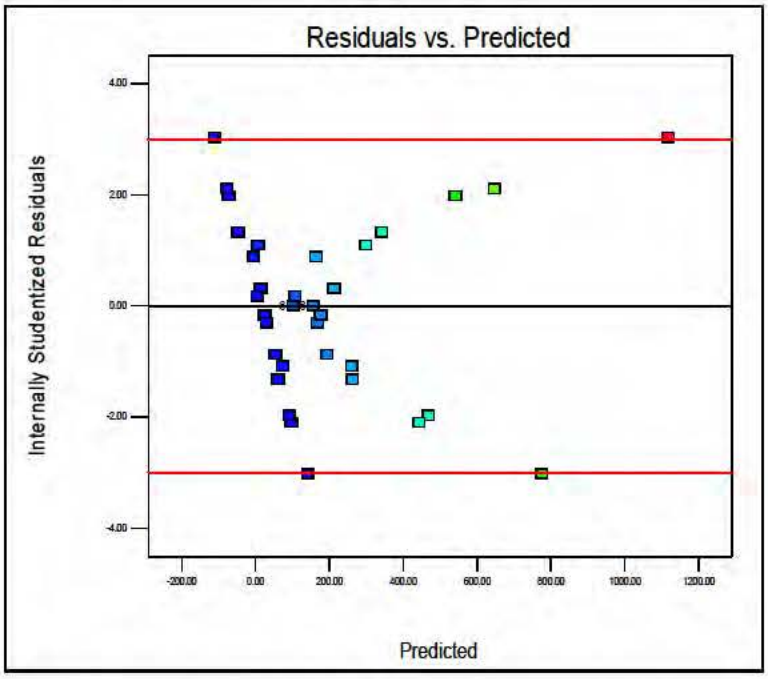

Figure 46. Residual vs. Predicted Data Showing Need for Transform for ΔP Data

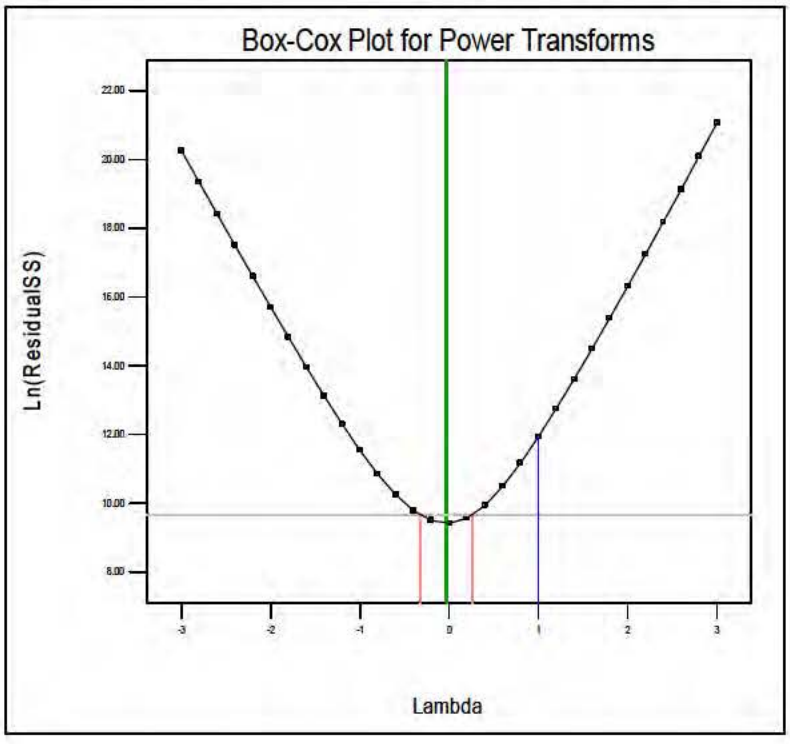

Figure 47. Box Cox Plot Suggesting Log(λ=0) Transform for ΔP Data

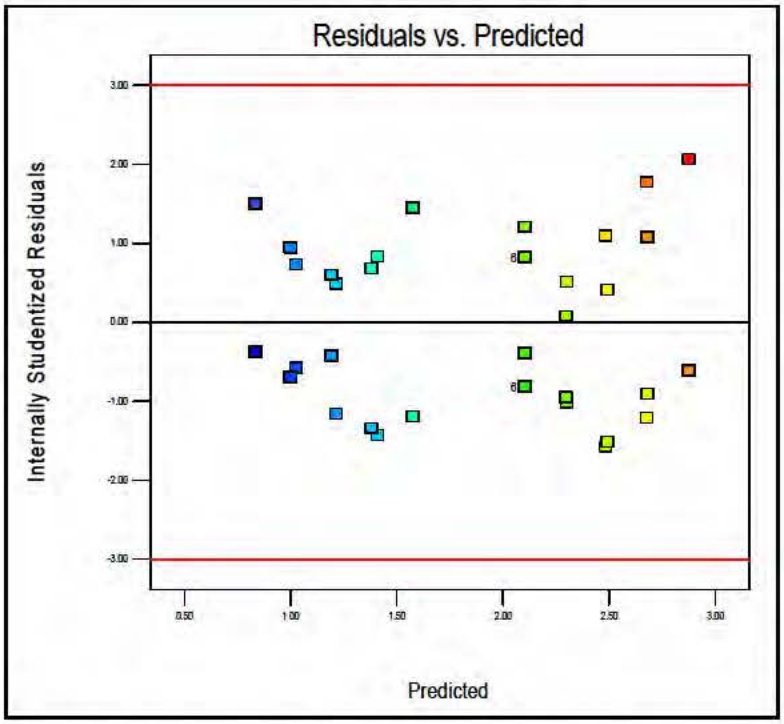

Figure 48. Residual vs. Predicted Data after Log Transform to ΔP Data

Table 27. Effects List for Transformed and Reduced 2FI ANOVA Model

	Term	Effect	SumSqr	% Contribtn
Model	A-Diameter	0.181794	0.264393	1.65008
Model	B-Spacing	0.193887	0.300738	1.87692
Model	C-HeatRateIn	-0.381559	1.1647	7.26893
Error	D-TfluidIn	-0.0172571	0.00238247	0.0148691
Error	E-mdot	-0.00508964	0.000207235	0.00129336
Model	F-OffsetAngle	0.0153933	0.00189562	0.0118306
Error	G-Geometry	-0.00353774	0.000100125	0.000624884
Error	AB	0.0203448	0.0033113	0.0206659
Error	AC	-0.0321236	0.00825541	0.0515223
Error	AD	0.00539444	0.0002328	0.00145291
Error	AE	-0.0092173	0.000679669	0.00424184
Model	AF	1.28472	13.204	82.4068

Finally, Equations 12-13 list the coded and actual factor equations for the transformed and reduced 2FI model. Due to the dominance of the AF interaction term for this response variable, a reduced main effects model contained no terms and thus an equation could not be generated. Even without the backward regression reduction the main effects model was not found to be statistically significant, as expected. Thus, main effects equations are not available for the ΔP factor.

Finally, response surface plots are found in Appendix C for the parsimonious model and at a glance at 5) shows the strong, nonlinear response of ΔP to input factors AF. The following section summarizes an initial validation exercise using the actual factor ANOVA model equations compared to ANSYS Fluent™ generated data for 8 additional runs not included in the baseline factorial experiment.

Equation 12. *Coded Factor Equation for Transformed and Reduced 2FI Model for ΔP*

$$Log_{10}(DeltaP) = +1.92 + 0.091 * A + 0.097 * B - 0.19 * C + 7.697E\text{-}003 * F + 0.64 * A * F$$

Equation 13. *Actual Factor Equation for Transformed and Reduced 2FI Model for ΔP*

$$Log_{10}(DeltaP) = +11.14115 - 3.67237 * Diameter + 0.038777 * Spacing - 2.54373E\text{-}003 * HeatRateIn - 0.21361 * OffsetAngle + 0.085648 * Diameter * OffsetAngle$$

5.4 ANOVA Model Comparison to CFD Results

Subsequent to the ¼ fraction experimental data ANOVA analysis and generation of surrogate model equations for the three response variables of interest, a comparison with CFD results for 8 additional runs was accomplished. The additional runs were outside the core ¼ fraction factorial design space but within the larger (128 run) full factorial space defined by the 7 input factors and their respective levels. Using the parsimonious actual factor equations listed in the previous sections for T_{max}, h_{avg}, and ΔP, values for the input factors from the 8 additional Fluent™ runs were used to calculate estimates of the response variables and compared to CFD results. In addition, response variables were also generated using the main effects only models as an additional comparison to explicitly show the utility of these models for main effects screening purposes. Table 28 is an organized summary of the input factor levels used a) and the results of the three calculations b).

Table 28. Input a) and Response Factor b) Values from a Comparison Calculation using CFD,

	Input Factors						
Run	Geometry	A-D (mm)	B-S (mm)	C-Q(W/cm^2)	D-T(^{0}C)	E-mdot(kg/s)	F-angle
1	cylinder	3.00E+00	4	50	60	0.6	30
2	cylinder	2.00E+00	4	200	60	0.6	60
6	cylinder	3.00E+00	9	50	60	0.1	60
7	cylinder	2.00E+00	9	200	60	0.1	30
10	square	2.00E+00	4	200	10	0.6	30
12	square	2.00E+00	9	200	10	0.1	60
14	square	3.00E+00	4	50	10	0.6	60
15	square	3.00E+00	9	50	10	0.1	30

a)

CFD Response Factors			Reduced 2FI Model Response			Main Effects Model		
T-max(^{0}C)	ΔP (Pa)	h (W/m^2-K)	T-max(^{0}C)	ΔP (Pa)	h (W/m^2-K)	T-max(^{0}C)	ΔP (Pa)	h (W/m^2-K)
77.4	710.928	10669	175.901	28.311	4395.906	156.107	N/A	7638.244
152	237.652	14355	242.208	8.015	7343.624	179.432	N/A	11392.328
96.9	83.50	6560	145.577	882.724	8979.331	104.257	N/A	5683.905
197	94.50	7265	201.359	232.906	12468.547	127.107	N/A	8525.198
86	622.568	6753	114.722	149.049	15507.459	98.916	N/A	10672.424
175	8.962	4693	100.648	12.524	5203.985	47.066	N/A	8336.066
30.6	646.970	8854	72.514	564.904	11583.276	76.066	N/A	7459.277
41.8	18.576	4265	68.015	44.239	2782.070	23.741	N/A	5178.854

b)

The first thing noticeable about the surrogate model results is that they are inconsistent and highly "variable" in their fidelity to the CFD values over the range of input factors assessed. This is not unexpected as the ¼ fraction design has utility primarily as a screening tool to identify the

factors of primary importance to a given response of interest. In other words, the ANOVA models at best have acceptable predictability within the factorial space and dubious utility for prediction outside that range. Table 29 quantifies the degree with which the reduced 2FI and main effects models agree with the deterministic CFD results. While not altogether unexpected, the main effects model is immediately seen to be superior to the reduced 2FI model in its' ability to yield results in better agreement with the CFD data. The lack of ΔP data for the main effects model is due to the fact that the ANOVA analysis showed that there were no main effects of statistical significance at the 5% level and the response was dominated by the highly nonlinear saddle shape AF interaction term (reference response surface plot in Appendix C). Thus, an ANOVA equation could not be generated for a main effects model. Furthermore as seen in the Table below, the 2FI reduced model for ΔP yields the greatest degree of inaccuracy compared to CFD response factor results. This is due to the highly nonlinear response of the dominant factor (AF) and the required inclusion of statistically insignificant terms to satisfy model hierarchy.

Table 29. Comparison of the Two ANOVA Models to the Fluent™ CFD Results

Reduced 2FI Model Response			Comparison to CFD Results		
T-max(^{0}C)	ΔP (Pa)	h (W/m^2-K)	% Error T_{max}	% Error (ΔP)	% Error (h)
175.901	28.311	4395.906	127.3	-96.0	-58.8
242.208	8.015	7343.624	59.3	-96.6	-48.8
145.577	882.724	8979.331	50.2	957.2	36.9
201.359	232.906	12468.547	2.2	146.5	71.6
114.722	149.049	15507.459	33.4	-76.1	129.6
100.648	12.524	5203.985	-42.5	39.8	10.9
72.514	564.904	11583.276	137.0	-12.7	30.8
68.015	44.239	2782.070	62.7	138.1	-34.8

Main Effects Model			Comparison to CFD Results		
T-max(^{0}C)	ΔP (Pa)	h (W/m^2-K)	% Error T_{max}	% Error (ΔP)	% Error (h)
156.107	N/A	7638.244	101.7	N/A	-28.4
179.432	N/A	11392.328	18.0	N/A	-20.6
104.257	N/A	5683.905	7.6	N/A	-13.4
127.107	N/A	8525.198	-35.5	N/A	17.3
98.916	N/A	10672.424	15.0	N/A	58.0
47.066	N/A	8336.066	-73.1	N/A	77.6
76.066	N/A	7459.277	148.6	N/A	-15.8
23.741	N/A	5178.854	-43.2	N/A	21.4

This comparison with additional CFD runs outside the core fractional factorial design space solidifies the notion that additional follow-on experiments must be accomplished to improve physical fidelity and surrogate model predictability. Main effects screening can be accomplished in various manners; response surface and/ contour plot behavior, half normal, ANOVA coefficients, or Pareto chart magnitude comparison. Each is equivalent but the Design Expert effects list enables a comparison of the standardized effects (2X ANOVA coefficients) and percent contribution to the results. If all terms have the same DOF then the percent contribution value is a direct measure of the significance of each included term. Therefore, for this analysis the Effects lists were compared for each response variable to define the primary input factors of importance. Table 30 shows the reduced 2FI and the main effects lists for the ANOVA analysis of the Tmax response variable.

Table 30. Effects List ANOVA Data for T_{max} a) 2FI and b) Main Effects Models.

a)

Reduced 2FI Effects List for T_{max} Response				
	Term	Effect	SS	% Contribtn
Model	D-TfluidIn	78.3875	49156.8	65.8071466
Model	E-mdot	42.0375	14137.21	18.9257541
Model	AF	-19.6875	3100.781	4.15107495
Model	C-HeatRateIn	19.425	3018.645	4.04111759
Model	CD	11.825	1118.645	1.49755138
Model	BC	-10.0625	810.0313	1.08440427
Model	B-Spacing	-10.05	808.02	1.08171177
Model	BD	-9.2	677.12	0.90647345
Model	DE	-6.5375	341.9112	0.45772311
Model	CE	5.025	202.005	0.27042794
Model	A-Diameter	-3.6625	107.3113	0.14365962
Error	BE	-2.375	45.125	0.0604097
Error	AD	-2.0875	34.86125	0.04666942
Error	BG	1.5375	18.91125	0.02531685
Error	AE	1.4625	17.11125	0.02290716
Error	AG	-1.125	10.125	0.01355453
Error	AC	0.45	1.62	0.00216872
Error	G-Geometry	-0.35	0.98	0.00131194
Error	CF	0.325	0.845	0.00113122
Error	BF	0.3	0.72	0.00096388
Model	F-OffsetAngle	0.2375	0.45125	0.0006041
Error	CG	0.0875	0.06125	8.1997E-05
Error	AB	-0.075	0.045	6.0242E-05

b)

Main Effects List for T_{max} Response				
	Term	Effect	SumSqr	% Contribtn
Model	D-TfluidIn	78.3875	49156.8	65.7733778
Model	E-mdot	42.0375	14137.21	18.9160424
Model	C-HeatRateIn	19.425	3018.645	4.0390439
Model	B-Spacing	-10.05	808.02	1.08115669
Model	A-Diameter	-3.6625	107.3113	0.1435859
Model	G-Geometry	-2.21729	39.33091	0.05262602
Model	F-OffsetAngle	0.2375	0.45125	0.00060379

As seen in the data, both models predict the same main effects of importance driving the maximum temperature response variable. In addition, the 2FI model shows a modest contribution from geometry interaction term AF, CD, BC and CE which are retained at the 5% level. This information will be used to identify the factors of focus for follow-on experiments that will be designed to yield surrogate models with a high degree of predictability. Of specific note with regards to the Tmax Effects List comparison is the fact that both models predict the order (D, E, C, B, A, G, and F) and % contribution with excellent agreement. The comparison tables for havg and P response variables are shown in Tables 31 and 32, respectively. The results of the Design Expert analysis for these two response factors mirrors that of Tmax in terms of agreement between reduced 2FI and main effects only modes when identifying the relative strength of the input factor main effects. In Table 31 we see that both models predict a dominance of main effect C, at 5%, followed by A, E, B, F, and, D. On the other hand, the main effects only model would miss the overwhelming dominance of geometry interaction term AF. Thus, in this case the main effects model accurate allocates contribution for the main input factors, the reduced 2FI model is required to identify the truly dominant effect, that being the diameter-offset angle geometry factor. $Heat_{ratein}$ is certainly a factor for h_{avg} since it is fundamentally defined as the proportionality coefficient for convective heat transfer. However, in the context of heat sink characteristics, the fin geometry is the dominant defining characteristic from a practical correlation equation standpoint. Similar results are seen for the 2FI and main effects model comparison for the ΔP data in Table 32. Again, the dominance of interaction term AF is the most significant input factor for consideration. Once again this is not surprising since fin geometry and layout drive the channel conductance (flow restriction). Consistent with the prior two analyses, the main effects order of importance is identical for the two models. In this case, the C factor was significant at approximately the 10%

level, above the 5% alpha cutoff selected for the ANOVA analysis. The minor contribution for this factor is likely due to the reduction in viscosity of water at higher temperatures.

Table 31. Effects List ANOVA Data for havg a) 2FI and b) Main Effects Models

a)

Reduced 2FI Effects List for h_{avg} Response				
	Term	Effect	SumSqr	% Contribtn
Model	AF	35.04898645	9827.451609	74.56462744
Model	C-HeatRateIn	9.155752194	670.622386	5.088268083
Model	A-Diameter	-8.98335682	645.605598	4.898456162
Model	E-mdot	7.752309759	480.7864528	3.64791038
Model	B-Spacing	-5.45181067	237.7779163	1.804111834
Model	DE	-5.3801772	231.570454	1.757013447
Error	BG	-2.47775992	49.11435375	0.372649354
Error	CE	1.709239713	23.37200316	0.177332311
Error	AG	1.381449137	15.26721375	0.11583818
Model	F-OffsetAngle	1.198749216	11.49599747	0.087224522
Error	CF	1.110677665	9.868839	0.074878649
Error	AC	0.854328041	5.839011214	0.044302807
Error	BE	0.761402363	4.637868466	0.035189279
Error	BC	-0.70225105	3.945252302	0.029934135
Error	AD	0.68572186	3.761715756	0.028541574
Error	AE	0.566743982	2.569589928	0.01949646
Error	CG	0.518440872	2.150247501	0.016314749
Error	AB	0.505899388	2.047473529	0.015534963
Model	D-TfluidIn	0.337373019	0.910564431	0.0069088
Error	BF	0.248854328	0.495427813	0.003759
Error	CD	0.230735806	0.425912097	0.003231558
Error	G-Geometry	-0.17367888	0.241314829	0.001830948
Error	BD	-0.14420534	0.166361429	0.001262248

b)

Main Effects List for h_{avg} Response				
	Term	Effect	SumSqr	% Contribtn
Model	C-HeatRateIn	9.155752194	670.622386	5.088268083
Model	A-Diameter	-8.98335682	645.605598	4.898456162
Model	E-mdot	7.752309759	480.7864528	3.64791038
Model	B-Spacing	-5.45181067	237.7779163	1.804111834
Model	F-OffsetAngle	1.198749216	11.49599747	0.087224522
Model	D-TfluidIn	0.337373019	0.910564431	0.0069088

Table 32. Effects List ANOVA Data for ΔP a) 2FI and b) Main Effects Models

a)

Reduced 2FI Effects List for ΔP Response				
	Term	Effect	SumSqr	% Contribtn
Model	AF	1.28472	13.204	82.4068
Model	C-HeatRateIn	-0.381559	1.1647	7.26893
Model	B-Spacing	0.193887	0.300738	1.87692
Model	A-Diameter	0.181794	0.264393	1.65008
Error	AC	-0.0321236	0.008255	0.0515223
Error	AB	0.0203448	0.003311	0.0206659
Error	D-TfluidIn	-0.0172571	0.002382	0.0148691
Model	F-OffsetAngle	0.0153933	0.001896	0.0118306
Error	AE	-0.0092173	0.00068	0.00424184
Error	AD	0.00539444	0.000233	0.00145291
Error	E-mdot	-0.00508964	0.000207	0.00129336
Error	G-Geometry	-0.00353774	0.0001	0.000624884

b)

Main Effects List for ΔP Response				
	Term	Effect	SumSqr	% Contribtn
Model	C-HeatRateIn	-0.38155937	1.1647	7.268930983
Model	B-Spacing	0.193887208	0.300738	1.876915009
Model	A-Diameter	0.181794013	0.264393	1.650081701
Model	D-TfluidIn	-0.01725714	0.002382	0.014869079
Model	F-OffsetAngle	0.015393273	0.001896	0.01183064
Model	E-mdot	-0.00508964	0.000207	0.001293361
Model	G-Geometry	-0.00353774	0.0001	0.000624884

In summary, the model comparison exercise highlighted two facts of relevance. First, the main effects model provided greater fidelity to the deterministic CFD model data which I am attributing to the necessary inclusion of insignificant terms in the reduced 2FI model to satisfy hierarchy. This results in an inflation of variance throughout the residuals ANOVA analysis leading to a less accurate model. This problem could be avoided or minimized if we had conducted a higher resolution design (> IV). The cost of 2X to 4X greater number of experimental runs was prohibitive in this case. Secondly, the main effects model was measurably better at predicting the expanded design space data points. However, for both the heat transfer coefficient and the pressure drop response factors, the main effects only model would have not identified the dominant AF interaction factor as relevant if used exclusively as a screening tool. Thus, both of

these point to the need to assess all the available data and analyses for statistical AND physical relevance. In addition, this analysis will be crucial in defining a follow-up designed experiment in which insignificant factors are eliminated and a higher resolution design approach taken. A review of the effects list Tables above, and the response surface 3D graphs in the Appendix lead to a conclusion that the Geometry (G) and Spacing (B) can be removed for subsequent experiment designs. Geometry had a very minor impact on any of the response factors and was not involved in any significant interactions. Spacing was a < 2 % contributing factor as a model term and physically can be derived from the pin diameter and offset angle factors if a lower limit is specified as a function of pin diameter. In addition, $Heat_{rarein}$ (C) would likely be better relegated to a fixed boundary condition rather than an input factor as it is actually better suited as an operational response variable for a power device electrical operating condition. It could also be a block variable in a subsequent higher resolution factorial design. However, before specifying follow-on design factors an optimization of the current fractional factorial design needs to be conducted. That is the subject of the following section.

6 Design Optimization

For simple designed experiments with 3 or fewer input factors, the process of determining the optimal settings for a desired response output can be accomplished quite readily using graphical methods. Contour plots or 3D response surface plots can be visually and/or analytically assessed to determine the direction of "maximum ascent" that an input variable must move in order to maximize or minimize a specific response. These expectation value surfaces, generated using the ANOVA equations, and their companion topography 2D contour plots, enable a visualization of the impact of design variable changes on a given response variable. Overlaying contour plots for assessing two input factors to determine a region of feasible settings leading to a desired response specification is straightforward process, as is moving a variable setting in the direction orthogonal to the contour lines of equal response value. However, 7 input factors require the simultaneous assessment of 15 contour plot pairs and are prohibitively difficult to accomplish manually. This is further exacerbated when 3 response factors require optimization as in this case. Fortunately, Design Expert has automated this process and it is readily executed by selecting limits for the input and response factors along with weights designating relative importance. Since we are considering a Res IV fractional design, we have left the input factor upper and lower limits the same as specified in the factorial space design. This is because of the poor predictability of the ANOVA model outside the design space.

Table 33 summarizes the design optimization routine settings copied from the Design Expert menu dialog for this experiment. T_{max} was selected for minimization along with the pressure drop across the test cell to minimize power device die temperature and coolant fluid pump size and weight, respectively. Maximization of convective heat transfer is achieved through a maximum value specification for h_{avg}. As seen in the table, T_{max} is selected as the highest optimization priority followed by h_{avg} and ΔP. The reasoning being that while they are all coupled, power component functionality and reliability necessitate that the die junction temperature remain below a fixed specification limit. Higher operating temperatures translate to reduced device life expectancy, while exceeding a specified upper limit leads to rapid, catastrophic failure.

Table 33. Design Expert Summary of the Numerical Optimization Algorithm

Constraints

Name	Goal	Lower Limit	Upper Limit	Lower Weight	Upper Weight	Importance
A:Diameter	is in range	2	3	1	1	3
B:Spacing	is in range	4	9	1	1	3
C:HeatRateIn	is in range	50	200	1	1	3
D:TfluidIn	is in range	10	60	1	1	3
E:mdot	is in range	0.1	0.6	1	1	3
F:OffsetAngle	is in range	30	60	1	1	3
Tmax	minimize	25.1	208	1	1	5
h_avg	maximize	2920.89	14333.4	1	1	4
DeltaP	minimize	6.22847	1246.31	1	1	3

Table 34 is an organized listing of the Design Expert optimization numerical routine results for the 10 best solutions (out of 47 found) given the parameter settings of the previous table.

Table 34. Top 10 Optimized Design Settings from Design Expert Numerical Routine

Solutions Number	Diameter	Spacing	HeatRateIn	TfluidIn	mdot	OffsetAngle	Geometry*	Tmax	h_avg	DeltaP	Desirability
1	2.00	4.09	200.00	10.00	0.11	30.10	*Circular*	38.1016	12431.6	148.821	0.885
2	2.00	4.10	200.00	10.81	0.10	30.00	*Circular*	38.2178	12389.2	150.383	0.883
3	2.00	4.00	198.85	10.00	0.19	30.02	*Circular*	46.6165	12903.1	149.035	0.880
4	2.00	5.13	196.40	10.00	0.10	30.06	*Circular*	34.1193	12056.4	167.23	0.878
5	2.00	5.65	200.00	10.45	0.10	30.01	*Circular*	34.0126	12003.3	172.497	0.876
6	2.00	4.07	169.94	10.00	0.10	30.42	*Circular*	34.4134	11858	171.194	0.870
7	2.02	5.79	200.00	10.54	0.10	30.00	*Circular*	34.2423	11779.4	165.933	0.869
8	2.00	4.33	148.95	10.00	0.10	30.01	*Circular*	32.5007	11650.6	206.905	0.860
9	2.00	4.00	159.43	12.35	0.16	30.10	*Circular*	43.8427	12205.3	187.326	0.858
10	2.00	8.85	200.00	10.01	0.13	30.01	*Circular*	29.9127	11440.9	229.684	0.854

The solutions are listed in rank order based on the desirability index. Immediately obvious from a perusal of the data is the fact that input factors A, D, E, and F are all selected at the lower limit of their respective input factor ranges. This is possibly an indication that subsequent experiment design should specify levels centered near these lower limits when physically practical. For instance, there is an obvious manufacturing lower limit for the pin fin diameter as well as a mechanical rigidity requirement. The requirement for a lower temperature working fluid is obvious from simple convective heat transfer ΔT considerations, although practical implementation factors would reject the inclusion of fluid refrigeration cost/volume/weight. In practice this is a variable quantity dependent upon the heat capacity of the fluid and the amount of energy absorbed. However, for heat sink design purposes this is a critical factor and realistic average fluid temperature value levels are an acceptable compromise. The fact that mass flow is optimized at its lower level is somewhat surprising. Typically, higher mass flow conditions result in larger Re numbers and an increase in heat transfer coefficient. It will be necessary to critically review the flow conditions in the CFD output to fully understand this, but it may be that geometry-restriction-flow conditions maximize heat transfer in the computation. Finally, the suggested low setting for the row offset angle factor requires exploration. Low (30^o) angle factors result in increased fin density and reduced fluid conductance. This in turn likely increases Re-number and certainly increases surface area in the flow field, both of which will increase convective heat transfer. Since our response factor pressure drop across the pin fin array is seen to be very small (~12-650 Pa) for all experiments in the design space, we can increase the pin fin density beyond that of the base experiment to improve heat transfer functionality without significant pumping penalty. Finally, factor C, heat rate input, is near its upper level (200 W/cm^2) for the entire top ten numerically calculated optimized solution set. This is likely in response to the specified maximization of the heat transfer coefficient ($q = h\Delta T$), which when coupled with the minimum T_{max} specification requires q be maximized to result in a large convective heat transfer coefficient h_{avg}. This is physically correct but highlights again that the heat rate input would be better suited for an external boundary condition limit. Large q is achieved only at the expense of a high junction temperature in the power semiconductor device. The subject design specified T_{max} as the temperature on the upper surface of the channel at the point where the pin fins attach. Finite thermal conductivity of the intermediate layers between this surface and the semiconductor die result in higher temperatures at the device level. High internal temperatures in the die result in larger magnitude temperature cycling during switching operation which mechanically fatigues die and wire bond attachment metallurgies shortening functional life. Thus, heat rate input will be a fixed boundary condition in subsequent designs while T_{max} may be moved to a grid point on the lower surface of the switching device for improved visualization of the critical device temperatures. Companion response surface summary plots for T_{max} are shown in Appendix D for the optimized solution settings associated with the maximum desirability ranking (0.885). Included on the 3D plots is the calculated minimum temperature design point.

After performing the initial optimization computation it was instructive to vary the range limit goals and view alternative "optimized" settings. Table 35 is a summary of the top 10 design settings in which the heat transfer coefficient was unrestricted and allowed to vary within its range (2921-14333 Wm^2K).

Table 35. Top 10 Optimized Design Settings with h_{avg} Specification within Range Only

Solutions Number	Diameter	Spacing	HeatRatein	Tfluidin	mdot	OffsetAngle	Geometry*	Tmax	h_avg	DeltaP	Desirability
1 Selected	2.81	8.62	199.99	10.00	0.10	44.82	*Circular*	33.6918	6709.51	72.6092	0.951
2	2.59	9.00	200.00	10.25	0.10	45.46	*Circular*	34.0123	7022.51	69.7968	0.950
3	2.79	9.00	200.00	10.00	0.10	51.53	*Circular*	30.498	7486.8	109.396	0.950
4	3.00	4.00	50.00	10.03	0.10	39.34	*Circular*	34.1168	4822.69	71.9363	0.949
5	2.83	4.00	50.00	10.00	0.10	39.73	*Circular*	33.2447	5414.68	83.2486	0.949
6	2.75	4.00	50.00	10.00	0.10	40.35	*Circular*	32.8228	5727.5	90.2468	0.948
7	2.44	4.00	50.01	10.02	0.10	42.88	*Circular*	32.3296	6639.84	102.357	0.946
8	2.89	4.43	53.74	10.00	0.10	37.42	*Circular*	35.6887	4863.01	67.7854	0.945
9	2.28	8.38	188.11	10.00	0.10	38.82	*Circular*	34.6787	7964.13	79.7429	0.945
10	2.06	4.00	50.01	10.00	0.10	42.67	*Circular*	32.522	7580.18	104.192	0.945

First noticeable effect is that the desirability is now closer to 1.00, which is expected since we removed restrictions on the possible solution set. Also notable is the fact that now factors A, B, C, and F are no longer pinned to their lower setting. In addition, the maximum temperature is slightly lower than the optimized design above, similarly for the ΔP response. h_{avg} is roughly half that from the previous optimization, and most notably several solutions contain the lower q_{in} value of 50 W/cm^2. Input factor D, fluid temperature, is still pinned to the low setting of 10^oC needed to realize the low ~35^oC T_{max} minimized response. As mentioned above, a practical consideration for coolant fluid necessitates evaluation of the use of warmer temperature operation. Thus, an additional optimization run was accomplished in which the fluid temperature was fixed at the level midpoint value of 35^oC. Table 36 shows the ten most "desirable" solutions for this optimization. Due to the coupled dependency of q_{in} and T_{fluid}, the heat rate optimal solution now favors the lower level to achieve minimum T_{max}, which is notable higher as expected but well within a reasonable range.

Table 36. Top 10 Optimized Design Settings with h_{avg} Specification within Range Only and $T_{fluid}=35^oC$

Solutions Number	Diameter	Spacing	HeatRatein	Tfluidin	mdot	OffsetAngle	Geometry*	Tmax	h_avg	DeltaP	Desirability
1	2.66	4.00	50.00	35.00	0.10	41.28	*Circular*	73.774	6507.36	97.1074	0.851
2	2.77	4.00	56.16	35.00	0.10	42.14	*Circular*	74.6945	6372.66	93.8228	0.849
3	2.74	4.13	50.00	35.00	0.10	49.62	*Circular*	71.0935	7077.15	144.52	0.849
4	3.00	9.00	189.29	35.00	0.10	46.62	*Circular*	74.5198	7079.07	102.779	0.848
5	2.32	4.00	50.00	35.00	0.11	32.73	*Circular*	71.5278	8092.18	144.593	0.848
6	2.48	6.13	51.08	35.00	0.10	32.63	*Circular*	73.1747	6642.97	125.641	0.847
7	2.62	4.00	62.43	35.00	0.10	47.69	*Circular*	74.5454	7083.71	107.285	0.847
8	2.64	9.00	180.72	35.00	0.10	51.87	*Circular*	75.486	7636.11	95.6763	0.846
9	2.40	9.00	158.99	35.00	0.10	32.32	*Circular*	75.1276	7775.2	102.753	0.846
10	2.85	9.00	124.31	35.00	0.10	40.93	*Circular*	76.0798	5785.58	90.2678	0.846

There are a prohibitively large number of alternative optimization settings that could be assessed. However, the primary purpose of this exercise for the ¼ fraction design is to point us in the direction of an optimized follow-on experiment to provide the fidelity required for prediction within the design space as well as to explore new areas. The combined results of the previous factor screening assessment and the present optimization summary should provide the information necessary to define the next experiment. A good exercise at this point would be to conduct additional CFD runs at several calculated optimization factor settings. Unfortunately, we have lost our CFD expertise and have yet to replace that resource. As a result, we are resigned to identify our follow-on design, which hopefully can be accomplished in the near future.

7 Summary

Based on what we have learned thus far and the information gained from the ¼ fraction design, it is recommended that we project our fractional 2^{7-2} experiment design onto a full 2^5 factorial design to further refine our models factor dependence, reduce error, and improve prediction fidelity. The optimization analysis conducted in the previous section has provided us with a good indication as to where the factor level settings (+/-) should be our follow-up design. As seen during the response analysis in the previous sections, the results obtained are suitable for factor screening of important input terms. In addition, we observed that factors such as pin spacing (B) and geometry (G) provide little advantage for our stated objectives. ANOVA analysis indicated the geometry was not a significant factor driving the response of any of our response variables and only a very slight advantage was attributed to the circular cross section shape. Furthermore, pin spacing (B) was involved as a main factor as a less than 2% contributor for any of the three response factors. Similarly for any statistically significant two factor B-interaction term (BC, BD for T_{max}) the percent contribution to the response results was approximately 1% or less. Thus, we can confidently demote these two input factors to yield 5 input factors remaining. Offset angle (F) was not identified as statistically significant, but the AF interaction was a dominant factor for both ΔP and h_{avg}, thus it must be retained. Previous discussion postulated that the $heat_{ratein}$ (C) factor may be better served as an external fixed boundary condition. On the other hand, in practice it is probably best characterized as a controllable nuisance variable (power module or component design), which may be best suited for design use as a blocking variable. However, due to the poor fidelity and predictability of the completed quarter fraction design, and the prominence of this factor in the ANOVA results, it has been determined that it would be best not to fundamentally change the design space until after the factorial process analysis is complete. Further model refinement may be necessary using RSM or other DOE design methodology. Table 37 is the input factor summary and design layout in standard order for the 2^5 full factorial design recommendation based on current project analysis and practical SME considerations. The lack of aliasing in the full factorial structure, coupled with the deterministic CFD experiments, will enable a good determination of optimal design settings and should enable reasonable surrogate model realization. Also included in the proposed design are 6 center points for estimation of curvature. One thing of note that has changed in terms of the level settings is the reduction of the low (-) settings for offset angle (B) and mass flow rate (E). These values were reduced based on the optimization analysis in which the lower values were consistently identified as optimal settings in the fractional factorial analysis. Thus, the angle reduction and mass flow rate low level adjustments should enable the full factorial follow-on experiment to further refine and identify the optimal settings in the direction (lower) suggested by the quarter fraction experiment analysis. Finally, Table 38 shows the DOF distribution from the Design Expert experiment evaluation for a 3FI model. As seen in the table, sufficient DOF are distributed across both Lack of Fit and Pure Error for complete residual analysis including confidence in detecting lack of fit. A 3FI model will be assessed initially since this model will in principle have higher fidelity and be able to identify possible higher order interactions of importance if they exist.

Table 37. Factor list and Design Layout for Recommended Follow-up Full Factorial Experiment

Name	Units	Type	Std. Dev.	Low	High
Diameter	mm	Factor	0	2	3
Offset Angle	degrees	Factor	0	25	60
HeatRateIn	W/cm2	Factor	0	50	200
TfluidIn	oC	Factor	0	10	60
mdot	kg/s	Factor	0	0.025	0.3
Tmax	oC	Response			
h_avg	W/m2K	Response			
DeltaP	Pa	Response			

		Factor 1	Factor 2	Factor 3	Factor 4	Factor 5
Std	Run	A:Diameter	B:Offset Angle	C:HeatRateIn	D:TfluidIn	E:mdot
		mm	degrees	W/cm2	oC	kg/s
17	1	2	25	50	10	0.3
28	2	3	60	50	60	0.3
19	3	2	60	50	10	0.3
35	4	2.5	42.5	125	35	0.1625
29	5	2	25	200	60	0.3
37	6	2.5	42.5	125	35	0.1625
32	7	3	60	200	60	0.3
6	8	3	25	200	10	0.025
20	9	3	60	50	10	0.3
36	10	2.5	42.5	125	35	0.1625
3	11	2	60	50	10	0.025
27	12	2	60	50	60	0.3
34	13	2.5	42.5	125	35	0.1625
25	14	2	25	50	60	0.3
38	15	2.5	42.5	125	35	0.1625
13	16	2	25	200	60	0.025
30	17	3	25	200	60	0.3
1	18	2	25	50	10	0.025
10	19	3	25	50	60	0.025
9	20	2	25	50	60	0.025
11	21	2	60	50	60	0.025
16	22	3	60	200	60	0.025
26	23	3	25	50	60	0.3
21	24	2	25	200	10	0.3
12	25	3	60	50	60	0.025
23	26	2	60	200	10	0.3
7	27	2	60	200	10	0.025
8	28	3	60	200	10	0.025
31	29	2	60	200	60	0.3
4	30	3	60	50	10	0.025
24	31	3	60	200	10	0.3
15	32	2	60	200	60	0.025
33	33	2.5	42.5	125	35	0.1625
14	34	3	25	200	60	0.025
22	35	3	25	200	10	0.3
18	36	3	25	50	10	0.3
2	37	3	25	50	10	0.025
5	38	2	25	200	10	0.025

Table 38. Design Matrix Evaluation for the 25 Factorial 3FI Model.

Degrees of Freedom for Evaluation	
Model	25
Residuals	12
Lack Of Fit	*7*
Pure Error	*5*
Corr Total	37

The subject project has provided an excellent platform for providing a much greater understanding of the DOE process and prospects. Actually having gone through the full process significantly enhanced the learning process, including experiencing making mistakes and understanding what works and is statistically valid and what constitutes degrading the process outcome. While struggling with a loss of CFD expertise hampered the completion of desirable additional runs at the optimized run settings, sufficient data was generated to follow most of the process through completion, including follow-on design definition. Especially illuminated was the lack of fidelity and predictability of a fractional design, beyond that stated on the pages of Montgomery's text. Real insight was gained by performing the ANOVA process for full, reduced, and main effects models, including data transforms when indicated. The impact to normality assumptions and predictability through changes to the aliasing structure, DOF distribution across residuals, and the inclusion of statistically insignificant terms in higher order models was enlightening beyond that obtainable from textbook erudition alone. Hopefully, this initial attempt at utilizing the DOE toolset to investigate the utility for simple heat sink design will lead to a more detailed thermal analysis study of the critical electronics cooling problem on more electric aircraft platforms. Much work remains to elevate the limited utility surrogate models generated here as a result, but insight was obtained and benefit was realized. Even follow-on model optimization will ultimately necessitate the validation of surrogate statistical models with empirical hardware and real life experimental data which mirrors the modeling conditions.

8 References

1. Kang, S. and Holahan, M. "The Thermal Resistance of Pin Fin Heat Sinks in Transverse Flow", Proceedings International Electronic Packaging Technical Conference and Exhibition, July 2003 Hawaii.
2. Peles, Y., Kosar, A., Mishra, C., Kuo, C-J., and Schneider, B. "Forced Convective Heat Transfer Across a Pin Fin Micro Heat Sink", International Journal of Heat and Mass Transfer 48 (2005) 3615-3627.
3. Cao, X., Ngo, D.T., and Lu, G-Q. "Thermal Design of Power Module to Minimize Peak Transient Temperature", Proceedings International Conference on Electronic Packaging Technology & High Density Packaging", 2009.
4. Kobus, C.J. and Oshio, T., "Development of a Theoretical Model for Predicting the Thermal Performance Characteristics of a Vertical Pin Fin Array Heat sink Under Combined Forced and Natural Convection with Impinging Flow", International Journal of Heat and Mass Transfer 48 (2005)1053-1063.
5. Heltzel, A., "Thermal Performance Modeling of Micro Pin Fin Heat Sinks for Aircraft Thermal Management", Proceedings 46th AIAA Aerospace Sciences Meeting and Exhibit, January 2008, Reno NV.
6. Sparrow, E., and Larson E., "Heat Transfer from Pin Fins Situated in an Oncoming Longitudinal Flow Which Turns to Crossflow", International Journal of Heat and Mass Transfer, Vol. 25 No. 5, pp 603-614, 1982.
7. Khan, W., and Yovanovich, M., "Effect of Bypass on Overall Performance of Pin Fin Heat Sinks", Journal of Thermophysics and Heat Transfer, Vol 21, No. 3, July-September 2007.
8. Siu-Ho, A., Qu, W., and Pfefferkorn, F., "Pressure Drop and Heat Transfer in a Single Phase Micro Pin Fin Heat Sink", Proceedings 2006 ASME International Mechanical Engineering Congress and Exposition, November 5-10, 2006, Chicago IL.
9. Ismail, L. and Velraj, R., "Studies on Fanning Friction and Colburn Factors of Offset and Wavy Fins Compact Plate Fin Heat Exchanger-a CFD Approach", Numerical Heat Transfer, Part A, 56: 987-1005, 2009.
10. Stanescu, G., Fowler, A., and Bejan, A., "The Optimal Spacing of Cylinders in Free-Stream Cross Flow Forced Convection", International Journal of Heat and Mass Transfer, Vol. 39, No. 2, pp. 311-317, 1996.
11. Khan, W., Culham, J., and Yovanovich, M., "Optimization of Pin Fin Heat Sinks Using Entropy Generation Minimization", Proceedings 2004 International Society Conference on Thermal Phenomena.
12. Lin, W., and Lee, D., "Second Law Analysis on a Pin Fin Array Under Crossflow", International Journal on Heat and Mass Transfer, Vol. 40, No. 8, pp. 1937-1945, 1997.

Appendix

A. Response Surface Plots for T_{max} using the Parsimonious 2FI ANOVA Model. 1-15

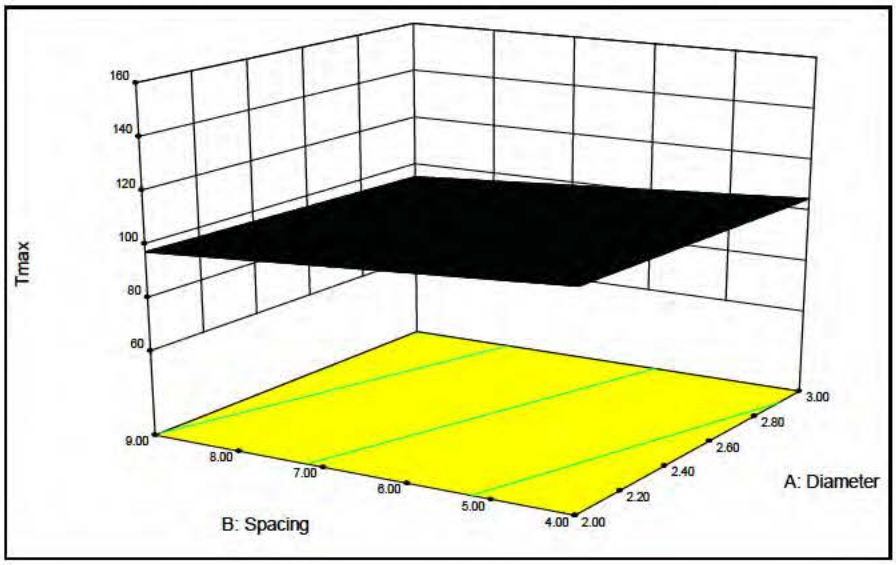

1)

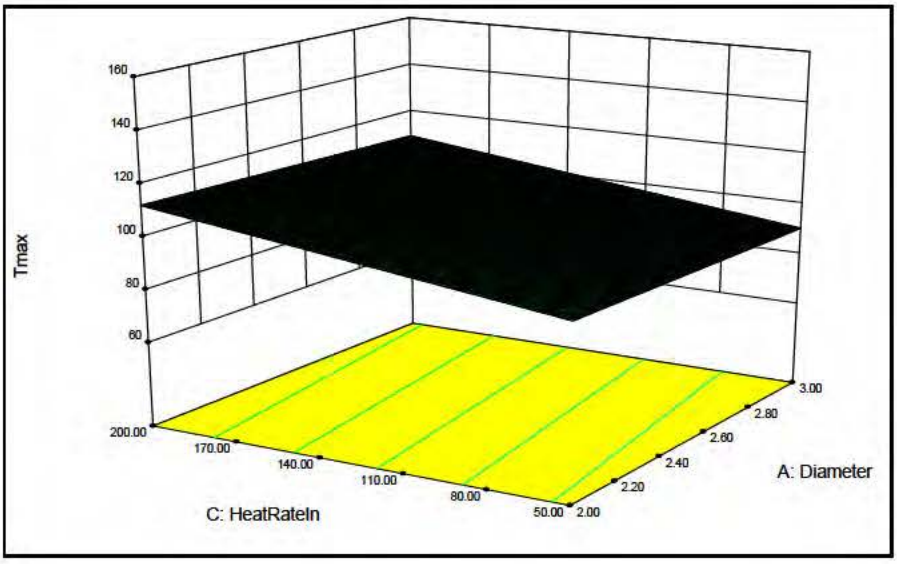

2)

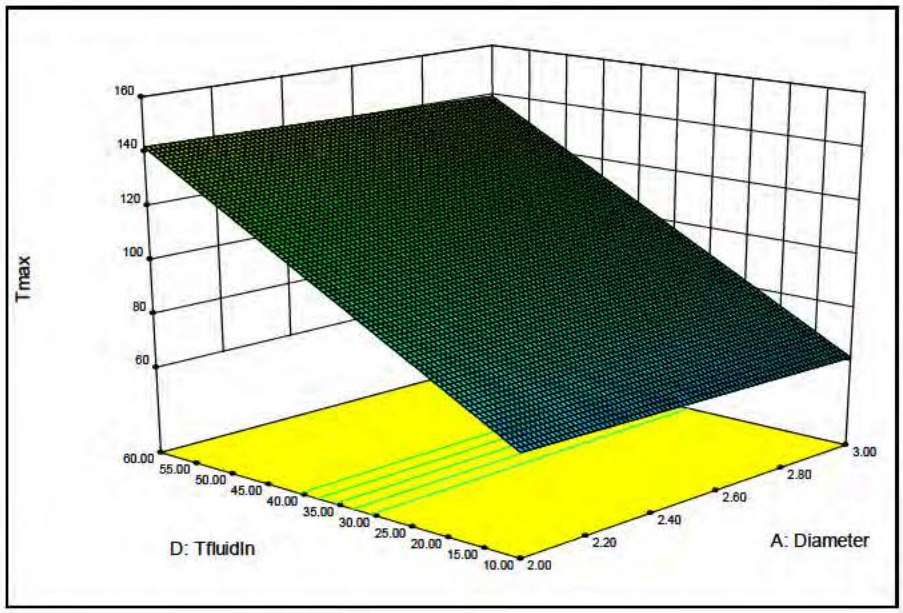

3)

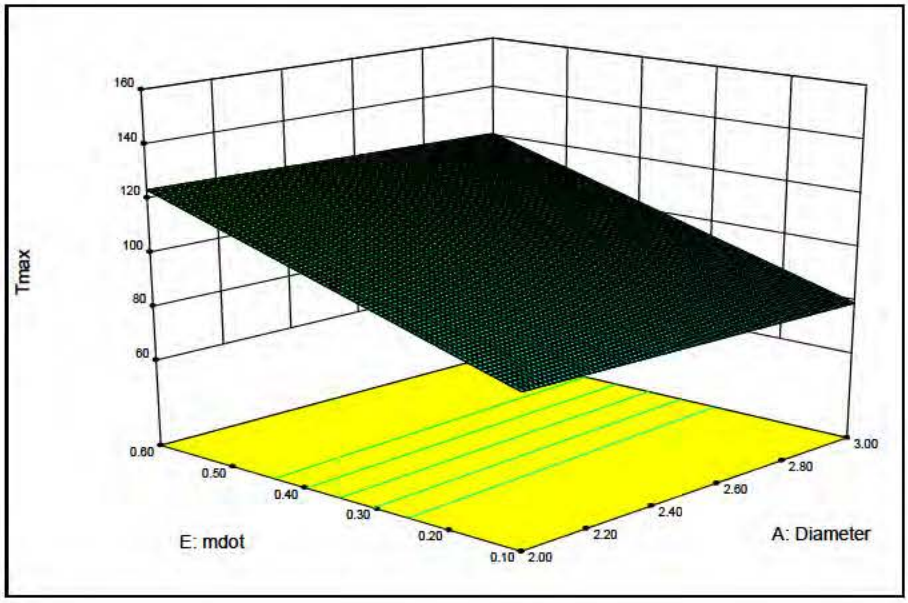

4)

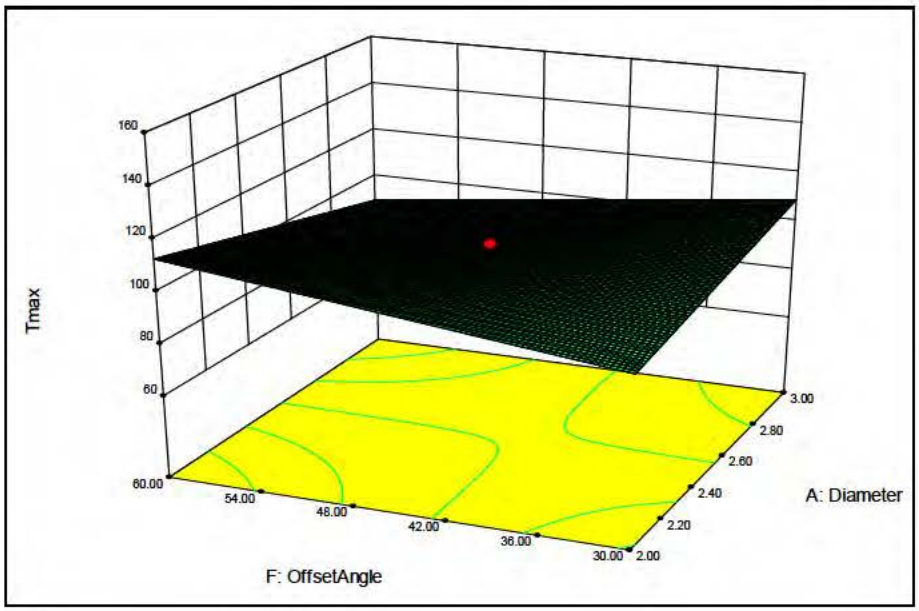

5)

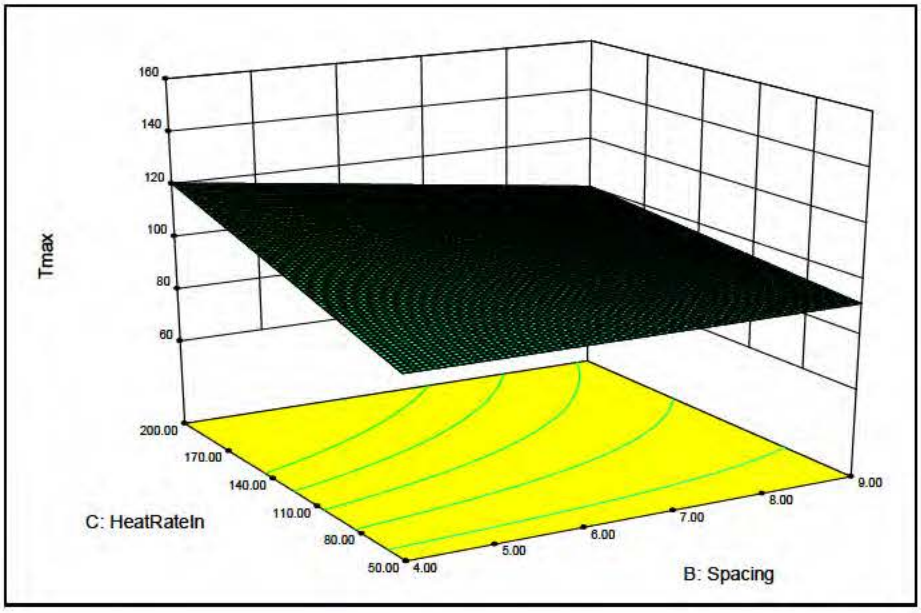

6)

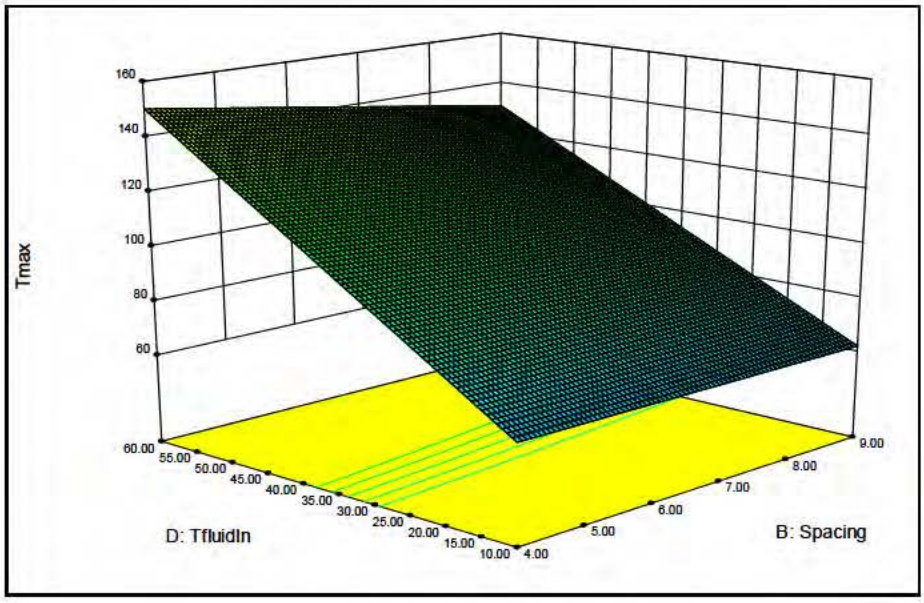

7)

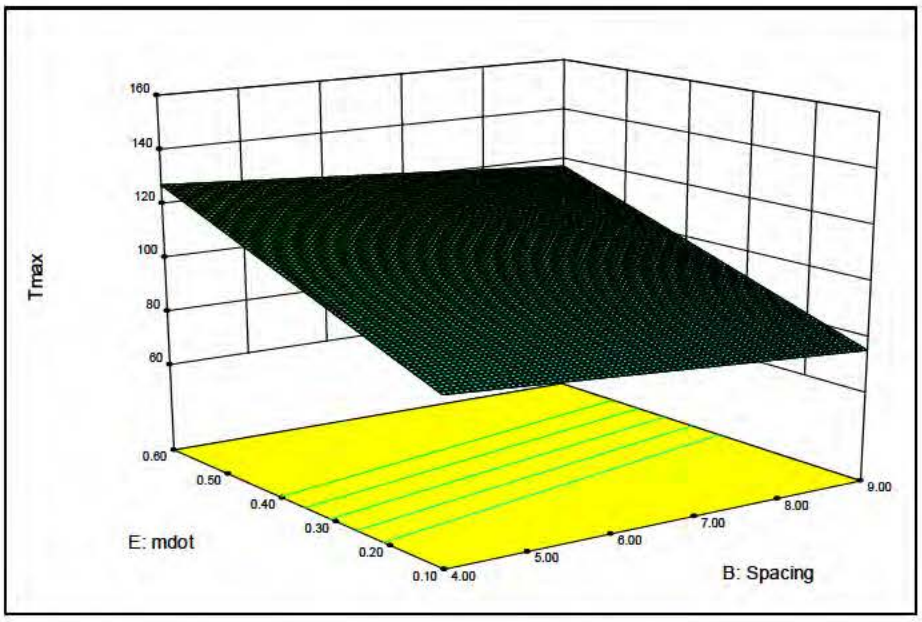

8)

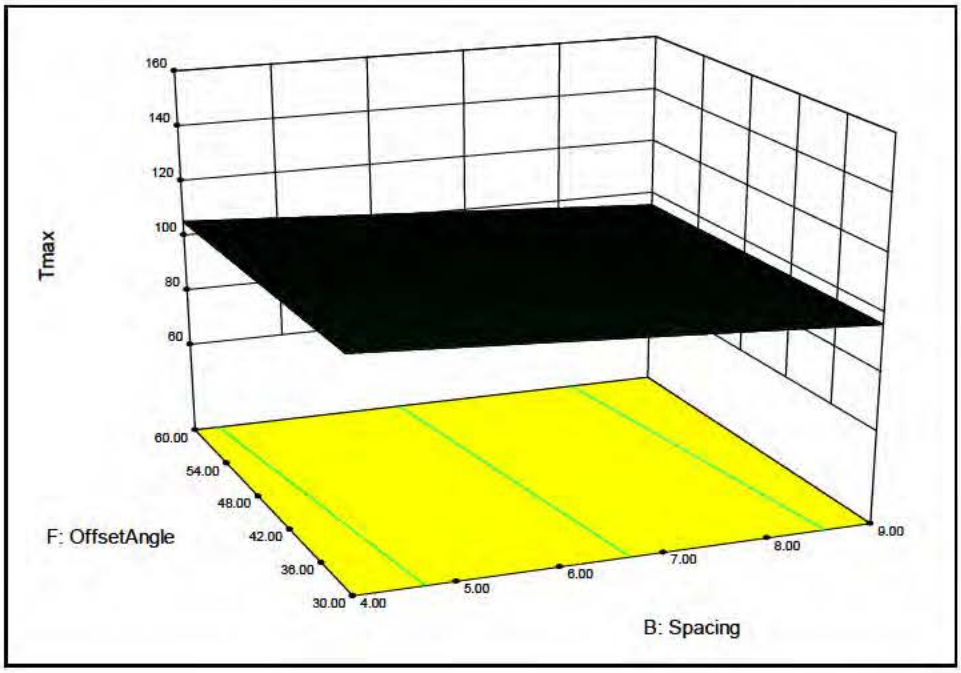

9)

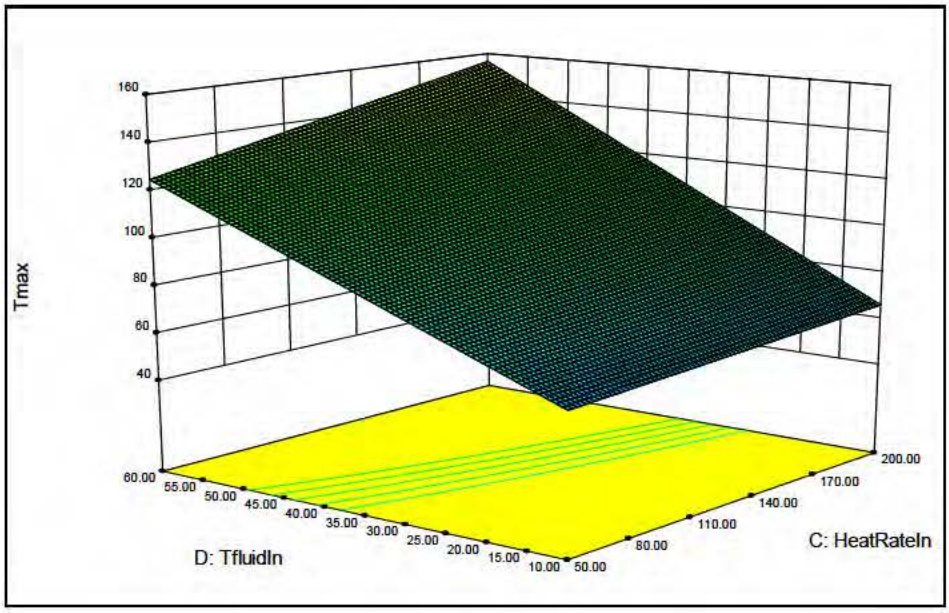

10)

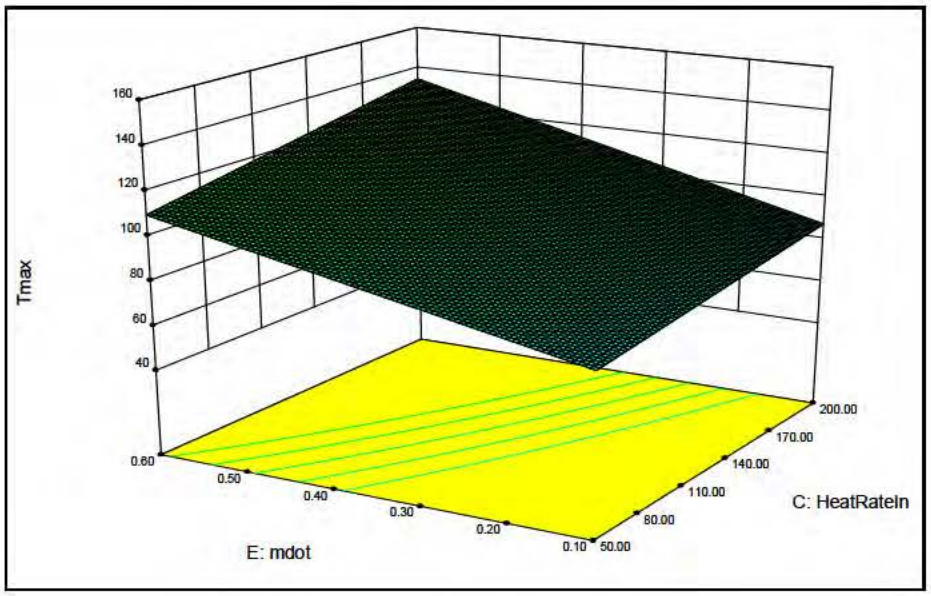

11)

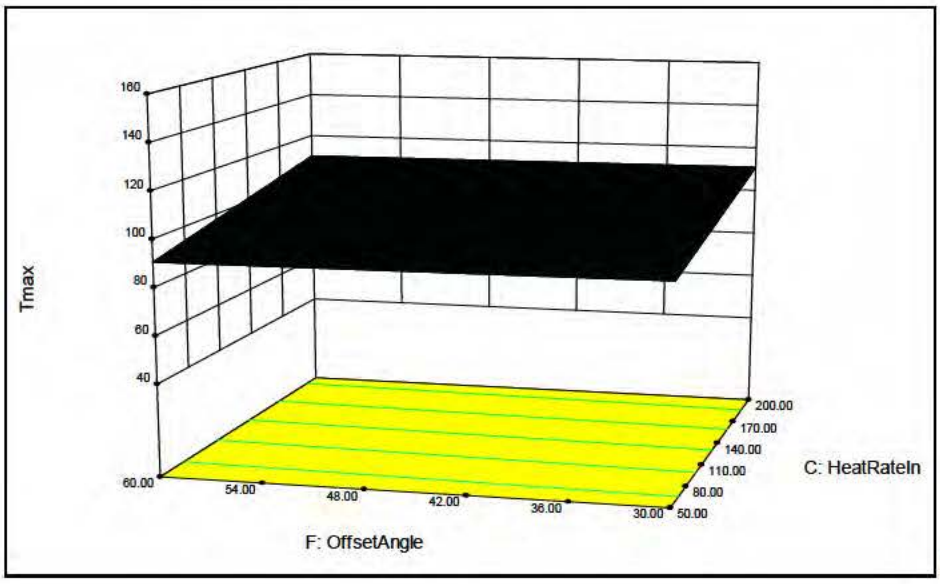

12)

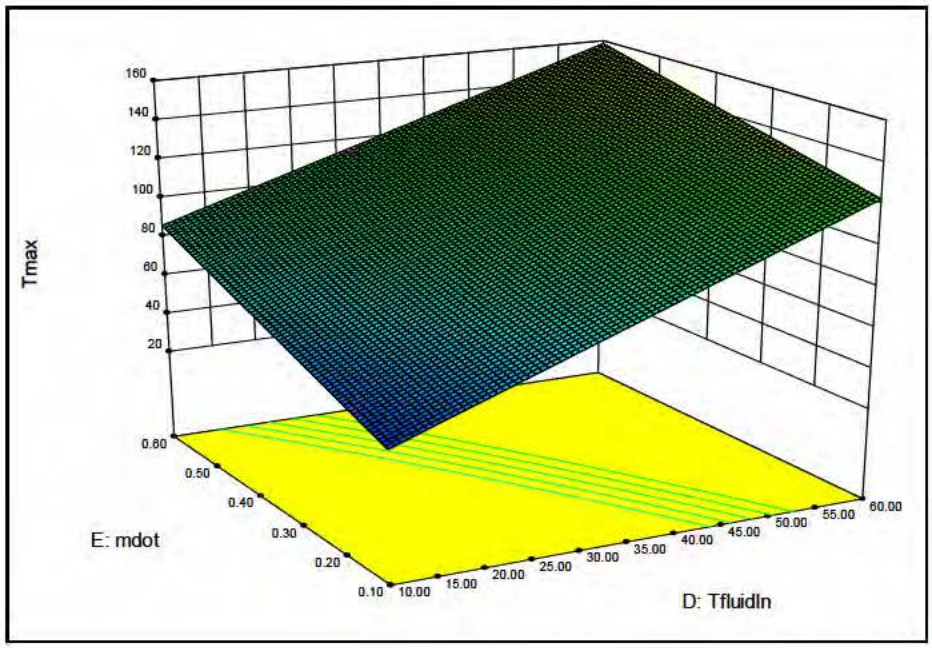

13)

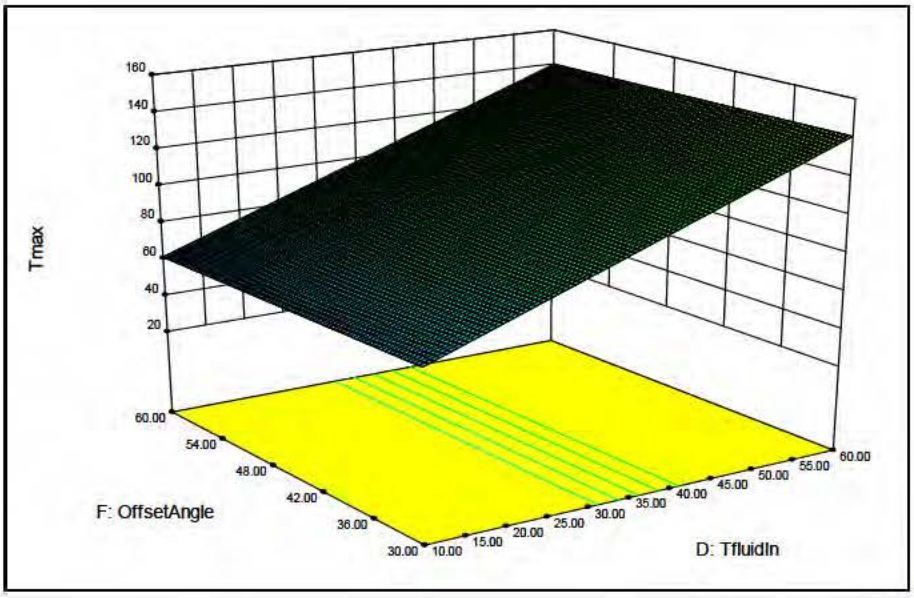

14)

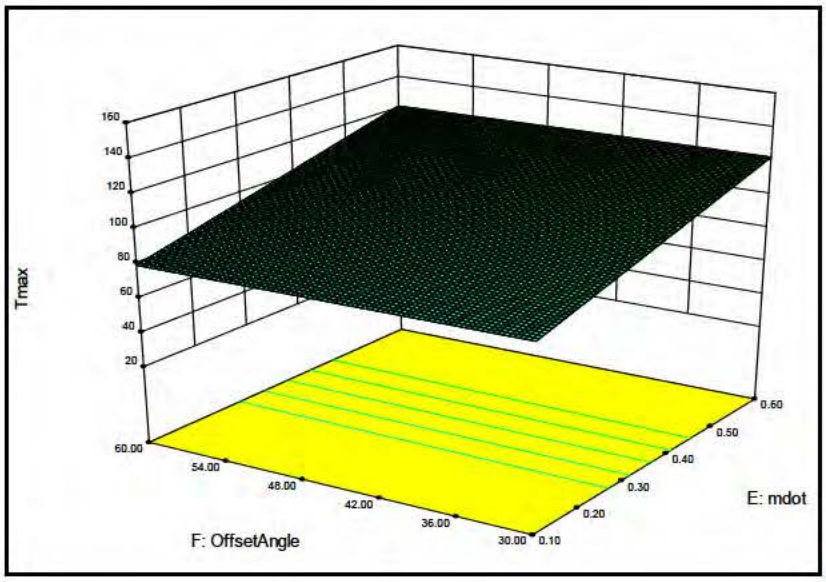

15)

B. Response Surface Plots for h_{avg} using the Parsimonious 2FI ANOVA Model. (1-15)

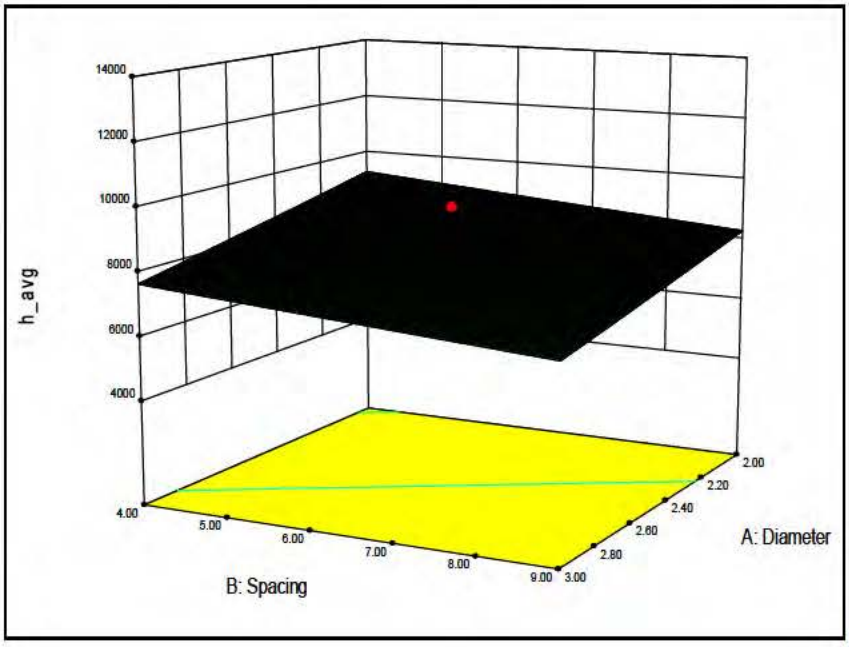

1)

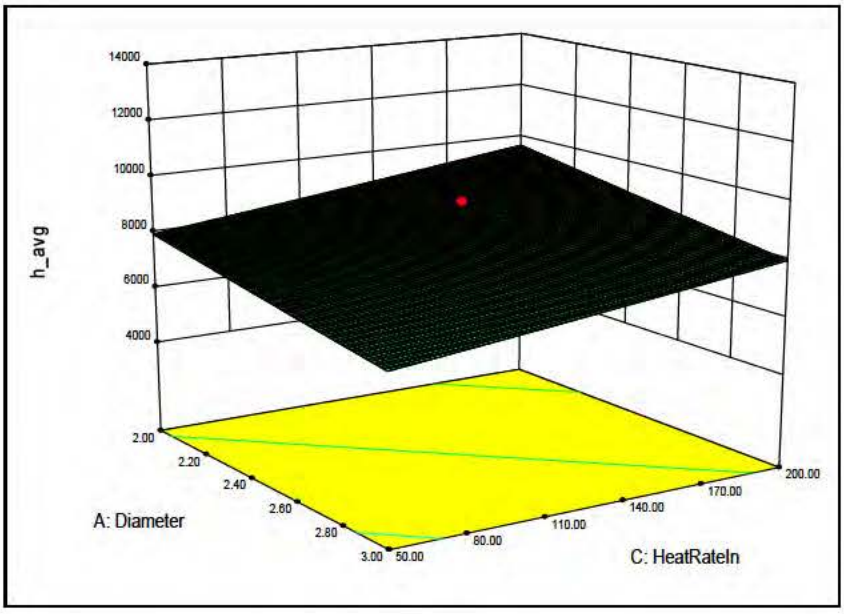

2)

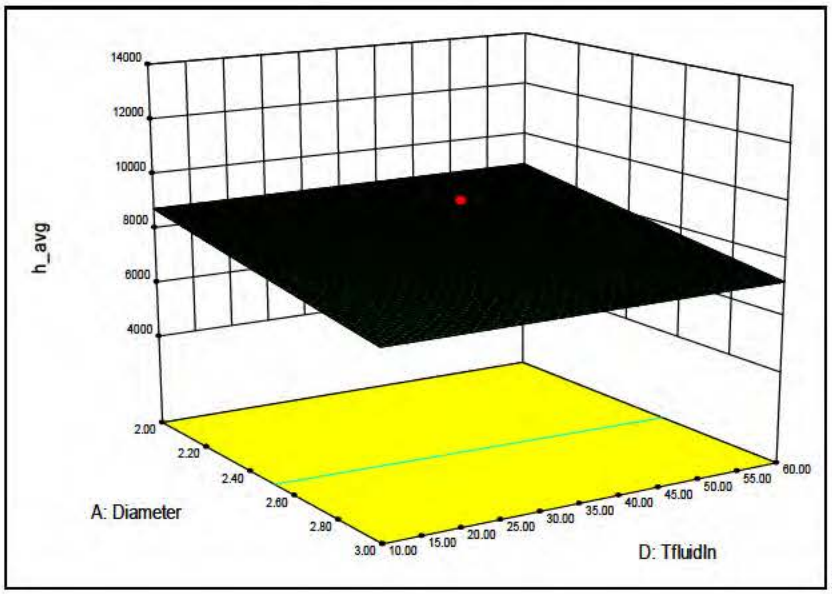

3)

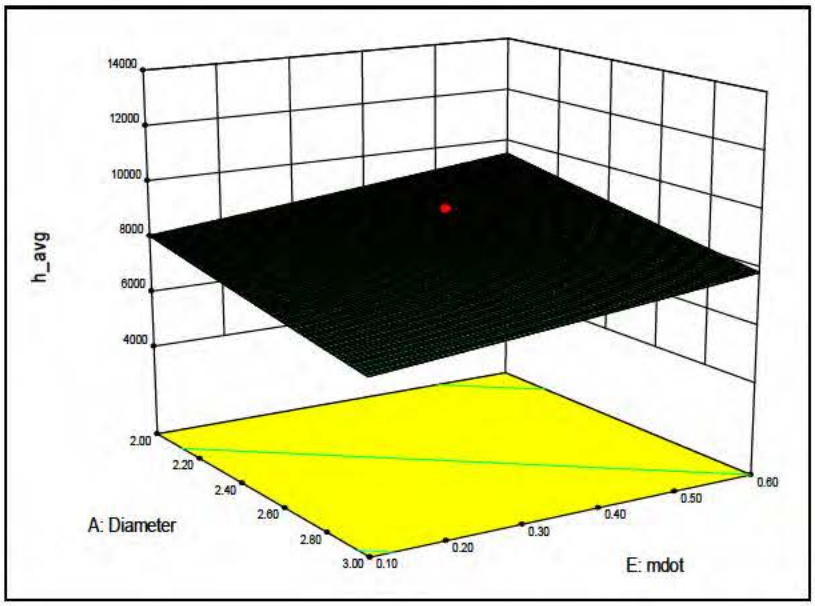

4)

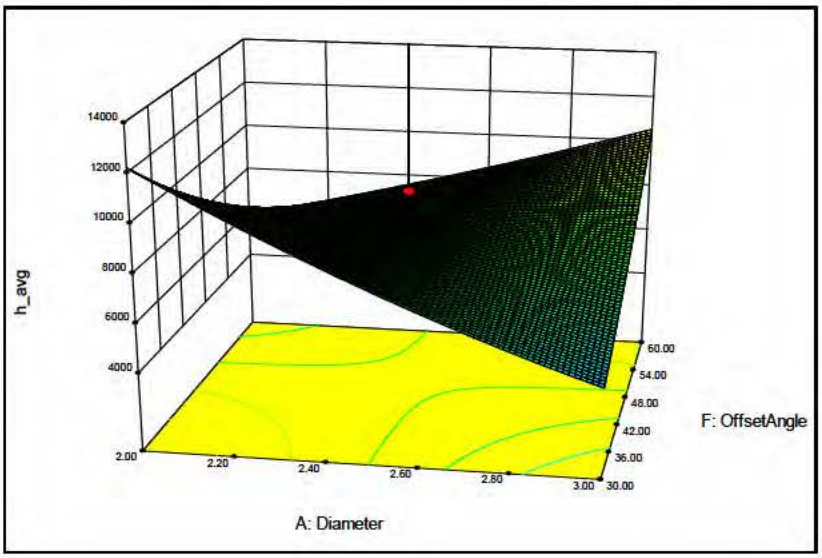

5)

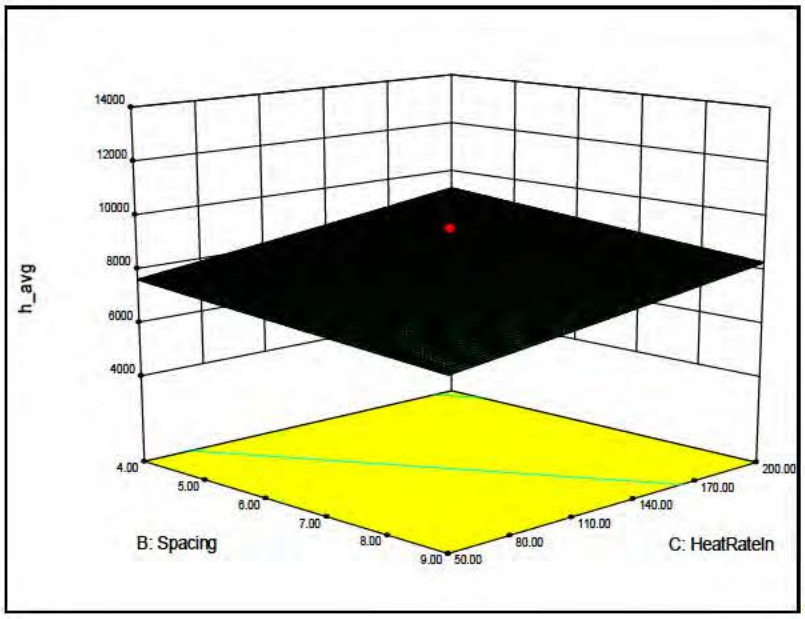

6)

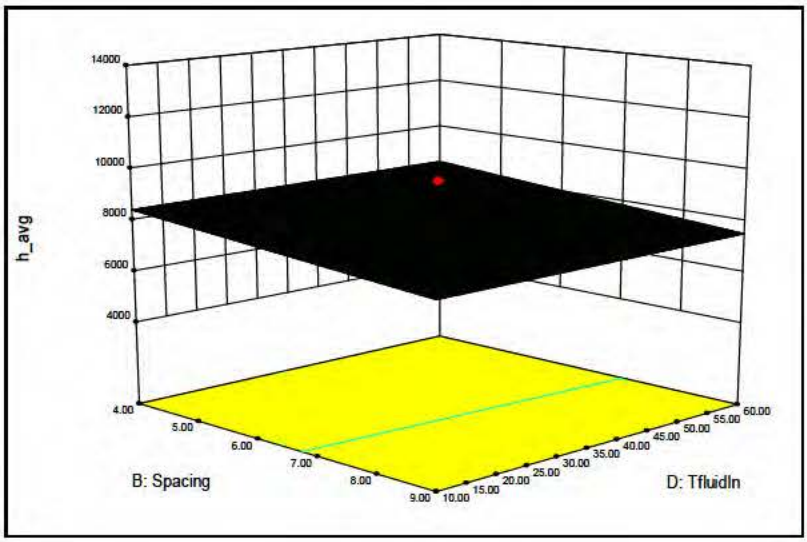

7)

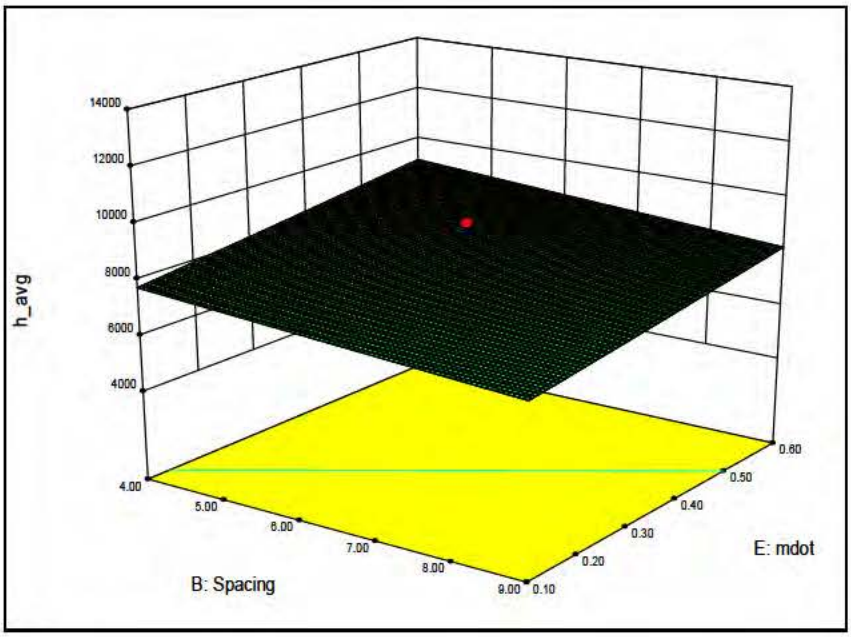

8)

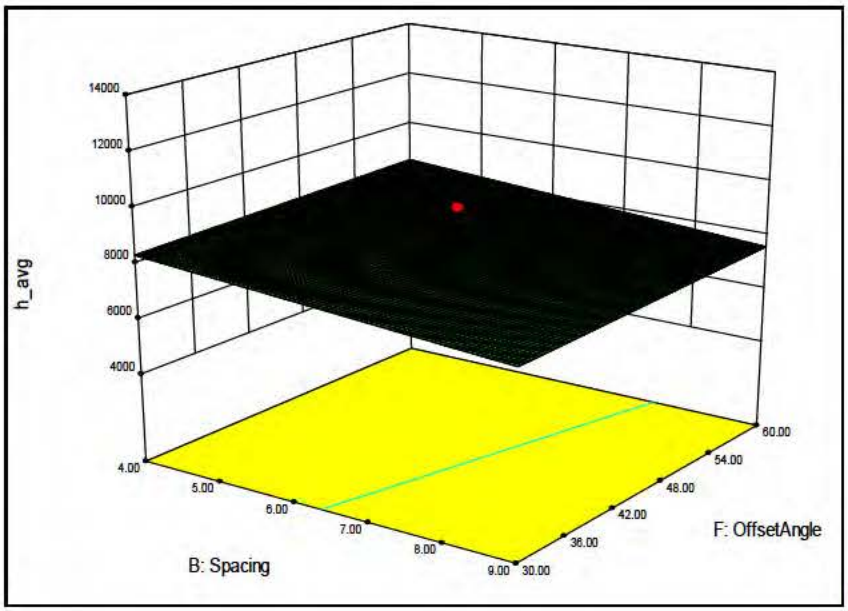

9)

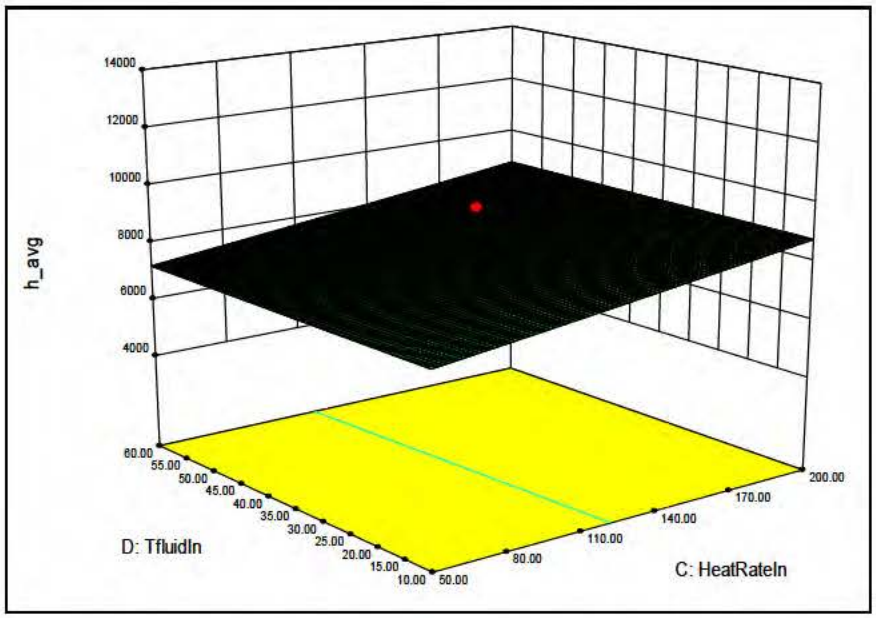

10)

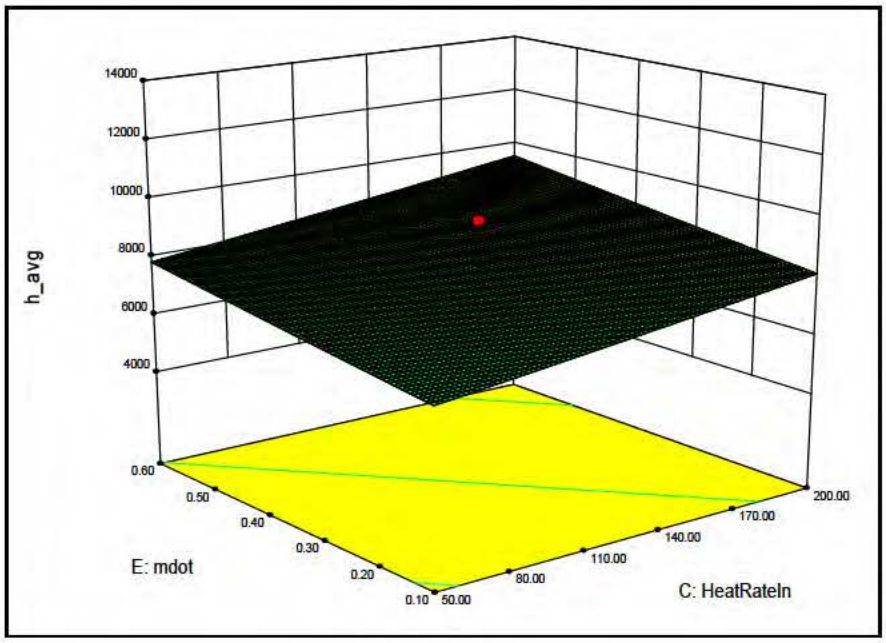

11)

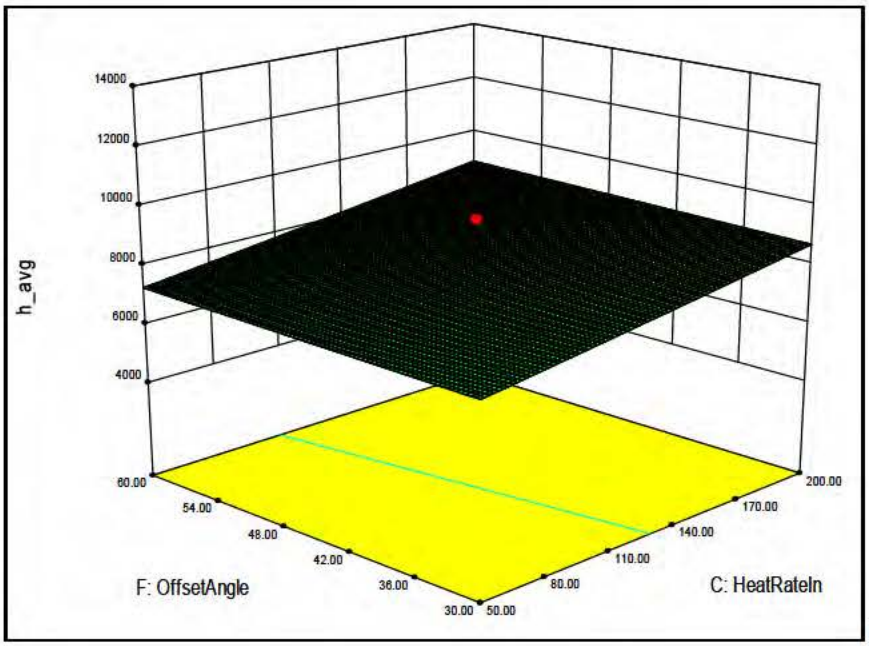

12)

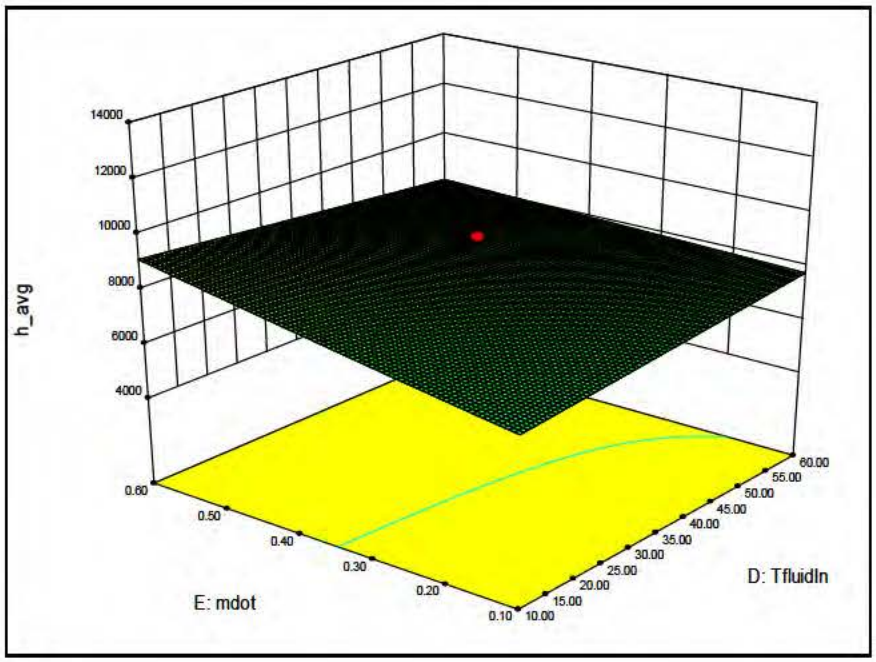

13)

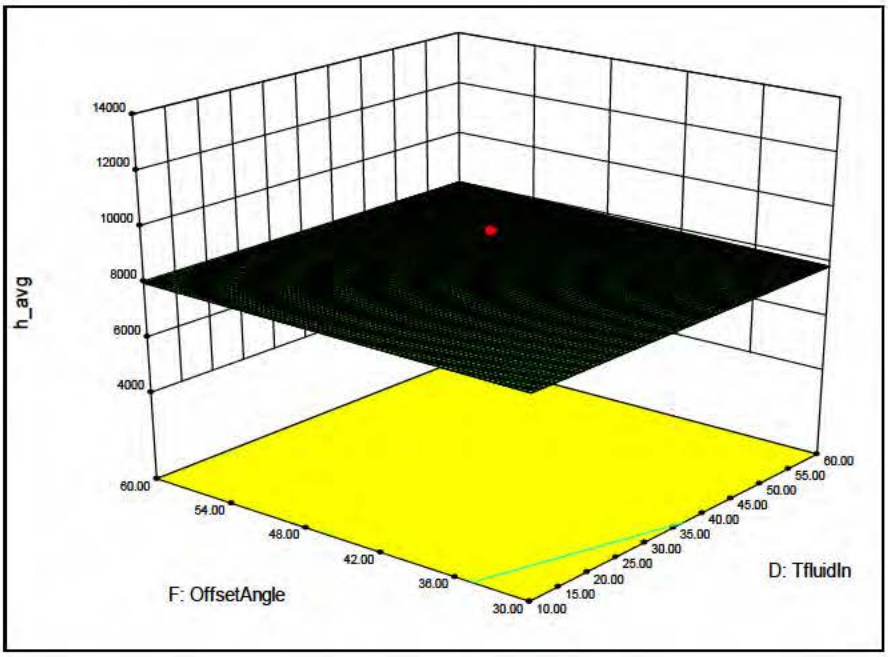

14)

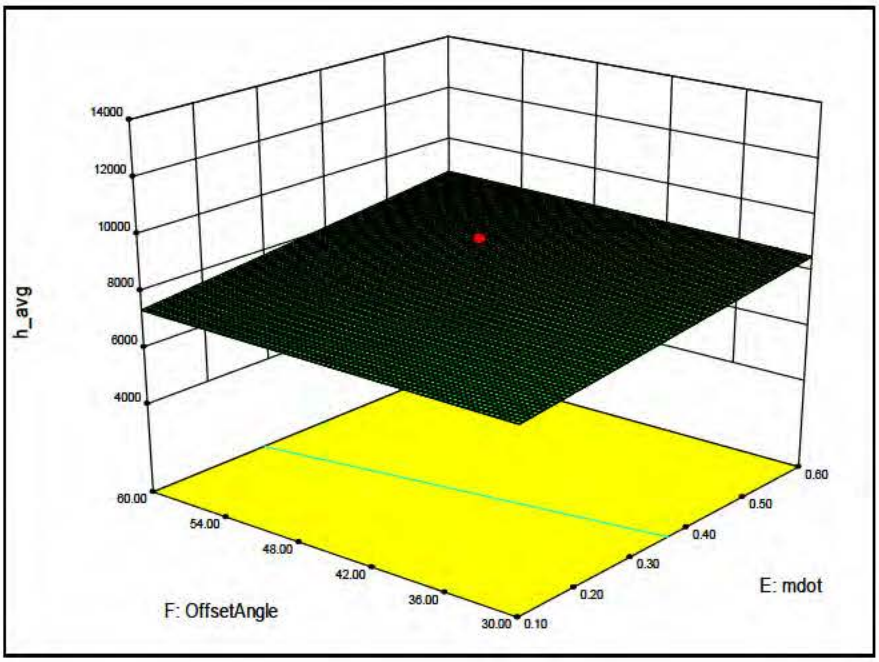

15)

C. Response Surface Plots for ΔP using the Parsimonious 2FI ANOVA Model. (1-15)

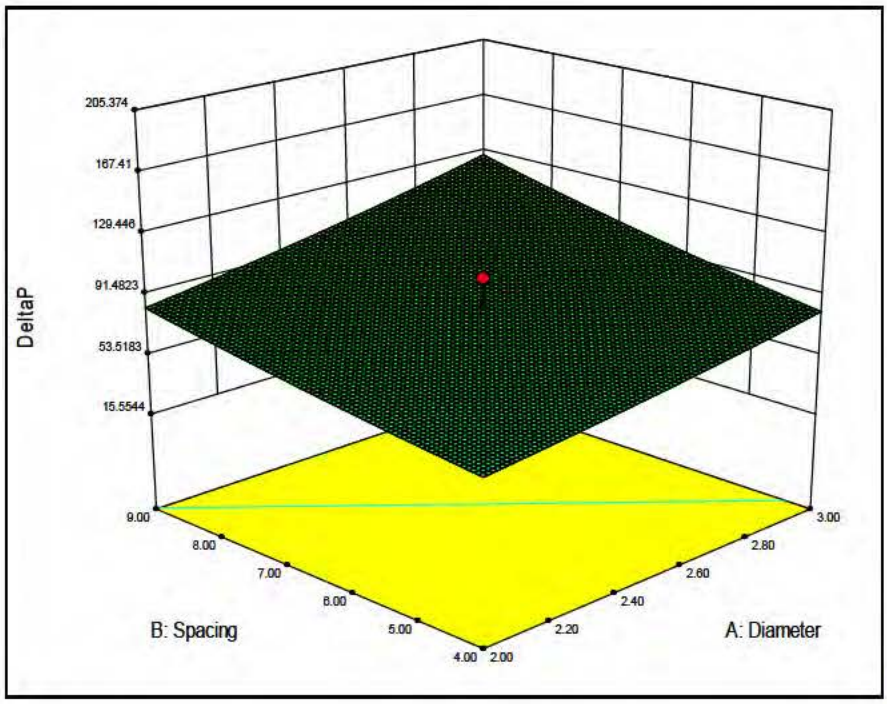

1)

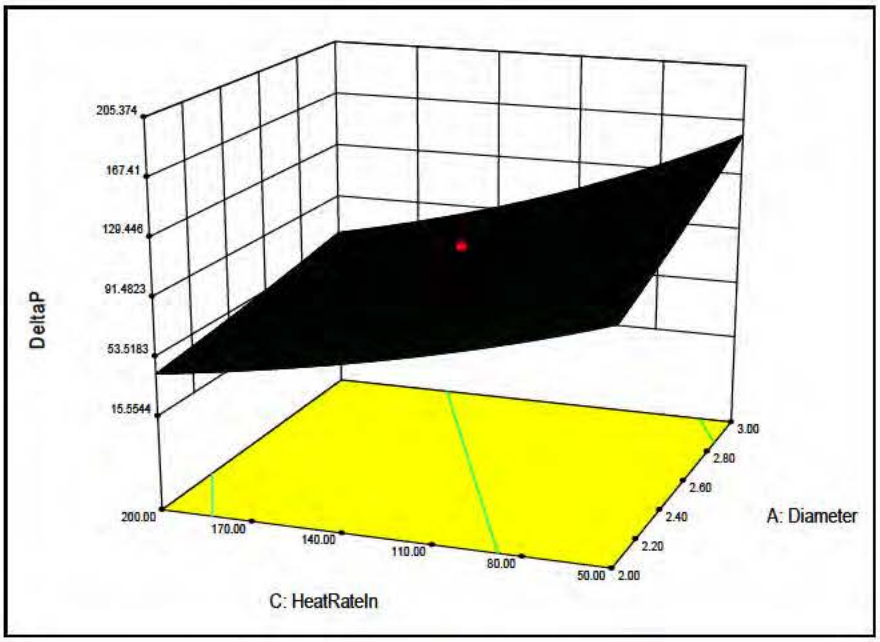

2)

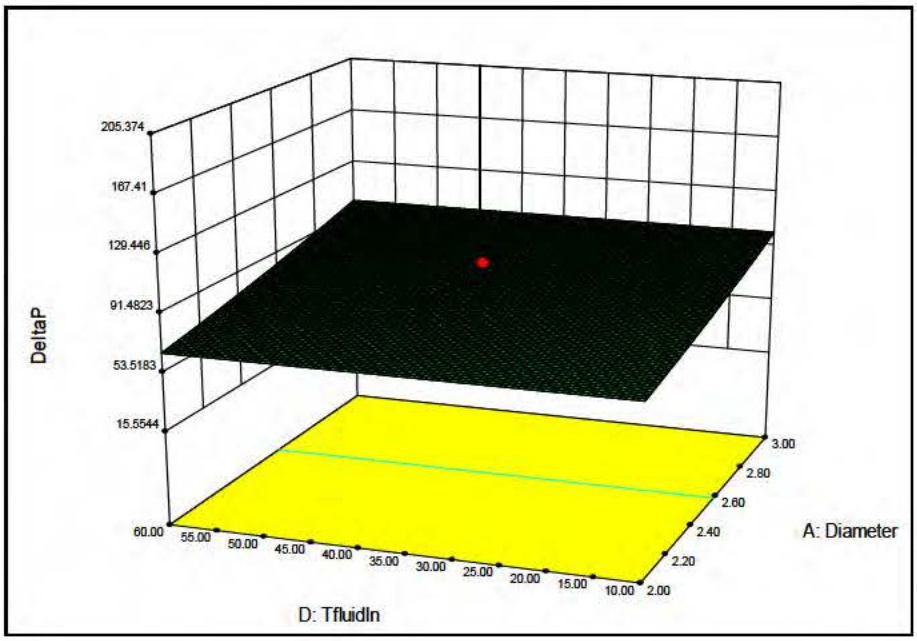

3)

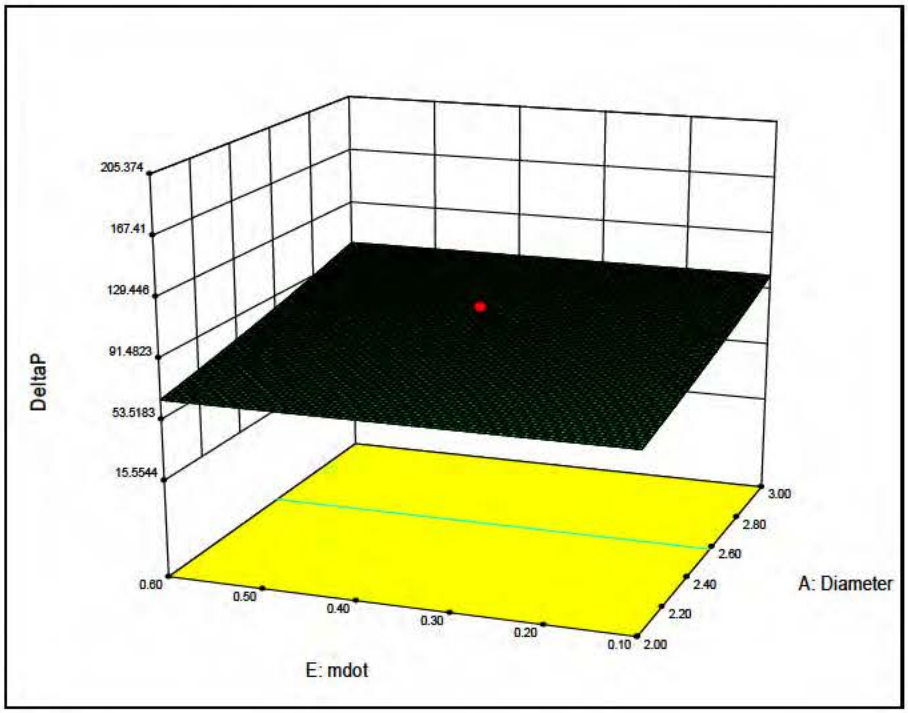

4)

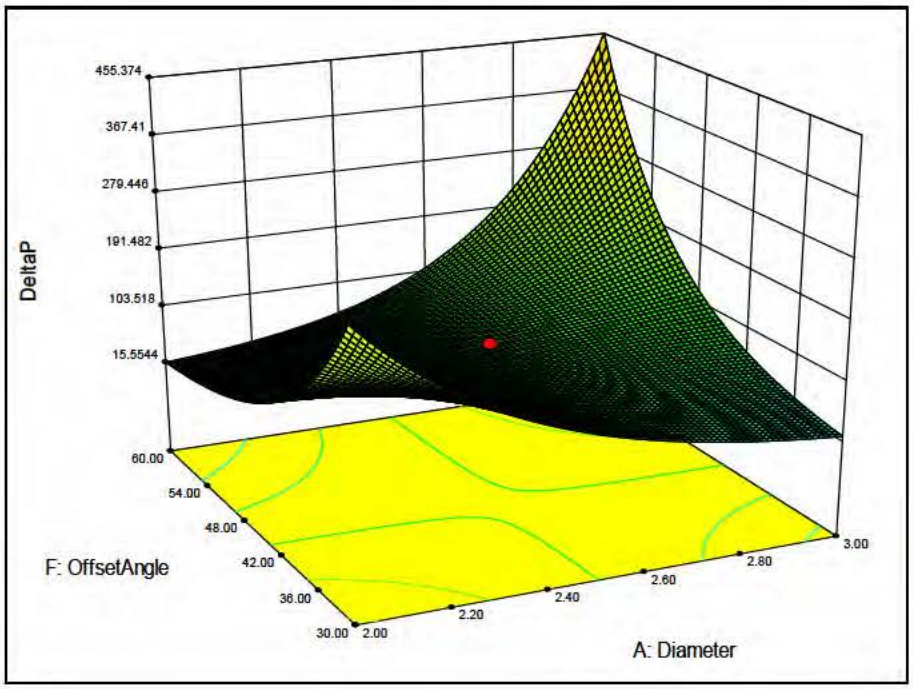

5)

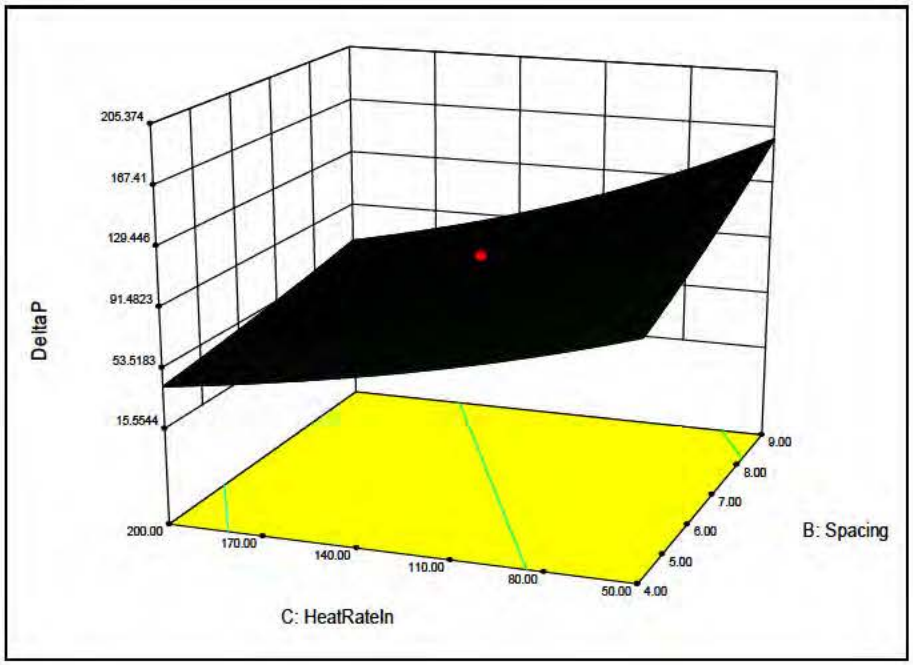

6)

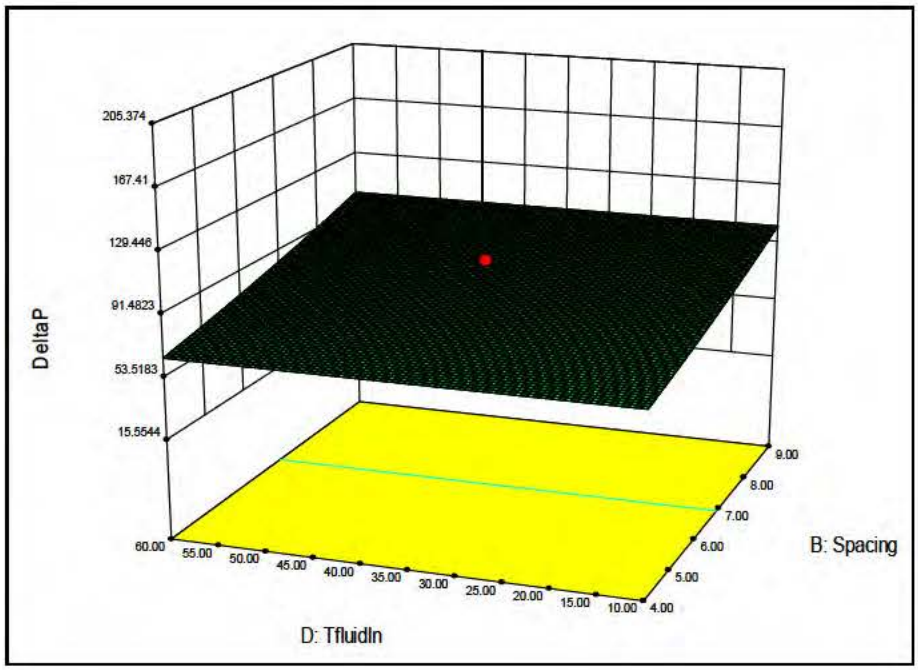

7)

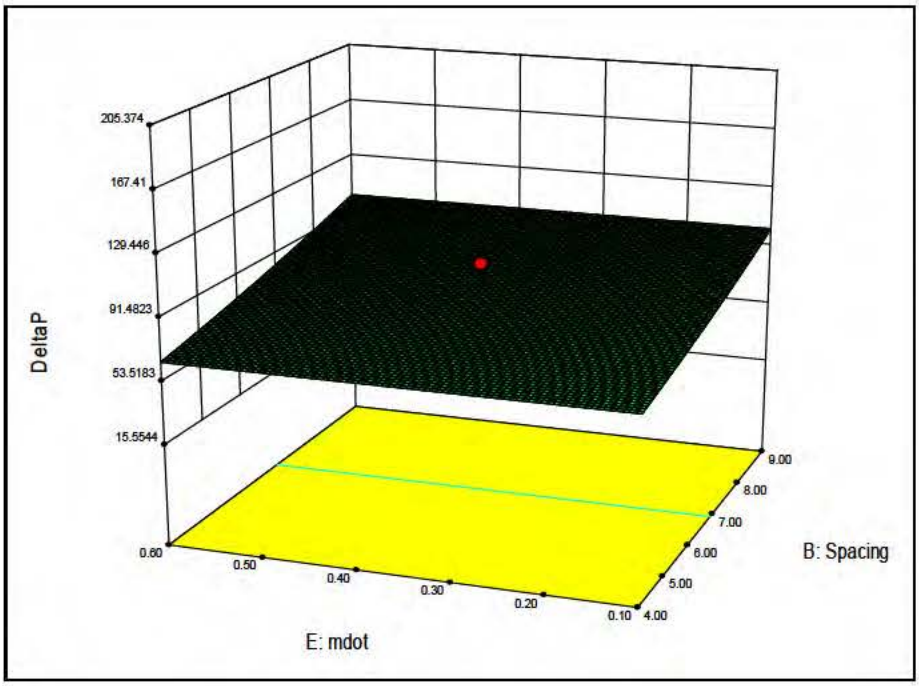

8)

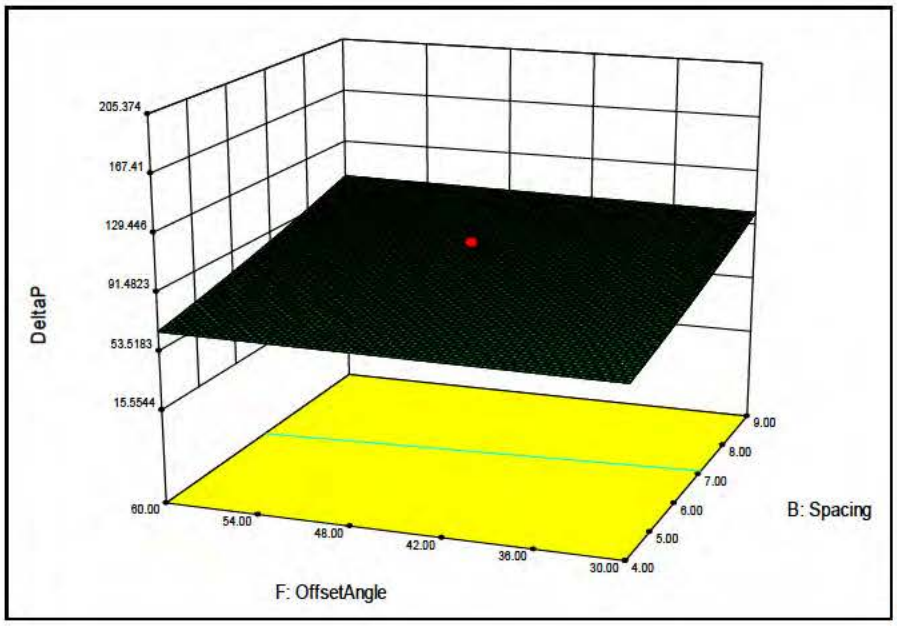

9)

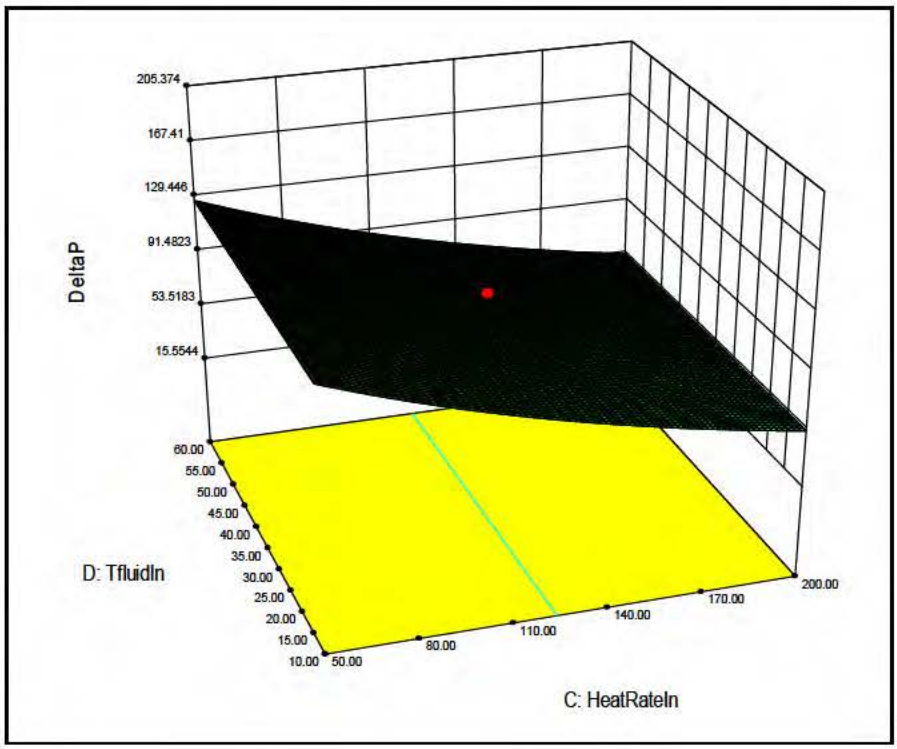

10)

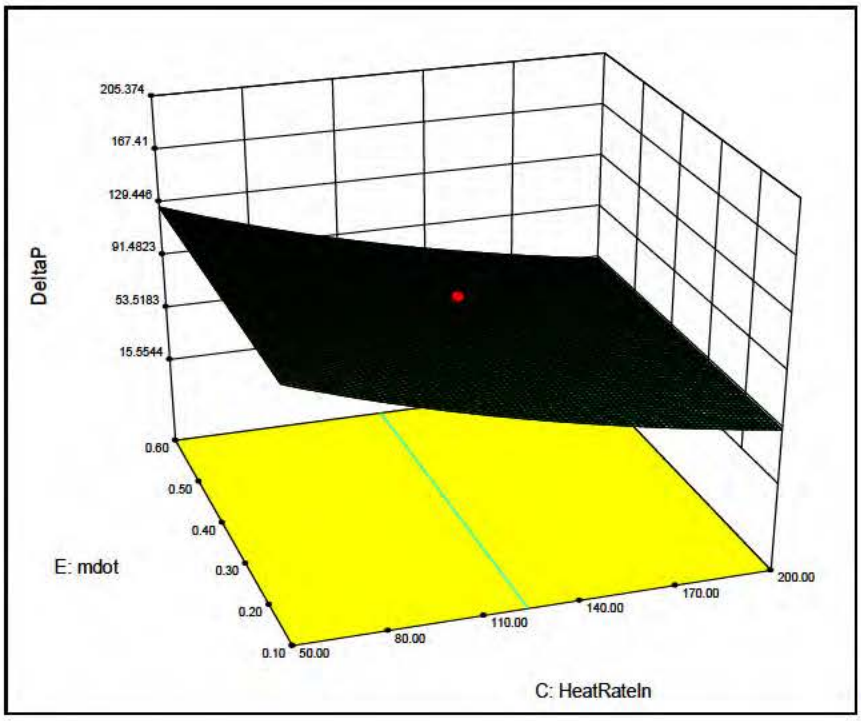

11)

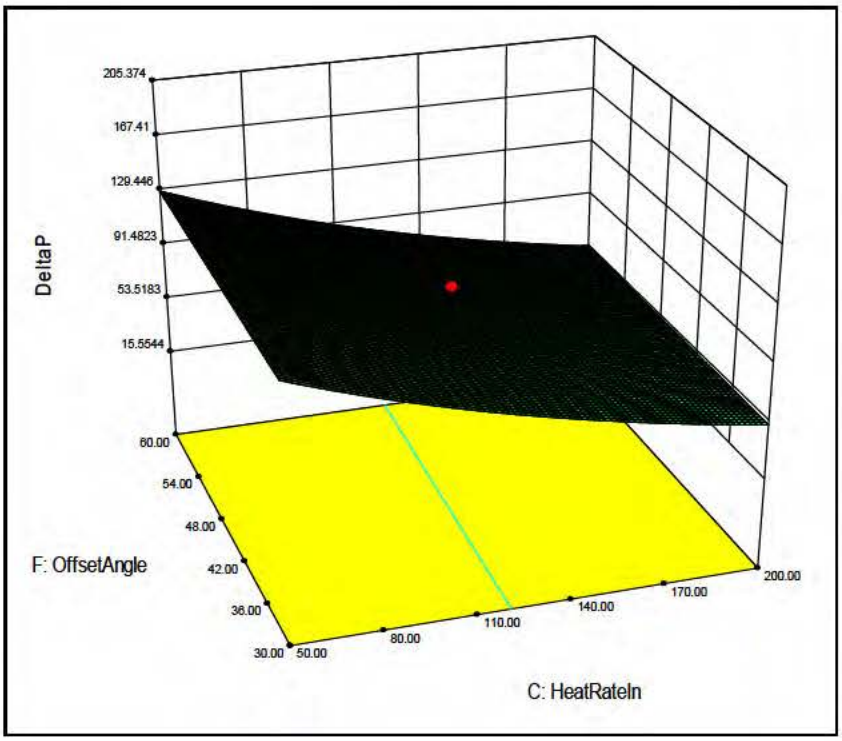

12)

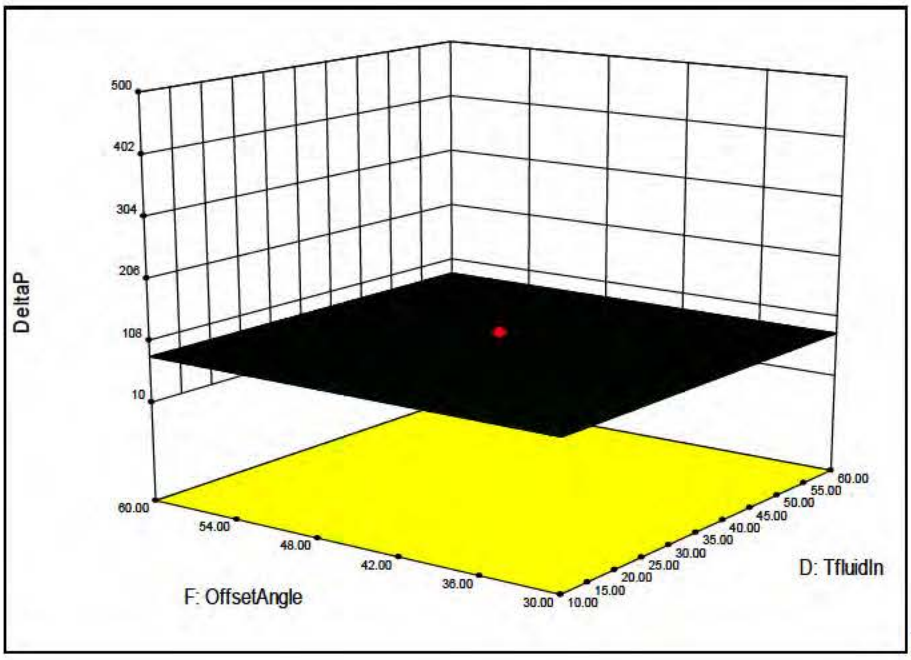

13)

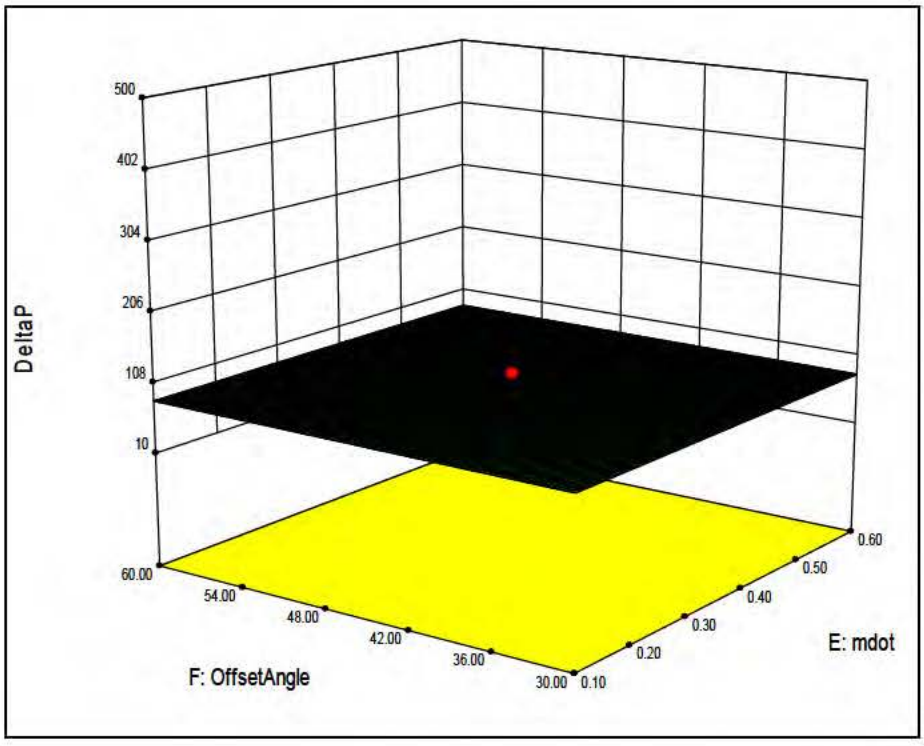

14)

D. Response Surface Plots for Optimized Run Factor Pairs. Minimzed T_{max} (1-15)

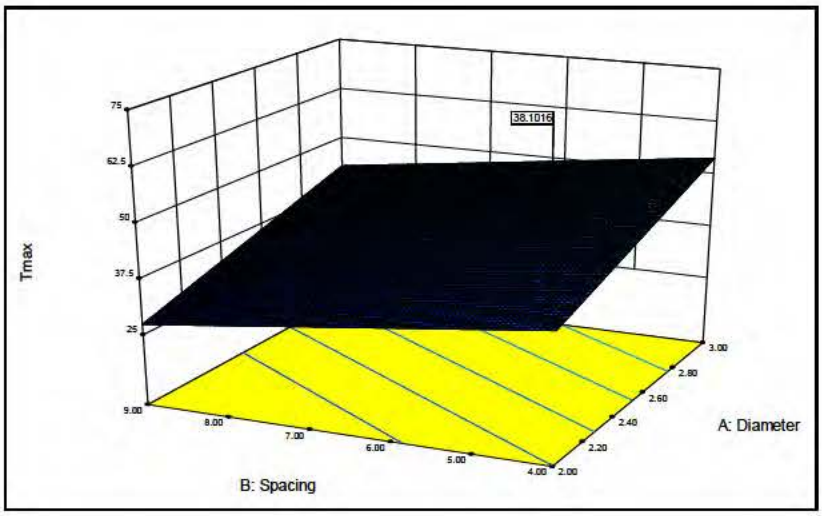

1)

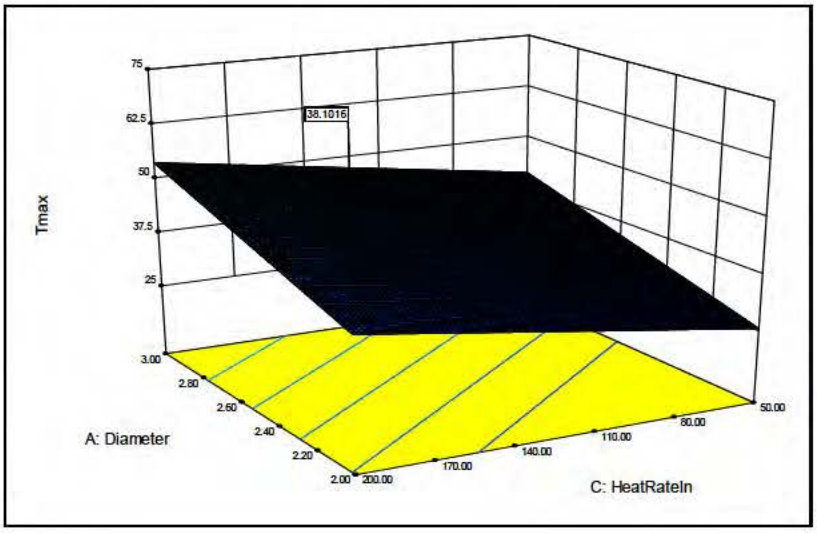

2)

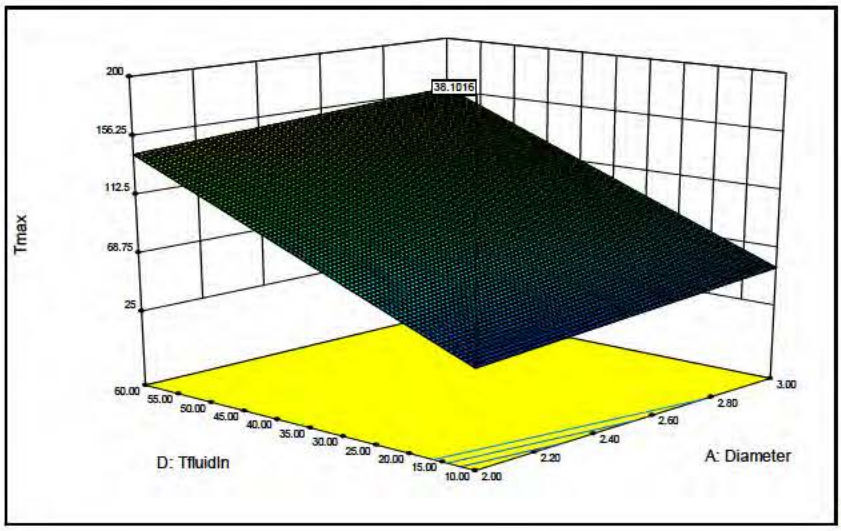

3)

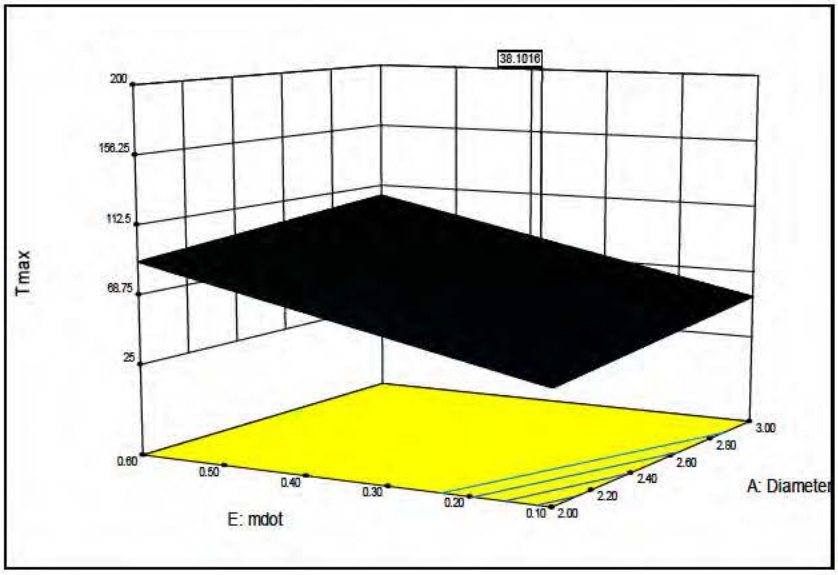

4)

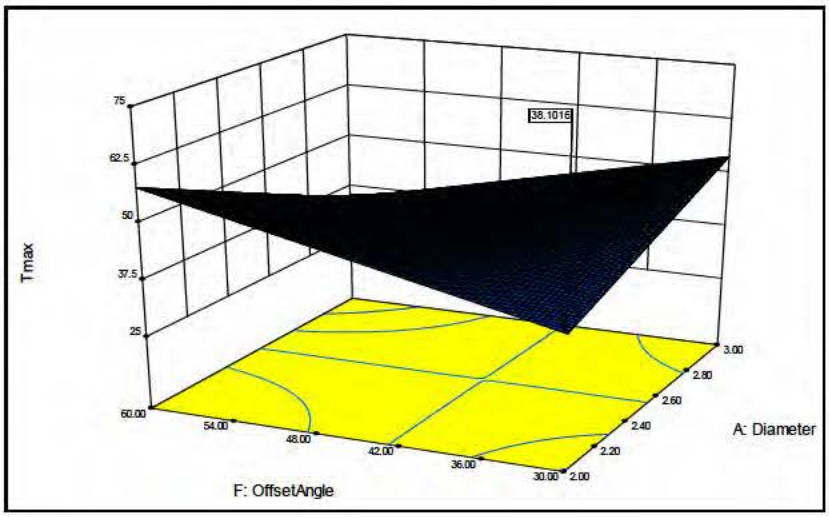

5)

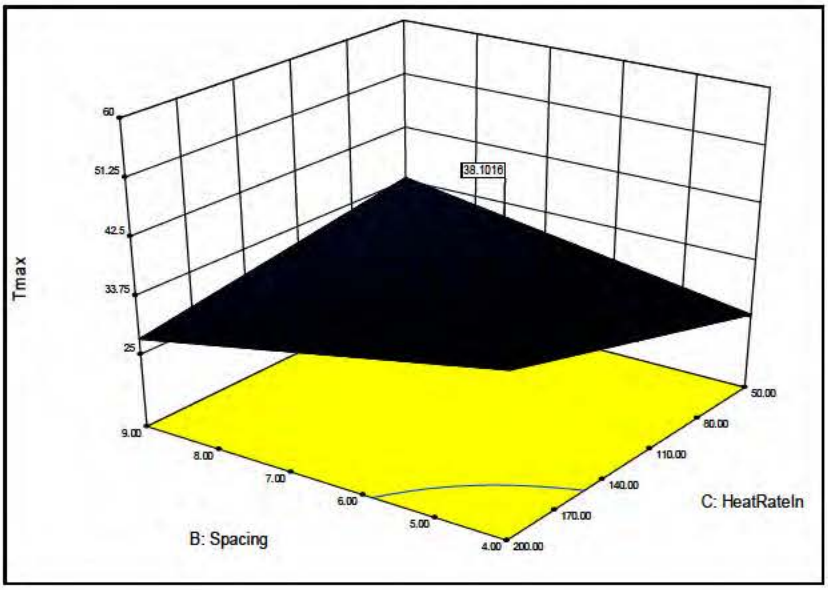

6)

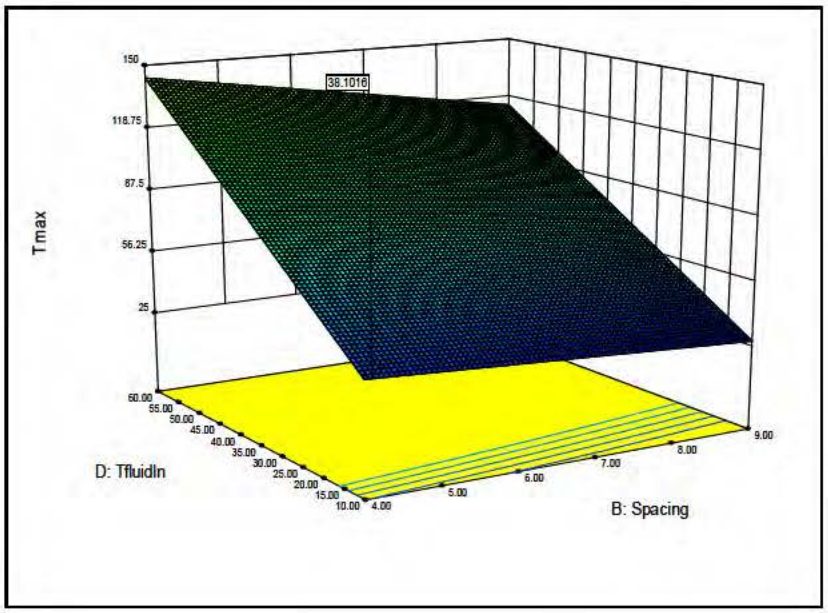

7)

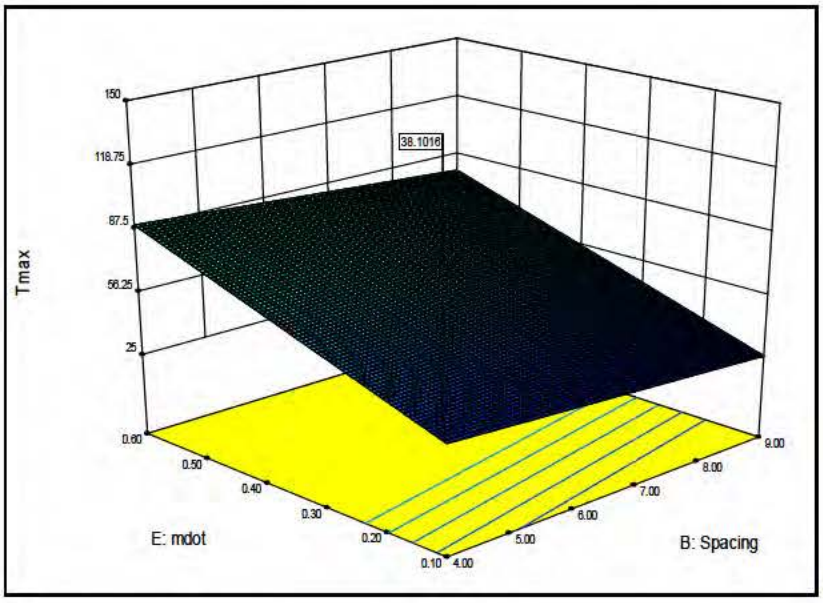

8)

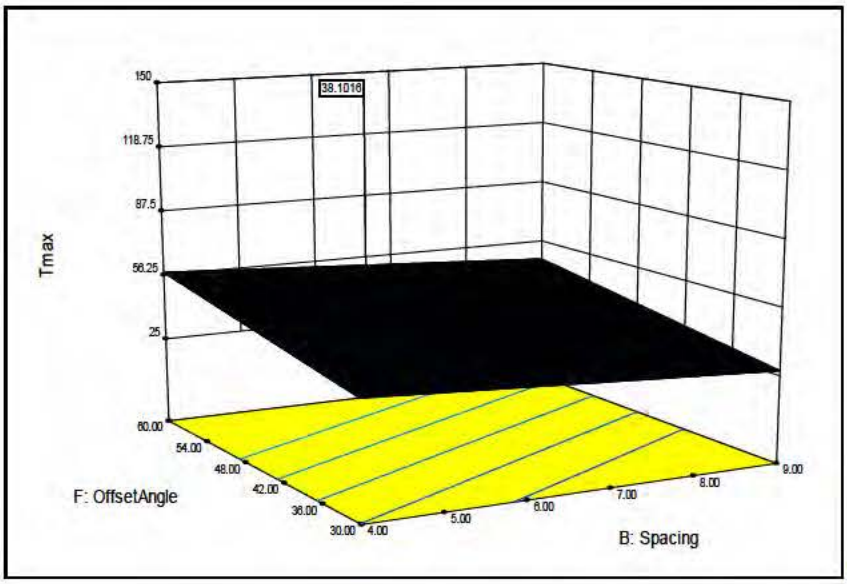

9)

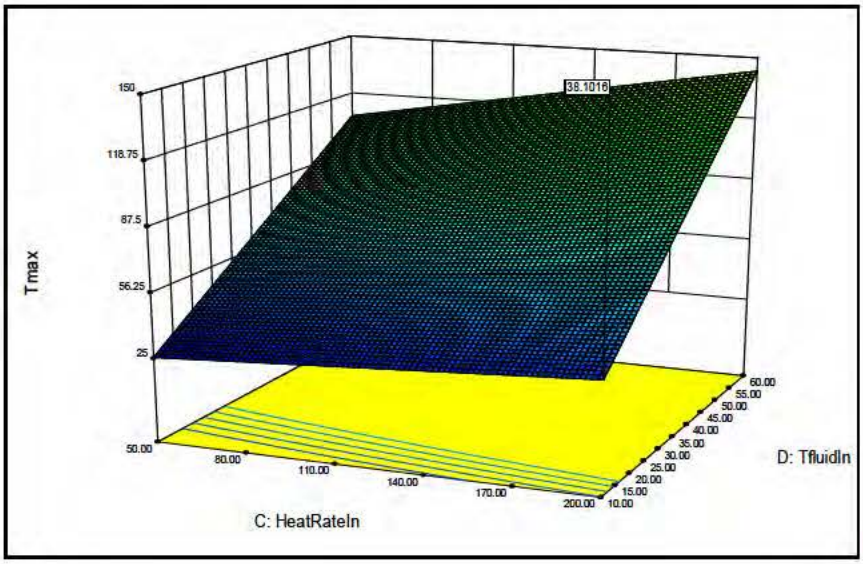

10)

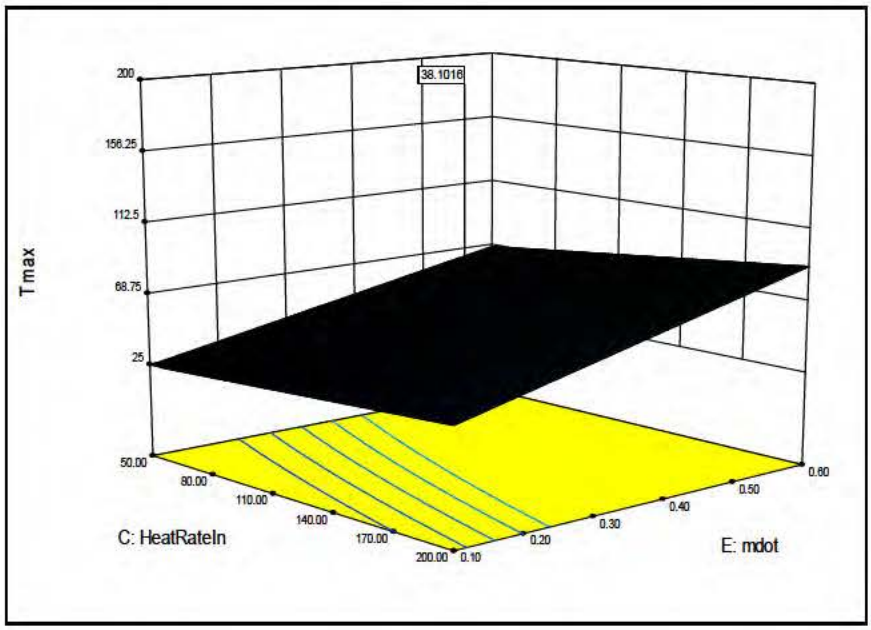

11)

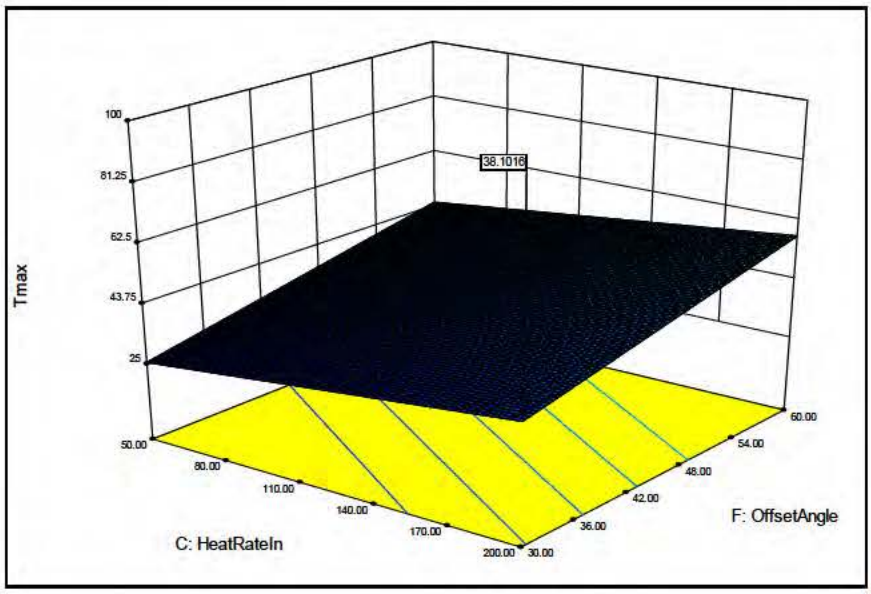

12)

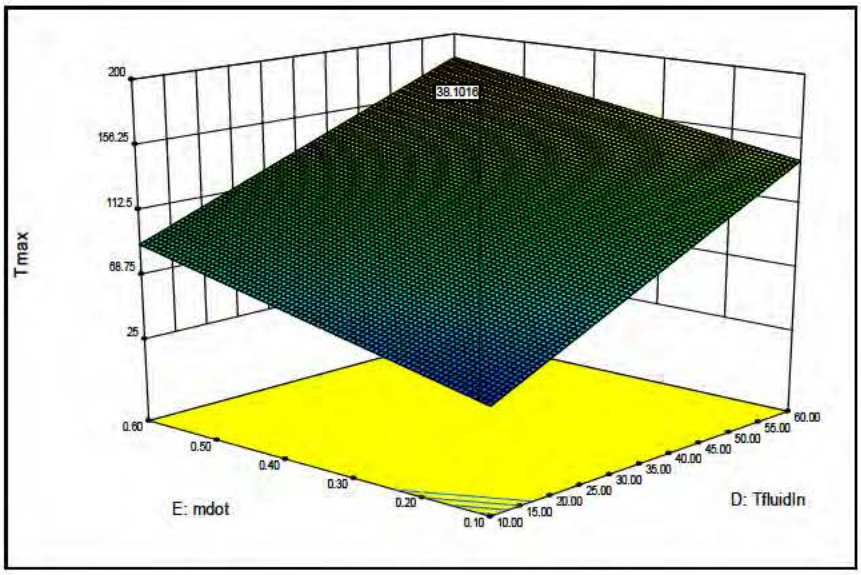

13)

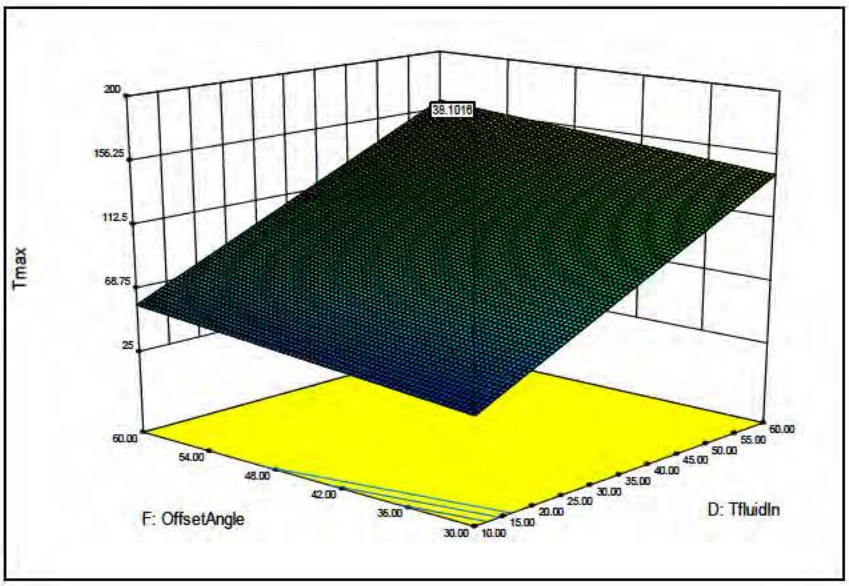

14)

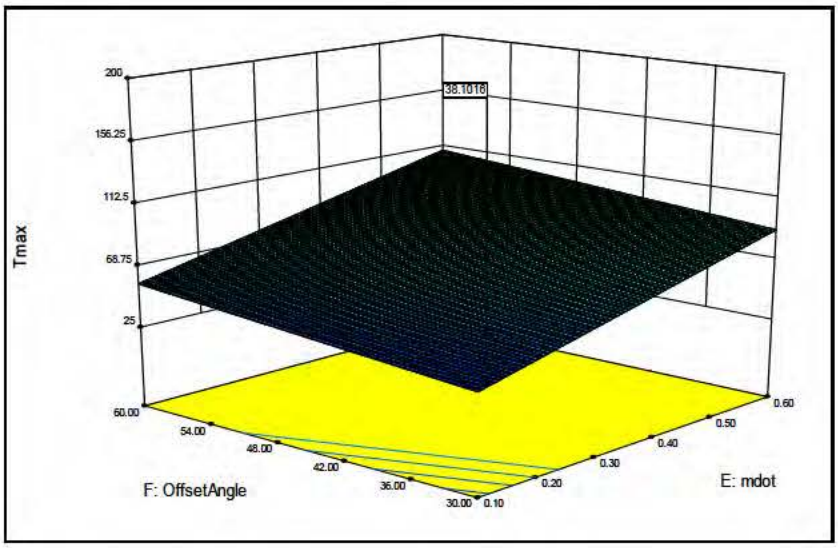

15)